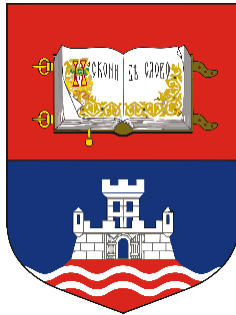UNIVERSITY OF BELGRADE
FACULTY OF TECHNOLOGY AND METALLURGY
AND
THE CATALAN INSTITUTE FOR WATER RESEARCH
UNIVERSITY OF GIRONA
FACULTY OF SCIENCES

Design, Development and Characterization of Atmospheric Plasma System for Wastewater Treatment

AMIT KUMAR

International Dual Doctorate

Belgrade, 2022

Advisors:

Prof. Dr. Dragan Povrenović, Full Professor at the Faculty of Technology and Metallurgy (FTM), University of Belgrade, Serbia.

Research Prof. Dr. Wolfgang Gernjak, Research Professor at the Catalan Institute for Water Research (ICRA), University of Girona, Spain.

Committee members:

Prof. Dr. Ivona Radović, Professor at the Faculty of Technology and Metallurgy (FTM), University of Belgrade, Serbia.

Prof. Dr. Zoran Lj. Petrović, Member of Serbian Academy of Sciences and Arts, Serbia.

Assoc. Dr. Vladimir Pavicević, Professor at the Faculty of Technology and Metallurgy (FTM), University of Belgrade, Serbia.

Research Prof. Dr. Jelena Radjenovic, Research Professor at the Catalan Institute for Water Research (ICRA), University of Girona, Spain.

Dr. Sara Rodríguez-Mozaz, Research Scientist at the Catalan Institute for Water Research (ICRA), Girona, Spain.

Prof. Dr. Zdenko Machala, Full professor in Physics at Comenius University Bratislava, Slovakia.

Acknowledgment

Funding source

The project NOWELTIES is funding this work. Under the Marie Skodowska-Curie grant agreement No. 812880, NOWELTIES was awarded financing from the European Union's Horizon 2020 research and innovation program. The main goal of NOWELTIES is to create a platform (European Joint Doctorate) for the education of tomorrow's water treatment experts. There are 14 separate research projects in total, all of which are targeted at developing innovative water treatment technology.
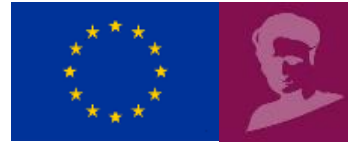
Design, Development, and Characterization of Atmospheric Plasma System for Wastewater Treatment

ABSTRACT

Water pollution is currently considered one of the most important environmental concerns on a global scale. Organic micropollutants (OMPs) are a type of emerging pollutant that is identified in a variety of water bodies and has the potential to impact aquatic life, agriculture, and human health. Some OMPs are frequently insufficiently eliminated by conventional convectional wastewater treatment plants, resulting in OMPs ending up in the environment. In this regard, several advanced oxidation processes (AOPs) have been investigated as efficient supplemental wastewater treatment techniques. Cold atmospheric plasma is a chemical-free AOP that has recently been recognized as an efficient and promising technology for the removal of OMPs from wastewater.

Cold atmospheric plasma is an abundant source of diverse reactive species at ambient conditions that are attracting attention due to its potential applications in commercial and scientific exploration, such as water treatment, agriculture, biomedical surface decontamination, and much more. In the case of water treatment, plasma and liquid interaction can generate chemically rich reactive species such as hydroxyl radical (HO·), atomic oxygen (O·), hydrogen peroxide (H_2O_2), ozone (O_3), and so on. These are the most important and strong oxidants that can cause OMPs to be oxidized and destroyed in water.

In this thesis, two separate cold atmospheric plasma sources known as 1-pin electrode and 3-pin electrode (also known as multi-electrode system) atmospheric pressure plasma jet (APPJ) were utilized to explore the degradation of OMPs in water. A multi-electrode-APPJ with a recirculation system was also investigated in order to optimize the plasma-liquid contact area and the degradation of OMPs.

In both cases, plasma was ignited using a high voltage RF power supply, and argon was chosen as a working gas. During the treatment, argon plasma was produced at the liquid surface in contact with the surrounding air. The plasma system was tested electrically and optically. Using voltage and current probes, the operating electrical discharge parameters (voltage and current) were investigated. The power deposition in two different circuits (at the source and in contact with the sample) was estimated using captured voltage and current waveforms. Optical emission spectroscopy (OES) and an intensified charge-coupled device (ICCD) camera were used to characterize plasma optically. OES techniques were used at various parameters to find evidence of numerous short-lived reactive species formed in the gas phase of a plasma system. OES spectra confirmed the presence of different reactive oxygen and nitrogen species (RONS) in a plasma discharge. The ICCD camera with a UV lens was utilized to obtain spectrally and temporally resolved images of the plasma discharge. The ICCD was utilized in combination with different band pass filters to capture the emission distribution of distinct RONS and excited argon in the plasma.

In this investigation, four different OMPs were chosen as target pollutants and treated with plasma, including two organic dyes (acid blue 25 dye and disperse red 1 dye) and one pharmaceutical (diclofenac) and one industrial chemical (para-chlorobenzoic acid). The treatments were carried out while taking into account many experimental parameters such as pollutant concentration, plasma treatment time, solution volume, input plasma power, and discharge gap. Characterization of plasma-treated samples was accomplished using a UV/Vis spectrophotometer, HPLC, and an Orbitrap-LC-MS. A pH and

conductivity analyzer was used to evaluate the pH and conductivity of the plasma-treated solution. Several kinetic models were assessed in order to investigate the various types of order of degradation and compute the oxidation rate of chosen OMPs. According to the study findings, plasma removed all of the mentioned pollutants through a distinct decomposition pattern. When compared to the other three OMPs, diclofenac showed the highest degradation. The energy yield was also calculated, which is an important measure for determining the energy efficiency of the plasma system. For comparison, the energy yield for 50 % pollutant removal was calculated; the highest energy yield was 6465 mg/kWh for diclofenac degradation.

In the present study, a pollutant, such as acid blue 25 dye, was treated indirectly (plasma was not in touch with dye solution) by using plasma-activated water (PAW). PAW was produced using pin-APPJ, then mixed with a dye-containing solution and studied for many days to identify the role of long-lived reactive species in dye degradation. PAW is a mixture of many stable RONS that can contribute to dye degradation in water.

Overall, the experimental results indicate that cold atmospheric plasma-based AOPs can be used to efficiently remove various OMPs from water. Cold atmospheric plasma-based treatment has significant potential as a unique, chemical-free approach to water purification that might be regarded as an alternative to traditional procedures. The findings of this study could be used to further research the development of plasma water treatment systems for the treatment of different types of polluted waters.

Keywords: Cold atmospheric plasma, electrical and optical characterization of plasma, treatment of organic micropollutants (OMPs)

Дизајн, развој и карактеризација плазма система на атмосферском притиску за прераду воде

АПСТРАКТ

Загађење воде се тренутно сматра једним од најважнијих еколошких проблема на глобалном плану. Органски микрозагађивачи (OMP) су нова врста загађивача који се налазе у различитим водама и имају потенцијал да утичу на живот у води, пољопривреду и здравље људи. Неки OMP немогу бити елиминисани применом конвенционалних конвекцијских постројења за пречишћавање отпадних вода, што доводи до тога да загађивачи заврше у животној средини. С тим у вези, актуелна су истраживања где се неколико напредних процеса оксидације (AOP) користе као ефикасне додатне технике третмана отпадних вода. Хладна атмосферска плазма је AOP без хемикалија који је недавно препознат као ефикасна и обећавајућа технологија за уклањање OMP из отпадних вода.

Хладна атмосферска плазма је извор различитих реактивних врста у амбијенталним условима који имају потенцијалне примене у комерцијалним и научним истраживањима, као што су третмани воде, пољопривреда, биомедицинска деконтаминација површина и још много тога. У случају третмана воде, интеракција плазме и течности може да генерише хемијски богате реактивне врсте као што су хидроксилни радикал (HO·), атомски кисеоник (O·), водоник пероксид (H_2O_2), озон (O_3) и тако даље. Ово су најважнији и најјачи оксиданти који могу изазвати оксидацију и уништавање OMP-а у води.

У овој тези, два одвојена извора хладне атмосферске плазме познати као плазма млаз на атмосферском притиску (APPJ) са једном шиљастом електродом и 3 шиљасте електроде (такође назван као мултиелектродни систем) су коришћени за истраживање деградације OMP у води. APPJ са више електрода са рециркулацијским системом је такође испитиван у тези у циљу оптимизације контактне површине плазме и течности и деградације OMP-а.

У оба случаја, плазма је реализована уз помоћ високонапонског радиофреквентног (РФ) напајања, а као радни гас је изабран аргон. Користећи ивор плазме на површини течности која је у контакту са околним ваздухом настала је аргонска плазма. Плазма систем је карактерисан из помоћ електричних и оптичких техника. Помоћу напонских и струјних сонди испитани су радни параметри електричног пражњења (напон и струја). Депоновање снаге у два различита дела кола (на извору и у контакту са узорком) је добијено коришћењем симљених сигнала напона и струје. Оптичка емисиона спектроскопија (OES) и камера са интензивираним детектором коришћене су за оптичку карактеризацију плазме. OES технике су коришћене за различите радне параметре да би се испитала производња различитих реактивних врста формираних у гасној фази тј. у пражњењу. Оптички емисиони спектри су потврдили присуство различитих реактивних врста кисеоника и азота (RONS) у пражњењу. За добијање спектрално и временски разложених слика плазме коришћена је камера са сочивом транспарентним у делу УВ спектра. Камера је коришћена у комбинацији са различитим филтерима из УВ и видљивог опсега да би се снимила просторна дистрибуција емисије различитих RONS и побуђеног аргона у плазми.

У овом истраживању, четири различита OMP су изабрана као циљни загађивачи који су третирани плазмом: две органске боје (AB25 боја и DR1 боја), фармацеутски производ (диклофенак) и

индустријска хемикалија (пара-хлоробензична киселина). Третмани су спроведени узимајући у обзир различите експерименталне параметре као што су почетна концентрација загађивача, време третмана плазмом, запремина третираног раствора, улазна снага плазме и растојање између извора плазме и узорка. Карактеризација узорака третираних плазмом је обављена коришћењем спектрофотометра, HPLC и LC-MS технике. Такође је мерен pH и проводљивости раствора третираних плазмом. Резултати су упоређени са неколико кинетичких модела да би се истражили различити типови редоследа деградације и израчунала брзина оксидације одабраних OMP. Према налазима студије, плазма је уклонила све поменуте загађиваче, сваки кроз специфичан образац разлагања. У поређењу са остала три OMP-а диклофенак је показао највећи степен деградације. Израчунат је и енергетски принос, што је важна мера за одређивање енергетске ефикасности плазма система. Израчунат је енергетски принос за уклањање 50 % загађивача, а највећи енергетски принос био је 6465 mg/kWh за разградњу диклофенака.

Поред тога у овој студији је загађивач AB25 боја третиран индиректно при чему плазма није била у додиру са раствором боје већ је коришћена вода активиране плазмом (PAW). PAW је произведен у третману дестиловане воде плазмом, а затим помешан са воденим раствором који садржи боју и након тога праћен током неколико дана да би се идентификовала улога дугоживећих реактивних врста у деградацији боје. PAW је мешавина многих стабилних RONS који могу допринети разградњи боје у води.

Све у свему, експериментални резултати показују да се AOP-и засновани на хладној атмосферској плазми могу користити за ефикасно уклањање различитих OMP-а из воде. Третман заснован на хладној атмосферској плазми има значајан потенцијал као јединствен приступ пречишћавању воде без хемикалија који се може сматрати алтернативом традиционалним процедурама. Налази ове студије могли би се користити за даље истраживање развоја система за третман плазма воде за третман многих врста загађених вода.

Кључне речи: хладна плазма на атмосферском притиску, електрична и оптичка карактеризација плазме, третман органских микрозагађивача (OMP)

Disseny, desenvolupament i caracterització de sistemes de plasma a pressió atmosfèrica per al tractament d'aigües residuals

RESUM

La contaminació de l'aigua es considera actualment una de les preocupacions mediambientals més importants a escala mundial. Els microcontaminants orgànics (OMP) són un tipus de contaminants emergents que s'identifiquen en una varietat de cossos d'aigua i tenen el potencial d'impactar en la vida aquàtica, l'agricultura i la salut humana. Alguns OMPs són sovint insuficientment eliminats a les plantes de tractament d'aigües residuals convencionals, resultant en OMPs que acaben en el medi ambient. En aquest sentit, diversos processos d'oxidació avançats (AOPs) han estat investigats com a tècniques de tractament d'aigües residuals suplementàries eficients. El plasma atmosfèric fred és un AOP lliure de productes químics que recentment ha estat reconegut com una tecnologia eficient i prometedora per a l'eliminació d'OMPs de les aigües residuals.

El plasma atmosfèric fred és una font abundant d'espècies reactives en condicions ambientals que atrau l'atenció a causa del seu potencial en l'exploració comercial i científica en el tractament de l'aigua, l'agricultura, la descontaminació de les superfície biomèdiques, i molt més. En el cas del tractament de l'aigua, el plasma i la seva interacció amb la superfície líquida poden generar espècies reactives com ara el radical hidroxil (HO·), l'oxigen atòmic (O·), el peròxid d'hidrogen (H_2O_2), l'ozó (O_3), i d´altres. Aquests són els oxidants més importants i forts que poden causar que els OMP s'oxiden i destrueixin en aigua.

En aquesta tesi, es van utilitzar dues fonts de plasma atmosfèric fred conegudes com a elèctrode de 1 pin i elèctrode de 3 pins (també conegut com a sistema multipin) per explorar la degradació dels OMPs en aigua. També es va investigar un multipin-APPJ amb un sistema de recirculació per optimitzar l'àrea de contacte plasma-líquid i la degradació dels OMPs.

En ambdós casos, el plasma es va encendre utilitzant una font d'alimentació de radiofreqüència (RF) d'alta tensió, i l'argó va ser triat com a gas de treball. Durant el tractament, es va produir plasma d'argó a la superfície líquida en contacte amb l'aire circumdant. El sistema de plasma es va provar elèctricament i òpticament. Utilitzant sonda de voltatge i corrent, es van investigar els paràmetres de descàrrega elèctrica en funcionament (voltatge i corrent). La deposició de potència en dos circuits diferents (a la font i en contacte amb la mostra) es va estimar utilitzant voltatge capturat i la forma de les ones de corrent. L'espectroscòpia d'emissió òptica (OES) i una càmera de dispositiu d'acoblament de càrrega intensificada (ICCD) es van utilitzar per caracteritzar el plasma òpticament. Les tècniques d'OES es van utilitzar en diversos paràmetres per trobar evidència de nombroses espècies reactives de curta durada formades en la fase gasosa del sistema de plasma. Els espectres OES van confirmar la presència de diferents espècies reactives d'oxigen i nitrogen (RONS). La càmera ICCD amb una lent UV es va utilitzar per obtenir imatges resoltes espectralment i temporalment de la descàrrega de plasma. L'ICCD es va utilitzar en combinació amb diferents filtres de pas de banda per capturar la distribució d'emissió de diferents RONS i argó excitat en el plasma.

En aquesta investigació, quatre OMPs diferents van ser escollits com a contaminants objectiu i vam ser tractats amb plasma, incloent-hi dos tints orgànics (blau àcid 25 i dispersa color vermell 1 tint) i dos fàrmacs (diclofenac i àcid paraclorobenzoic). Els tractaments es van dur a terme tenint en compte molts paràmetres experimentals com la concentració de contaminants, el temps de tractament del plasma, el

volum de la solució, l'energia del plasma d'entrada i el buit de descàrrega. La caracterització de mostres tractades amb plasma es va realitzar utilitzant un espectrofotòmetre UV/Vis, HPLC, i un UPLC-Orbitrap. El pH i la conductivitat de la solució tractada amb plasma també es va analitzar. Es van avaluar diversos models cinètics per investigar els diferents tipus d'ordre de degradació i calcular la taxa d'oxidació dels OMPs escollits. D'acord amb les troballes de l'estudi, el plasma va eliminar tots els contaminants esmentats mitjançant un patró de descomposició diferent. En comparació amb els altres tres OMPs, el diclofenac va mostrar el grau de degradació més alta. També es va calcular el rendiment energètic, que és una mesura important per determinar l'eficiència energètica del sistema de plasma. En comparació, es va calcular un rendiment energètic per a l'eliminació de contaminants del 50 %; el rendiment energètic més alt va ser de 6465 mg/kWh per a la degradació de diclofenac.

En l'estudi actual, un contaminant, com el blau àcid 25 tint, va ser tractat indirectament (el plasma no estava en contacte amb la solució del tint) mitjançant l'ús d'aigua (PAW) activada pel plasma. La PAW es va produir utilitzant pin-APPJ, després es va barrejar amb una solució que contenia tint i va estudiar durant una llarga exposició per identificar el paper de les espècies reactives de llarga vida en la degradació del tint. La PAW és una barreja de molts RONS estables que poden contribuir a la degradació dels tints en l'aigua.

En general, els resultats experimentals indiquen que els AOPs basats en plasma atmosfèric fred es poden utilitzar per eliminar de manera eficient diversos OMPs a l'aigua. El tractament basat en el plasma atmosfèric fred té un potencial significatiu com un enfocament únic i lliure de productes químics per a la purificació de l'aigua que podria considerar-se una alternativa als procediments tradicionals. Els resultats d'aquest estudi podrien ser utilitzats per a investigar més el desenvolupament de sistemes de tractament d'aigua amb plasma per tractar diferents tipus d'aigua contaminada.

Paraules clau: plasma atmosfèric fred, caracterització elèctrica i òptica del plasma, tractament de microcontaminants orgànics (OMP)

Diseño, desarrollo y caracterización de sistemas de plasma a presión atmosférica para el tratamiento de aguas residuales

RESUMEN

La contaminación del agua se considera actualmente una de las preocupaciones medioambientales más importantes a escala mundial. Los microcontaminantes orgánicos (OMP) son un tipo de contaminantes emergentes que se identifican en una variedad de cuerpos de agua y tienen el potencial de impactar en la vida acuática, la agricultura y la salud humana. Algunos OMPs son a menudo insuficientemente eliminados por las plantas convencionales de tratamiento de aguas residuales, resultando en OMPs que acaban en el medio ambiente. En este sentido, varios procesos de oxidación avanzados (AOPs) han sido investigados como técnicas de tratamiento de aguas residuales avanzadas eficientes. El plasma frío a presión atmosférica es un AOP libre de productos químicos que recientemente ha sido reconocido como una tecnología eficiente y prometedora para la eliminación de OMPs de las aguas residuales.

El plasma frío a presión atmosférica es una fuente abundante de especies reactivas en condiciones ambientales que atraen la atención debido a su potencial en la explotación comercial y científica en el tratamiento del agua, la agricultura, la descontaminación de superficie biomédicas, y mucho más. En el caso del tratamiento del agua, el plasma y su interacción con la fase líquida pueden generar especies reactivas diversas como el radical hidroxilo (HO·), el oxígeno atómico (O·), el peróxido de hidrógeno (H_2O_2), el ozono (O_3), y otros. Estos son los oxidantes más importantes y fuertes que pueden causar que los OMP se oxiden y destruyan en agua.

En esta tesis se utilizaron dos sistemas de fuentes de plasma frío en forma de chorro a presión atmosférica con electrodo de aguja (APPJ, del inglés "atmospheric plasma pin jet"), denominadas como electrodo de 1 aguja y electrodo de 3 agujas (también denominado sistema multipin) para explorar la degradación de los OMPs en agua. También se investigó un multipin-APPJ con un sistema de recirculación para optimizar el área de contacto plasma-líquido y la degradación de los OMPs.

En ambos casos, el plasma se encendió utilizando una fuente de alimentación radiofrecuencia (RF) de alta tensión, y el argón fue elegido como gas de trabajo. Durante el tratamiento, se produjo plasma de argón en contacto con el aire circundante que impactó a la superficie líquida. El sistema de plasma se analizó respecto sus características eléctricas y ópticas. Utilizando sondas de voltaje y corriente, se investigaron los parámetros de descarga eléctrica en funcionamiento. La deposición de potencia en dos circuitos diferentes (a la fuente y en contacto con la muestra) se estimó utilizando voltaje capturado y la forma de las ondas de corriente. Se utilizó la espectroscopia de emisión óptica (OES) y una cámara de carga acoplada e intensificada (ICCD) para caracterizar el plasma ópticamente. Las técnicas de OES se utilizaron para evidenciar la existencia de numerosas especies reactivas de corta duración formadas en el sistema de plasma. De este modo, se confirmó la presencia de diferentes especies reactivas de oxígeno y nitrógeno (RONS). La cámara ICCD con una lente para el ultravioleta (UV) se utilizó para obtener imágenes resueltas espectral y temporalmente de la descarga de plasma. El ICCD se utilizó en combinación con diferentes filtros de banda para capturar la distribución de emisión de diferentes RONS y argón excitado en el plasma.

En esta investigación, cuatro OMP diferentes fueron escogidos como contaminantes objetivo y tratados con plasma, incluyendo dos tintes orgánicos (azul ácido 25 rojo disperso 1), un fármaco (diclofenac) y

un compuesto industrial (ácido paraclorobenzoico). Los tratamientos se llevaron a cabo teniendo en cuenta diferentes parámetros experimentales como la concentración de contaminantes, el tiempo de tratamiento mediante el plasma, el volumen de la solución, la energía del plasma depositada y la distancia entre electrodo y superficie del líquido. La caracterización de muestras tratadas con plasma se realizó utilizando un espectrofotómetro UV/Vis, HPLC, y un UPLC-Orbitrap así como se analizaron pH y conductividad de la solución tratada con plasma. Se evaluaron varios modelos cinéticos para investigar los diferentes tipos de orden de degradación y calcular la tasa de oxidación de los OMP escogidos. De acuerdo con los hallazgos del estudio, el plasma eliminó todos los contaminantes mencionados mediante un patrón de descomposición diferente. En comparación con los otros tres OMP, el diclofenac mostró la degradación más alta. También se calculó el rendimiento energético, que es una medida importante para determinar la eficiencia energética del sistema de plasma. Se calculó el rendimiento energético para la eliminación del 50 % de los contaminantes. El rendimiento energético más alto fue de 6465 mg/kWh para la degradación de diclofenac.

En el presente estudio, un contaminante, como el azul ácido 25 tinte, fue tratado de forma indirecta (el plasma no estaba en contacto con la solución del tinte) mediante el uso de agua activada por el plasma (PAW). La PAW se produjo utilizando pin-APPJ, después se mezcló con una solución que contenía tinte y se estudió mediante exposición larga la degradación para identificar el papel de las especies reactivas de larga vida en la degradación del tinte. La PAW es una mezcla de muchos RONS estables que pueden contribuir a la degradación de los tintes en el agua.

En general, los resultados experimentales indican que los AOPs basados en el plasma frío a presión atmosférica se pueden utilizar para eliminar de manera eficiente varios OMPs del agua. El tratamiento basado en el plasma frío a presión atmosférica tiene un potencial significativo como un enfoque único y libre de productos químicos para la purificación del agua que podría considerarse una alternativa a los métodos tradicionales. Los resultados de este estudio podrían ser utilizados para investigar más el desarrollo de sistemas de tratamiento de agua con plasma para el tratamiento de diferentes tipos de agua contaminada.

Palabras claves: plasma frío a presión atmosférica, caracterización eléctrica y óptica de plasma, tratamiento de microcontaminantes orgánicos (OMP)

TABLE OF CONTENTS

LIST OF FIGURES

LIST OF TABLES

ABBREVIATIONS

CAP	Cold atmospheric plasma
OMPs	Organic micropollutants
WHO	World health organization
AOPs	Advanced oxidation processes
COD	Chemical oxygen demand
BOD	Biological oxygen demand
TSS	Total suspended solids
APPJ	Atmospheric pressure plasma jet
PAW	Plasma activated water
DBD	Dielectric barrier discharge
AB25	Acid blue 25
DR1	Disperse red 1
DCF	Diclofenac
pCBA	Para-chlorobenzoic
C_o	Initial pollutant concentration
C	Concentration after treatment
V_0	Initial sample volume
ῃ	Removal efficiency
slm	Standard liter per minutes
FWHM	Full width at half maximum
Te	Electron temperature
Tg	Gas temperature
Ti	Ion temperature
RMS	Root means square
ROS	Reactive oxygen species
RNS	Reactive nitrogen species
RF	Radio frequency
BPF	Band pass filter
UV	Ultraviolet
DC	Direct current
AC	Alternative current
SPS	Second positive system
FNS	First negative system
FPS	First positive system
OES	Optical emission spectroscopy
LC	Liquid chromatography
MS	Mass spectrometry

CHAPTER 1

1. Introduction

1.1. Motivation and objective

Organic micropollutants (OMPs), which contain a variety of chemical compounds (pharmaceuticals, organic dyes, pesticides and so on), have become one of the world's most significant sources of water pollution. Anthropogenic activities have resulted in the detection of several OMPs in water bodies. Several million tons of OMPs are dumped into water bodies each year from diverse effluents, where their persistence causes serious environmental and health hazards. Chemical stability and low concentrations make various OMPs highly resistant to degradation by existing wastewater treatment plants (WWTPs). In order to detoxify harmful persistent wastewater effluents, sophisticated advanced oxidation processes (AOPs) have been investigated. Cold atmospheric plasma-based AOPs are a new, fast-emerging technology and a new possibility in water purification. Cold atmospheric plasmas can eliminate a wide range of OMPs without the use of any additional oxidants.

Cold atmospheric plasmas have gained prominence in recent years due to their potential applications in a variety of industries, including water treatment, agriculture and the food industry, among others. Atmospheric plasmas can provide a chemically rich environment that allows for a variety of species interactions to occur at ambient conditions (close to room temperature). The plasma-liquid contact produced a combination of reactive chemical species (HO•, O•, H_2O_2, O_3….) that have a high oxidation potential and can interact with most OMPs, mineralizing them in the liquid. Plasma-based treatment methods are solvent and chemical-free, as well as environmentally beneficial. As a result, cold atmospheric plasmas could be exploited as an alternative approach to wastewater treatment.

The goal of the thesis is to design, construct and characterize a 3-pin Atmospheric Pressure Plasma Jet (APPJ) system for removing OMPs (such as organic dyes, pharmaceutical, and industrial chemical) from water. The entire work has been shown with these key objectives:

- Design and development of cold atmospheric plasma source.
- The generation of cold atmospheric plasma in contact with liquid.
- Electrical and optical diagnostics of cold atmospheric plasma at various parameters.
- The use of a cold atmospheric plasma source to remove specific OMPs from water.
- The characterization of plasma-treated liquids.

Figure 1.1 depicts the work aim graphically, together with the essential tasks. Figure 1.1 (a) depicts the plasma source, power supply utilized to ignite plasma, and plasma diagnostic. Figure 1.1 (b) demonstrates parametric variation in contaminant treatment and characterization of plasma treated liquid samples, such as degradation analysis of all four selected pollutants by product analysis for diclofenac.
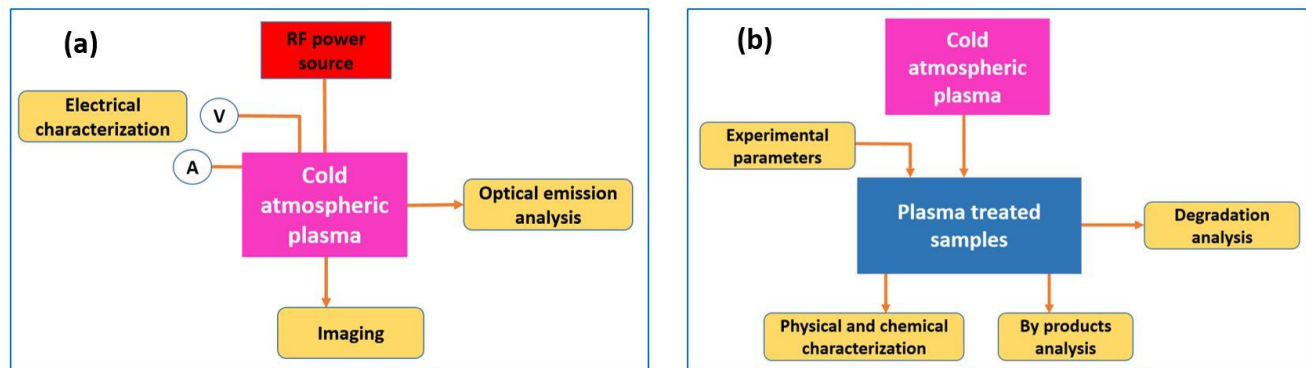
Figure 1.1. Schematic description of the research.

In order to achieve the goal, a cold atmospheric plasma source with a pin-type electrode shape was constructed. A radio frequency (RF) power supply has been selected as a high voltage source. Plasma was successfully ignited and generated in contact with the liquid surface. Complete characterization of plasma operating with various parameter settings was carried out utilizing a variety of measuring techniques, including electrical and optical plasma measurements. Electrical measuring techniques were utilized to determine discharge parameters such as voltage, current and power delivered to the plasma system. Optical measurements offered a satisfying understanding of plasma chemistry, allowing the identification of critical reactive species involved in the destruction of OMPs.

Cold atmospheric plasma was used to treat various contaminants diluted in water under various experimental conditions and the degradation pattern of each contaminant was investigated. A variety of analytical approaches were employed to characterize the plasma-treated liquid environment and understand the kinetics and mechanisms that contribute to OMPs degradation in the plasma treatment process. The plasma device was optimized in order to achieve plasma conditions that would allow for efficient wastewater treatment of various forms of OMPs. The characteristics of the plasma source, the treatment of OMPs and the relevance of experimental parameters are briefly outlined in the sections below.

1.2. Thesis outline

The objective of this thesis is the design, development and characterization of a multi-needle APPJ system for wastewater treatment. Cold atmospheric plasma sources investigated included already existing pin-APPJ and newly constructed multi-needle electrodes-APPJ for the treatment of certain contaminants.

The thesis is divided into seven chapters. The thesis outline and goal are the first topics covered in this chapter. The literature review is described in chapters two and three. The second chapter covered an overview of the worldwide wastewater scenario, the incidence and classification of OMPs and the treatment of OMPs using certain available AOPs. The third chapter covered the fundamentals of plasma technology as well as the current state-of-the-art in plasma-liquid interactions. It covers a review of the literature on cold atmospheric plasma-based OMPs (such as pharmaceuticals, organic dyes and pesticides) treatment, with a focus on plasma sources, reactor setup and various operating parameters that affect OMPs degradation. After providing introductory information about several types of plasma sources, chapter three goes into detail about methodologies used to degrade organic dyes, pharmaceuticals and pesticides.

The fourth chapter discusses a few of the OMPs that have been chosen as targets (Acid Blue 25, Disperse Red 1, Diclofenac, Para-Chlorobenzoic). Plasma source arrangement, experimental settings, instrumental equipment and analytical procedures are also part of this chapter.

The treatment outcomes are detailed in chapters five and six. The fifth chapter includes electrical and optical diagnostics of the pin-APPJ, as well as the treatment of various OMPs and parametric analyses. The effects of pollutant concentration, treatment period and power deposition are all considered in the plasma treatments.

The electrical and optical diagnostics of multi-needle electrodes-APPJ were examined in chapter six. It is discussed how OMPs are treated with and without a recirculation system. In chapter six, the transformation products derived from diclofenac were also discussed.

Finally, in chapter seven, the general conclusion and future work on cold plasma-based wastewater treatment are discussed.

CHAPTER 2

2. Literature review on wastewater

This chapter covers an overview of worldwide water demand, water pollution and the sources of OMPs in water. Several AOPs have also been studied for the degradation of OMPs in wastewater.

2.1. Global water scenario

The world's water crisis is escalating. It is estimated that due to huge population growth over the last 100 years, global water demand has surged by 600 % [1,2]. The worldwide water need for all purposes, which is currently roughly 4,600 km^3 per year, is expected to rise until 2050 [2,3]. Irrigation presently consumes more than 70 % of available fresh water, making it one of the most water-intensive sectors [4]. Water has been used in industry at a rate of roughly 20 %, with 75 % going to energy generation and the remaining 25 % going to manufacturing [5]. Domestic use accounts for approximately 10 % of the total volume and this is expected to increase considerably between 2010 and 2050 [2].

Water shortages already affect each continent. According to UN estimates, more than one-third of the world's population now lives in countries experiencing severe to serious water stress [6]. Over 2 billion people live in countries where there is severe water scarcity for at least one month of the year, while 4 billion live in nations where there is severe water stress [7]. According to Population Action International, more than 2.8 billion people in 48 countries may face water stress or scarcity by 2025, as illustrated in Figure 2.1, based on UN Medium Population Projections [8]. For example, by 2025, around 230 million Africans, or 16 % of the projected population, would face water scarcity, with 460 million living in water-stressed areas [9]. Water scarcity will affect the majority of Asian countries. Climate change is already influencing the water cycle and is expected to have a significant influence on global water access. Climate change and water stress will worsen as the demand for water rises [10,11].
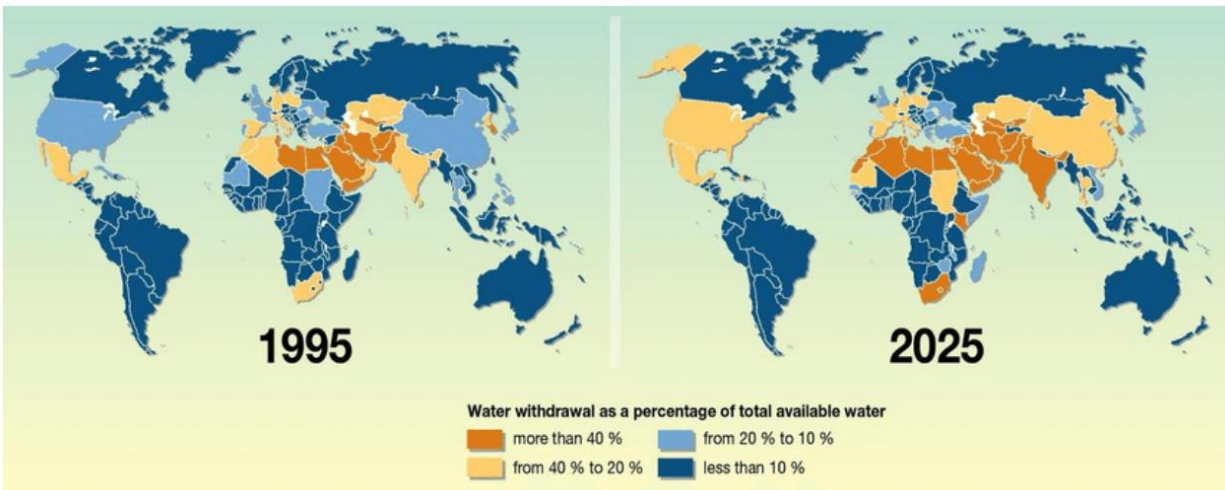
Figure 2.1. Water stresses around the World (United Nations Environmental Programme-UNEP) [8].

2.2. Water pollution

Pollution of surface and ground waters is currently one of the most pressing environmental issues, impacting people all around the world [12,13]. Toxic and chemical waste that finds its way into our rivers can make people sick and endanger marine life that lives nearby [14,15]. According to the study, harmful contaminants are already wreaking havoc on our biodiversity and ecosystems in numerous areas [16,17].

The ecosystem, as well as social and economic progress, needs clean water [18]. Sanitation and safe drinking water are regarded as basic human rights because they are essential for sustaining healthy livelihoods and upholding the dignity of the individual [19,20]. However, a growing global population, unrelenting urbanization and an increasing scarcity of high-quality water supplies are all contributing to the rapid depletion of adequate water resources [21]. According to the UN World Water Development Report 2003, approximately 1500 cubic kilometers of liquid waste are produced every day all over the world, including around over 2 million tons of waste being discharged into receiving streams every day [22]. Over 80 % of this water is not collected or treated and up to 90 % of it flows untreated into rivers, lakes, as well as other highly-productive regions in developing nations [23].

According to the World Health Organization, over 3.4 million deaths are caused by poor water supply, sanitation and hygiene, with the majority of these deaths occurring in poorer nations [24]. However, 884 million people worldwide do not have access to safe drinking water and 2.6 billion do not have access to adequate sanitation [25].

2.3. Source of organic micropollutants to environment

Water pollution is caused by the increased use of chemicals and the careless discharge of toxic materials into water bodies around the world [26,27]. Numerous emerging OMPs that are dangerous to the environment, including pharmaceuticals, personal care items, textiles, human waste, food wastes, sewage treatment discharge and agricultural runoff, have been found in water systems and contribute to water contamination [28–30].

Figure 2.2 highlighted the primary sources of OMPs [31,32]. OMPs reach the environment via a number of sources and pathways, including industrial, agricultural, residential, and municipal wastewater treatment plants [30,31]. When released from a variety of sources, certain OMPs linger in the environment for an extended period of time and can travel considerable distances. These OMPs were also found in amounts ranging from ng/L to g/L in groundwater, surface water, and even drinking water [33,34].
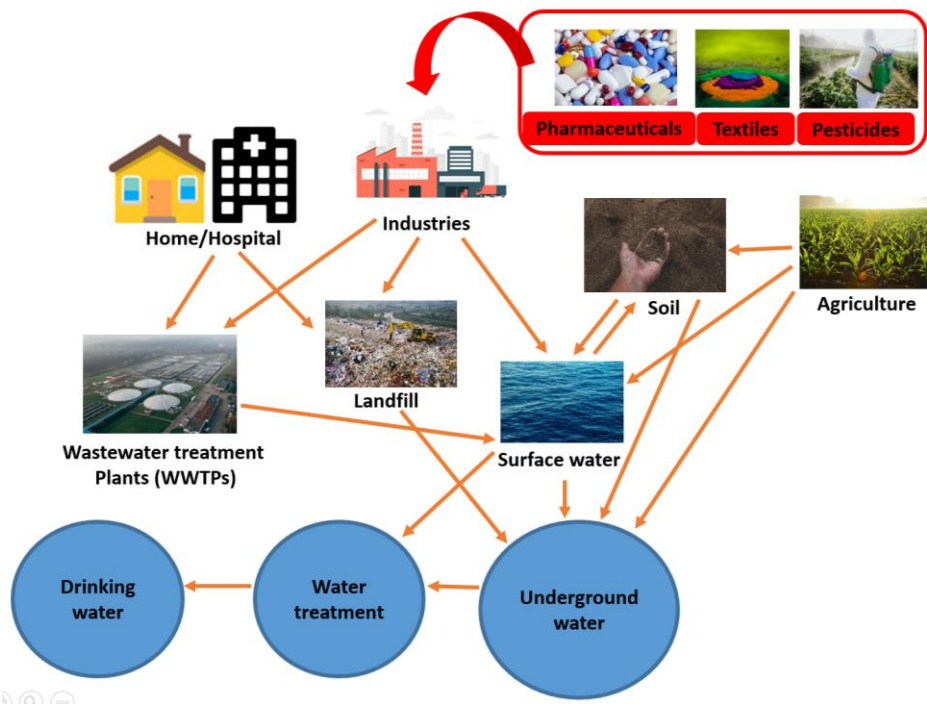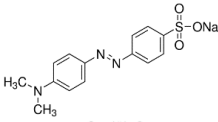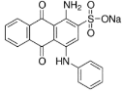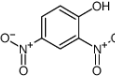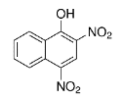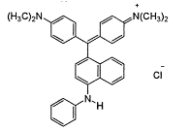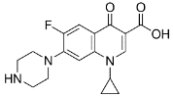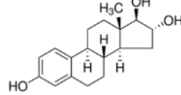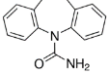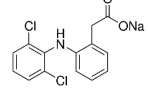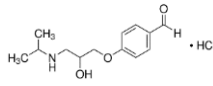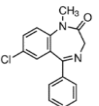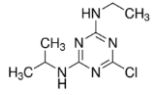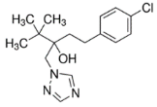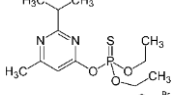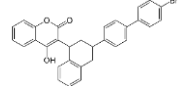
Figure 2.2. The paths by which OMPs enter the environment and how they flow.

The OMPs found in the environment are classified into several categories, some of which are mentioned with their subgroups in Table 2.1. Of course, several OMPs have been detected in water bodies, but these contaminants have been used as examples. OMPs have the potential to withstand biodegradation, are harmful to people, and have been related to negative environmental effects, including accumulation in both aquatic and agricultural environments.

Table 2.1. Classification of OMPs.

Class of OMPs	Sub-categories	Examples		Ref.
		Compounds	Chemicals structure	
Organic dyes	Azo	Methyl orange		[35]
	Anthraquinone	Acid Blue 25		[36]
	Sulfur	Sulphur Black 1		[37]
	Nitro	Martius yellow		[38]
	Triarylmethane	Basic Blue 26		[39]
Pharmaceuticals	Antibiotics	Ciprofloxacin		[40]
	Hormones	Estriol		[41]
	Anticonvulsants	Carbamazepine		[42]
	NSAIDs	Diclofenac		
	Antihypertensives	Metoprolol		[43]
	Antidepressants	Diazepam		[44]
Pesticides	Herbicides	Atrazine		[45]
	Fungicides	Tebuconazole		[46]
	Insecticides	Diazinon		[47]
	Rodenticides	Brodifacoum		[48]

Physical and chemical composition study of diverse wastewater effluents has been investigated by several researchers. Because a significant proportion of OMPs are non-biodegradable, they discovered that many wastewater effluents have a significant amount of pollutants. Table 2.2 illustrates the typical properties of wastewater from the textile, pharmaceutical, pesticide, cosmetic and domestic industries. The first four wastewater discharged are industrial effluents. According to the findings, the greater chemical oxygen demand (COD) to biological oxygen demand (BOD) ratios found in all cases suggests that the wastewater contained a significant quantity of resistant organic compounds. Such data suggests that there is an urgent need to address the wastewater treatment issue. To avoid harming living creatures and the ecosystem, this type of effluent should be disinfected before even being released into the environment.

Table 2.2. Some examples of wastewater effluents.

Physico-chemical parameters

	COD	BOD	pH	TSS	Ref.
Textile	3300-3500	2100-2300	8.2-9.6	350-410	[49]
Pharmaceuticals	4000-6000	300-1500	6.5-8.0	600-700	[50]
Pesticides	6000-7000	2000-3000	12-14	250-300	[51]
Cosmetic	34000-38000	7700-6700	7-7.2	8700-7300	[52]
Household	182-1818	116-1168	6-8.2	44-1396	[53]

All values are in mg/L except pH,

Many conventional wastewater systems rely on biological treatment techniques [54,55]. One of the key benefits of biological treatment approaches is their relatively inexpensive. Municipal wastewater as well as some industrial effluent are widely and effectively treated using biological treatment techniques [56]. Because of their complicated and persistent molecular structures, traditional WWTPs are unable to effectively remove several kinds of OMPs [57]. As a result, organic residuals have been discovered in water treatment plant effluents, groundwater, surface water and drinking water [32,58].

2.4. Advanced oxidation processes

Because several studies have demonstrated that traditional WWTPs only partially eliminate a variety of OMPs, a variety of AOPs (as seen in Figure 2.3) have been designed to address the limitations of traditional approaches [59–61]. There are two forms of AOP: homogeneous and heterogeneous systems, which have been explored in various papers. Homogeneous processes are usually relied on reagents, while catalysts are frequently used in heterogeneous processes. AOPs have been touted as a viable and long-term treatment option due to their capacity to remove a large number of pollutants while avoiding the production of harmful byproducts [62]. AOPs can be used on their own or in conjunction with other physical, chemical, as well as biological processes [63]. Other approaches (for example, membrane-activated carbon-based and others) have been investigated to remove OMPs through adsorption and while they remove many pollutants successfully, they do not degrade them [64]. As a result, adsorbed pollutants, as well as rejection trash in membrane-based treatment techniques, may contribute to pollution in the environment until they are incinerated.
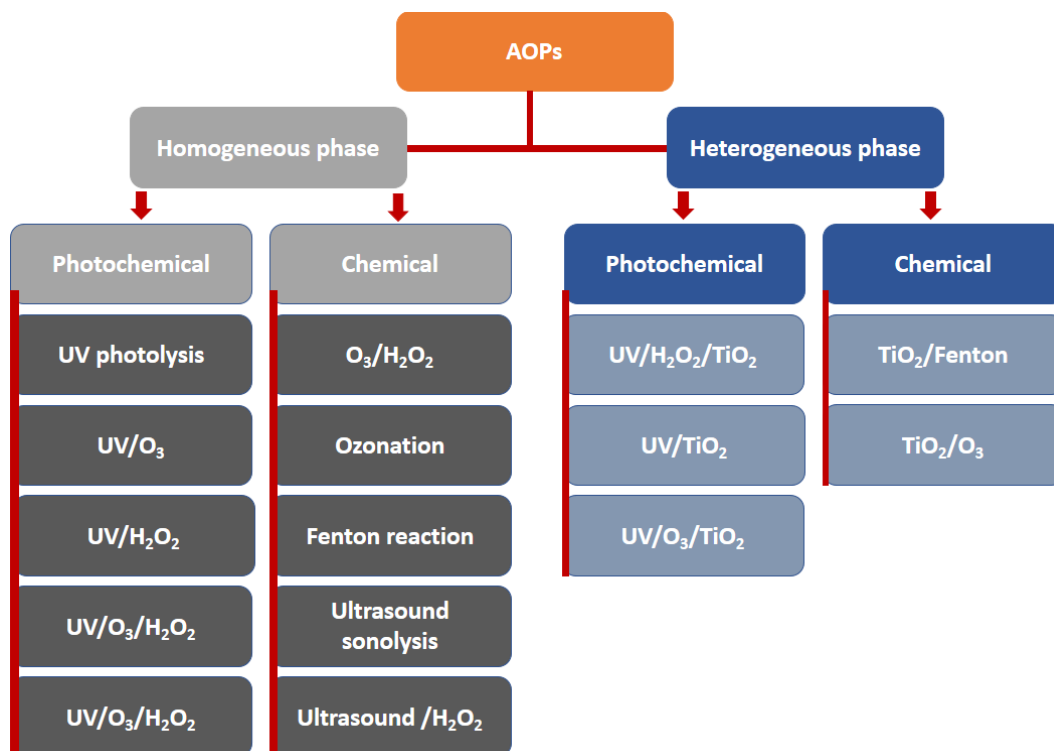
Figure 2.3. AOPs (homogeneous and heterogeneous) for the elimination of OMPs that are commonly used.

AOPs are known to produce hydroxyl radicals (HO•) [59,60,65]. HO• is highly suggested for treating extremely non-biodegradable wastewater treatment plant effluents. The mechanisms of HO• generation have been thoroughly investigated by a number of researchers and info can be obtained in multiple reviews [59,63]. The kind of AOPs influences the generation of HO• radicals. Table 2.3 shows the chemical pathways that can be used to produce HO• in various AOPs [65].

Table 2.3. HO• generation mechanism by various AOPs.

AOPs processes	Reaction steps
H_2O_2 – Fenton	$H_2O_2 + Fe^{2+} \rightarrow Fe^{3+} + HO• + OH^-$
UV/TiO2	$TiO_2 + h\nu \rightarrow e^- + h^+$ $h^+ + H_2O \rightarrow H^+ + HO•$
O_3/H_2O_2	$2O_3 + H_2O_2 \rightarrow 2\ HO• + 3O_2$
UV/H_2O_2	$H_2O_2 + UV \rightarrow 2\ HO•$
$UV/H_2O_2/O_3$	$2O_3 + UV + H_2O_2 \rightarrow 2HO• + 3O_2$
Ultrasound/UV/O_3	Ultrasound $+ UV + O_3 \rightarrow HO•$

Compared to other oxidizing agents, HO• has been deemed a powerful non-selective oxidant with a very high oxidation capability (can be seen in Table 2.4) [65,66]. Many non-biodegradable stable organic compounds can be successfully attacked and destroyed by HO• via hydrogen bond abstraction, electrophilic addition and electron transfer mechanisms [67]. Many researchers have observed that the

reactivity of HO• to most OMPs ranges between 10^6–10^{10} $M^{-1}s^{-1}$, depending on the type of organic pollutants [68].

Table 2.4. The oxidation potential of regularly used oxidants.

Oxidants	Oxidation potential (V)
Hydroxyl radical (HO•)	2.80
Atomic oxygen (O•)	2.42
Ozone (O_3)	2.07
Hydrogen peroxide (H_2O_2)	1.78
Hydroperoxyl radical (HO_2•)	1.70
Chlorine (Cl_2)	1.36

Cold atmospheric plasmas are getting popular among AOPs as a means of addressing wastewater treatment difficulties [69–71]. Cold atmospheric plasmas are regarded to be a viable method for eliminating dissolved OMPs [65,72]. Plasma technology is becoming more popular as a source of AOPs because it produces a large number of reactive species all at once and at a rapid rate, which helps to decompose OMPs [73–75]. Plasma technology is extremely popular due to its quick removal and environmentally friendly operations. Moreover, unlike previous efforts, no chemicals are used in the operation, plasma functions at ambient condition and the amount of OMPs can be reduced to a safe level via plasma treatment [65]. Multiple plasma sources with varied reactor configurations have already been utilized to examine the elimination of many model OMPs from water in the past few years [13,65,70].

CHAPTER 3

3. Cold atmospheric plasma technology

Irving Langmuir, an American physicist and scientist, created the term "plasma" in 1928, characterizing it as an electrically ionized gas [76–78]. Figure 3.1 depicts plasma as the fourth fundamental type of matter after solids, liquids and gases [78–80]. Plasma is a massive cloud of particles that includes high-energy electrons, reactive species and negative and positive ions [77,78,81,82]. Aside from ions and electrons, plasma contains a wide number of neutral species, metastables and photons of various wavelengths that contribute to the acceleration of chemical reactions [81,83].
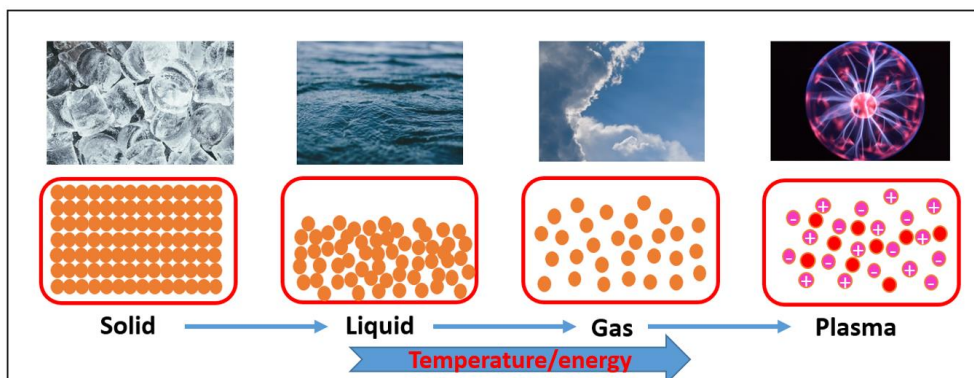
Figure 3.1. Plasma state of matter.

3.1. Non-equilibrium low temperature (cold) plasma at atmospheric pressure

Many researchers are already investigating how plasma technology might help protect the environment by eliminating contaminants from the air and water [84,85]. In general, the two forms of plasmas investigated in the laboratory are distinguished primarily by temperature differences [86,87]. Plasmas are categorized into two types: thermal plasma and non-thermal plasma. The term "thermal plasma" refers to a plasma that is in local thermodynamic equilibrium, i.e. all of its species have the same temperature (T_e: electron temperature and T_g: gas temperature, are similar). Plasma welding arcs and plasma cutting are frequent ways to visualize thermal plasma, where very high current and lower voltage are required [77].

Cold or non-equilibrium non-thermal plasmas are plasmas produced at or near room temperature [77,81]. Non-thermal plasmas are also known as non-equilibrium cold plasmas due to the temperature differential between electrons (T_e) and other plasma species (ions and neutrals) and because the total gas temperature (T_g) in active plasma volume is close to ambient [65,87,88]. In cold plasmas, momentum transfer between electrons and heavy particles is ineffective, therefore the temperature of the electrons (T_e) is significantly higher than the temperature of the heavy particles. As a result, high-energy electrons play a crucial role in initiating chemical reactions and directing plasma chemistry in these plasmas via processes such as excitation, ionization and dissociation [77,81,85].

Table 3.1 contrasts two types of plasma in terms of electron temperature, electron density and gas temperature. Both types of plasma, with varying electrical and optical configurations, as well as other operational qualities, were researched for a variety of purposes and applications [65,77,81]. The plasma

source, discharge, voltage signal, working gas and other factors all influence the range of plasma characteristics. It was observed that because cold plasma runs at low temperatures, its power consumption is lower than that of a thermal plasma system [80,87,89].

Table 3.1. Properties of non-thermal plasma and thermal plasma.

	Non-thermal plasmas	**Thermal plasmas**	**Ref.**
Plasma state	Te>>Tg	Te≈Tg	
Electron temperature	1 - 10 eV	~1 eV	
Electron density	Lower electron density ($<10^{19}$ m^{-3})	High electron density ($<10^{21}$-10^{26} m^{-3})	[82,90]
Gas temperature	300 - 1000 K	10000 K	
Discharge type	Corona, Glow, Streamer	Arc plasma	

$1eV \approx 10000$ K

The simplest method for inducing plasma discharge is to use a potential difference between two electrodes with different gases and pressures [81]. When the applied voltage exceeds a particular threshold, an electric current is formed in the dielectric gas volume, which causes a gas breakdown between the electrodes [88]. Even if the majority of the species is neutral, electrons and ions produced by voltage potential difference and accelerated in an applied electric field form a conducting channel. Fast-moving electrons interact with atoms and molecules, producing additional electrons and ions along the route, resulting in a self-sustaining plasma state. In the case of cold plasma, energy is largely transmitted to electrons since they are lighter and receive energy from the applied electric field. It is well accepted that the temperature of electrons in cold plasmas can exceed 10^4 to 10^5 K [65,80,81]. On the other hand, ions and neutral species may endure at a lower temperature, which is often close to room temperature. Due to several orders of magnitude differences in energy between plasma species, cold plasmas initiate and accelerate chemical processes at close to room temperature.

Cold plasmas operating at low pressures have been employed for decades in a number of sectors for applications such as microelectronics, etching, coating, textiles, and so on due to their controllable and chemical-rich chemistry [79,83,91,92]. As a result, atmospheric pressure plasma technologies have been deemed a feasible alternative to low-pressure plasma techniques, owing to a large range of applications that include samples that cannot be vacuumed and a reduction in apparatus sophistication [78,81,93–95]. However, owing to the substantially greater breakdown voltage as well as a set of discharge characteristics that usually sit in the unfavorable section of Paschen's curve, starting and maintaining stable cold atmospheric pressure plasmas is extremely challenging [96–98]. The limits were overcome by using noble gases (argon and helium) as working gases, modifying the electrode design, operating frequency and power supply type, among other things.

Paschen curves make it straightforward to understand the formation of plasma discharge in various gases at low and atmospheric pressures [81]. Paschen curves show how electrode distance (d), pressure (p) and gas type influence breakdown voltage, are shown in Figure 3.2 [98,99]. At fixed electrode spacing, the breakdown voltage rises quickly as pressure rises. Curves indicate that producing cold plasma at atmospheric pressure while maintaining suitable breakdown and non-equilibrium plasma conditions necessitates a small size as well as a short gap in the electrode configuration. Noble gases have lower breakdown potentials and require less energy to form a plasma in ambient conditions; as a result, noble

gases are widely used to generate cold plasma at atmospheric pressure, either alone or in combination with molecular gases.
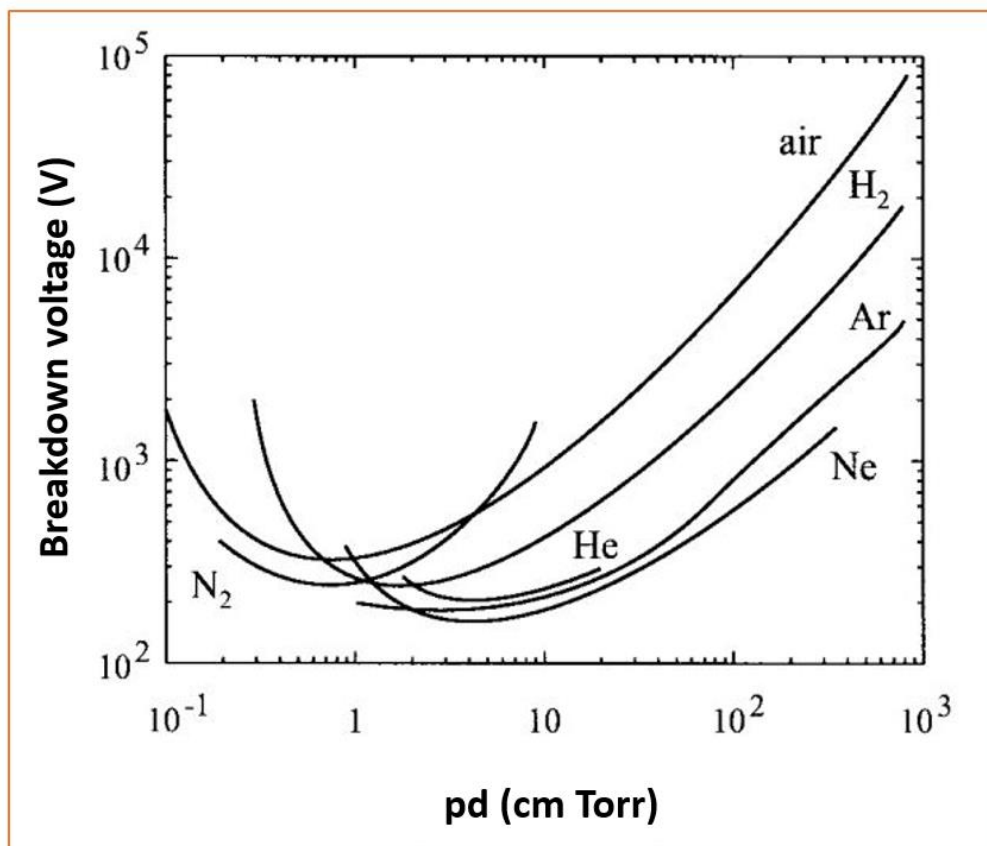
Figure 3.2. Breakdown voltage of the number of gases vs pressure×electrode distance [98–101].

Cold atmospheric plasmas have attracted great scientific interest in water and wastewater treatment due to their ability to produce a significant number of highly reactive species at room temperature. Various cold plasma devices (including corona discharge, streamer discharge, APPJ, gliding arc and others) operating at atmospheric pressure have been used and constructed. Cold atmospheric plasmas offer a wide range of applications in sectors such as material science, agriculture, medical, aerospace and aeronautical engineering, textile technology and so on [77,81,83,91,102,103].

3.2. Gas phase plasma chemistry at atmospheric pressure

Plasma generated in the gas phase at atmospheric pressure creates a complex and rich chemical environment, resulting in the creation of enormous amounts of radicals as well as ions, metastables and UV rays [81,88,94,95,104]. The creation of gas-phase plasma can entail a variety of chemical processes. Gas-phase plasma in contact with liquid and surfaces provides a lot of exciting chemistry due to a variety of chemical processes [95,105]. The chemistry that takes place in plasma is often extremely complicated and includes a wide range of elementary reactions (A and AB are the components), as seen in Figure 3.3 [81,86,106]. Gas composition (argon, helium, nitrogen and air), plasma source type, electrode geometry, power supply and other variables can all have a significant impact on gas-phase chemistry.
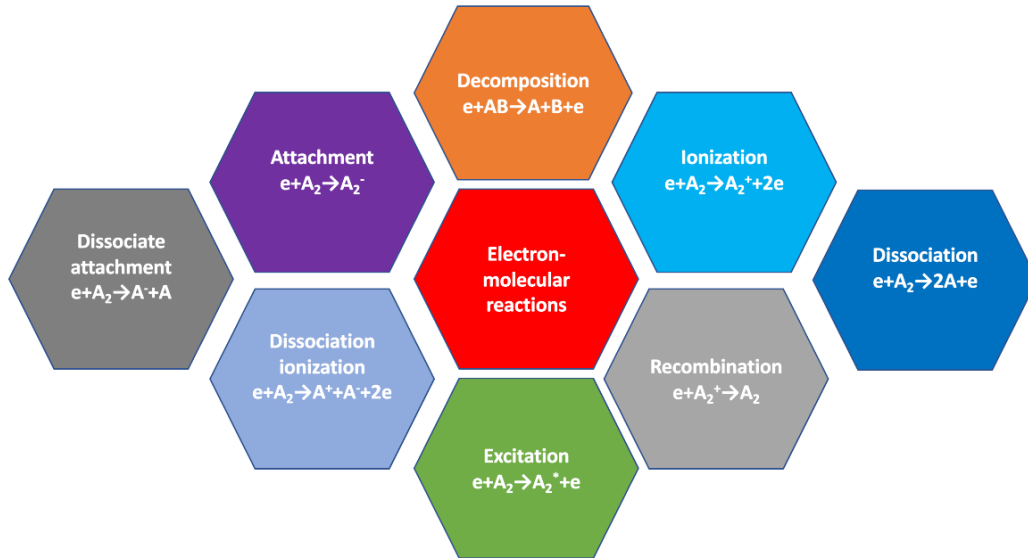
Figure 3.3. Possible chemical reactions that can occur during a gas phase plasma discharge.

The primary sorts of reactions that occur in plasma, for instance, are classified into many reaction steps [81,85,86]. One short of reaction that is frequently produced by inelastic collisions between electrons and heavier species or collisions between heavy species. These common reactions, for example, are shown in Figure 3.4. Ionization occurs when an electron collides with a neutral substance, resulting in the formation of positively charged particles. Electron impact excitation reactions produce electrically excited and metastable species. Electrons can react with molecules and dissociate without emitting ions. When electron impact dissociation produces an ion, the chemical process is known as dissociative ionization. Collisions of excited metastable species with neutrals can also cause them to dissociate and ionize. It is possible for two ions to combine again and produce molecules. All of the processes and phenomena that occur in gas phase plasma can occur across a wide variety of time periods, with a difference in duration of around twelve orders of magnitude, as shown in Figure 3.4 [86,107,108].
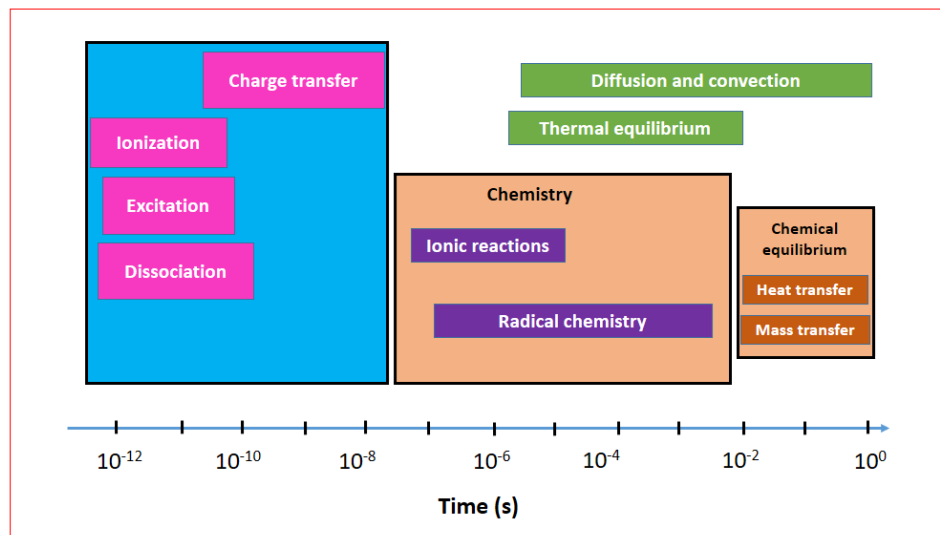
Figure 3.4. The time scale of several reaction processes.

Some of the examples of plasma sources utilized to create discharge in the gas phase are atmospheric pressure plasma jets (APPJs), corona discharges and dielectric barrier discharges (DBD) etc [65,72,73,81,95]. The reactive species produced by diverse plasma sources in the gaseous phase have been investigated for a wide range of applications, including plasma treatment of liquids and different surfaces [81,91,103]. In the case of liquid treatment, for example, the reaction products of gas-phase plasma could interact with the liquid, resulting in complex chemistry, creating different substances in the liquid and playing an essential role in water purification [65,85]. The researchers observed that gaseous plasma is more energy-efficient than liquid phase plasma, owing to the lower voltage required for the breakdown and sustaining of the discharge in the gas phase at atmospheric pressure compared to, say, discharge within the liquid [65,70,71,109,110]. A brief review of the chemistry involved in the interactions between in-liquid and gas-phase plasma is shown in the next section.

Plasma diagnostics are critical for estimating basic plasma properties and characterizing the formation of reactive species and chemical reactions inside the gaseous phase of plasma [81,86,88,111]. Over the last decade, gas-phase characterization of cold atmospheric plasmas has evolved dramatically and a wide variety of diagnostics and techniques for the characterization of cold atmospheric plasmas have been described [86]. The researchers use Stark broadening, Thompson scattering and Rayleigh scattering as methods for estimating plasma density and electron temperature [86,111]. Methods like laser-induced fluorescence or absorption, as well as spectral emission of molecular nitrogen or HO· bands, are widely employed to measure gas temperature [86]. Optical emission spectroscopy, mass spectrometry and laser-induced fluorescence were used to detect reactive components in plasma's gaseous phase [88,112,113].

3.3. Plasma-liquid interaction

In recent years, the application of cold atmospheric plasma for the removal or complete degradation of both dangerous OMPs and pathogenic microorganisms in wastewater has grown and developed [65,72–75,110,114].

Plasma-liquid interaction is a very complex field that includes non-equilibrium processes involving all states of matter and it has the potential to change the way to treat water. A variety of chemically reactive species are produced when plasma interacts with liquid. For example, when plasma interacts with liquid, much reactive oxygen (ROS) and nitrogen species (RNS) are formed, including HO•, O•, HO_2•, H_2O_2, NO•, ONOOH, O_3 and others, which are particularly efficient in removing a wide spectrum of organic contaminants from water [6,65,89,115,116]. Plasma can also generate solvated electrons within a liquid, which can be utilized to eliminate perfluorinated compounds [72]. Plasma in contact with water can be used for a variety of purposes, including water treatment, agriculture and medicine [68,81,85,96].

Several researchers have examined the process of wastewater purification by cold atmospheric plasmas, which may be grouped based on plasma-phase distribution or reactor working principle, primarily into three groups [65,72,85].

- Plasma discharge over the liquid surface.
- Plasma discharge in bubbles
- Direct plasma discharge within the liquid.

Figure 3.5 depicts schematics of common configurations, however, there are numerous electrode designs utilized to generate plasma in specific studies in all three categories.
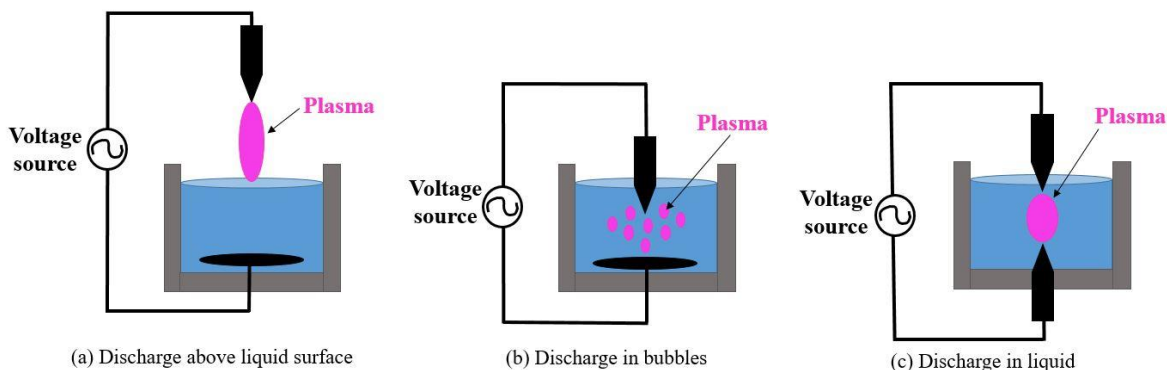
Figure 3.5. Schematic illustration of experimental sets utilized in the research of liquid treatments with cold plasma.

Plasma creation above the liquid surface and in bubbles are the most prevalent forms of plasma sources utilized in wastewater treatment, although direct discharge into the liquid is also not uncommon [65,117]. When a discharge occurs above the liquid surface, plasma species form in the gaseous phase at the liquid surface and are transported within the liquid sample, where they promote OMPs breakdown in water [85,118,119]. In the scenario of liquid bubbles, plasma is produced in the gaseous phase inside the bubble and reactive species emerge from different plasma locations and reach inside the sample. As a consequence, the mechanisms underlying these two techniques are remarkably similar. Plasma species creation over liquid has been examined and it is greatly influenced by plasma source, electrode geometries, operating gas, reduced electric field and so on.

When cold plasma is placed above a liquid surface in the presence of air, the interacting environment is separated into three components, as graphically represented in Figure 3.6: gaseous plasma, plasma-liquid interaction and bulk liquid phase [65,85,109,114,118,119]. Various RONS, for example, can be created directly in the gas phase region and at interfaces as a result of interactions between plasma-driven energetic species and feeding gas (or ambient gas) molecules. These species are relatively short-lived and can be transformed to secondary or long-lived species in an ambient environment. The chemistry of RONS (reactive oxygen and nitrogen species) production varies with the surrounding environment, plasma source type, and other experimental conditions.
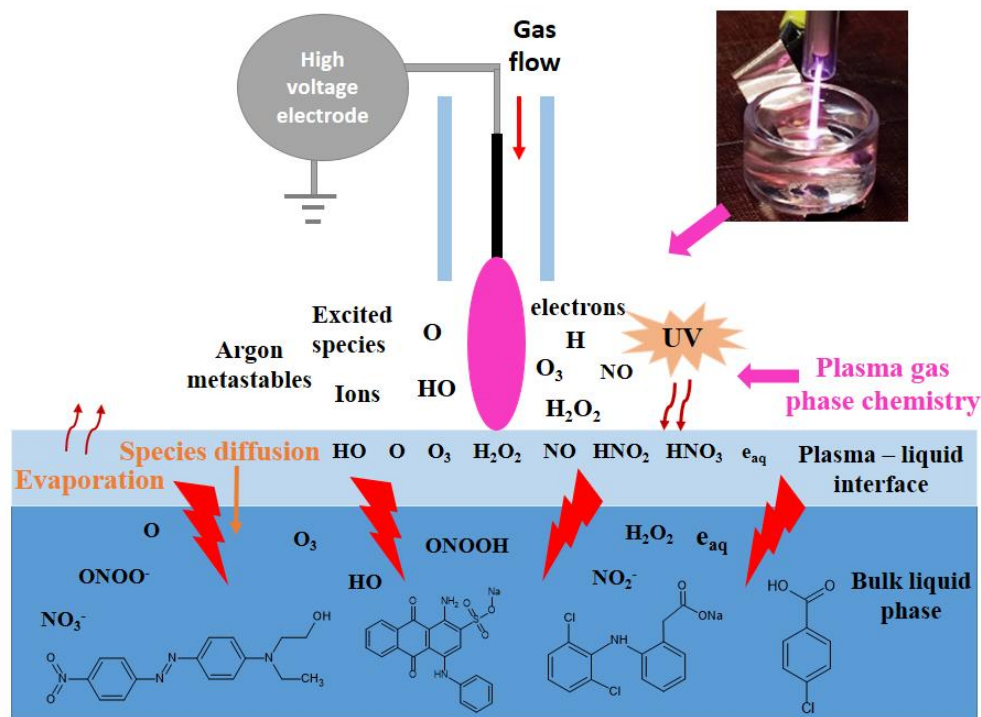
Figure 3.6. Schematic illustration of plasma-produced short and long-lived species in various phases [65].

Many species produced in the gas phase and interface can transfer to the liquid and dissolve in the bulk solution, producing additional RONS in the process. For example, RONS generated in the gas phase can diffuse into the water via Henry's law ($p = k_h.c$), where p signifies the partial pressure above the liquid, c is the concentration within the liquid and k_h is Henry's law constant [116]. The removal of OMPs from the water will be dependent on the presence of a plasma-rich chemical environment throughout all phases [65,120].

The previous researchers also looked at the quantification of diffused reactive species in liquids [68,110]. In the case of HO• radicals, for example, the lifespan and diffusion constant in the gaseous phase are usually in the range of 10^{-5} s and 10^{-10} m^2/s, respectively, yet they can have diffusion lengths of many tens of μm [110,121]. Dissolved HO• has a lifespan of about 10^{-6} to10^{-7} s and penetration lengths of about 10^{-5} to 10^{-6} m [110]. Several scholars have investigated the dissolved HO• in water utilizing various chemical detectors such as terephthalic acid, indigo carmine solution and so obviously the HO• concentration changed with different types of plasma sources and other variables [104]. Other distributed reactive species have been discovered using various approaches, such as scavengers and other probes.

Apart from plasma discharge above the liquid's surface, plasma could also be created within the liquid without the usage of an additional gas source. Many scientists have reported plasma discharges inside bubbles as a novel technique to remove various OMPs while also delivering green chemistry with low energy consumption when compared to direct discharge inside liquid [65,71,72,122]. The formation of a discharge within bubbles may enable the development of a large volume of plasma within liquids with a low breakdown voltage. Bubble discharge facilitates the creation and transport of aqueous chemical agents for particular applications due to its huge interfacial surfaces and lengthy residence durations. External gas bubbling can also help to increase the bulk phase species mass transfer velocity. The

reactions at the bubble-liquid interface are the most challenging aspect of understanding the plasma discharge inside the bubble.

The most commonly utilized plasma sources for the formation of discharge within bubbles are diverse corona discharge with varied geometries and DBD sources [123]. There have been a few studies done on the situation of direct discharge in liquid [124,125]. For example, corona discharge using electrode designs was primarily employed to initiate a discharge directly within liquid without the usage of feed gases. The procedure of creating plasma discharge directly within a liquid is difficult and energy-intensive.

There are various plasma sources that have been studied for treating wastewater, including corona, APPJ, DBD, gliding arcs, as well as others. They work with a variety of power source signals (like pulsed DC and AC at a wide frequency range – Hz to kHz, pulsed voltage signals and so on) [65,109,118]. Numerous electrode shapes were investigated, including needle-to-plate, pin-to-ring, pin-to-pin and others. A wide range of operating gases and associated compositions (for example, air, oxygen, argon and so on) have been thoroughly researched for the degradation of dissolved OMPs.

Some basic configurations of different plasma sources operating at atmospheric pressure are illustrated in Figure 3.7 [86,88,109]. Each form of discharge has its own set of parameters, such as electron temperature, electron density and gas temperature, among others. DBD can be made using two powered metal electrodes and one dielectrically covered electrode (glass, quartz, etc.) [77]. The dielectric insulation prevents the transition to an arc discharge. Corona is essentially a cocktail of highly energized particles such as electrons and ions that are driven by an electric field. Corona is a non-uniform discharge that can take numerous forms according to the orientation of the field and the morphological layout of the electrodes [74]. This sort of discharge occurs in an asymmetric electrode pair arrangement and necessitates a short spacing between electrodes, requiring pointed electrodes or point plane gaps in particular [65]. Sharp electrodes provide an electric field with high gradients, allowing gas breakdown to begin fast and the production of a powerful plasma discharge.
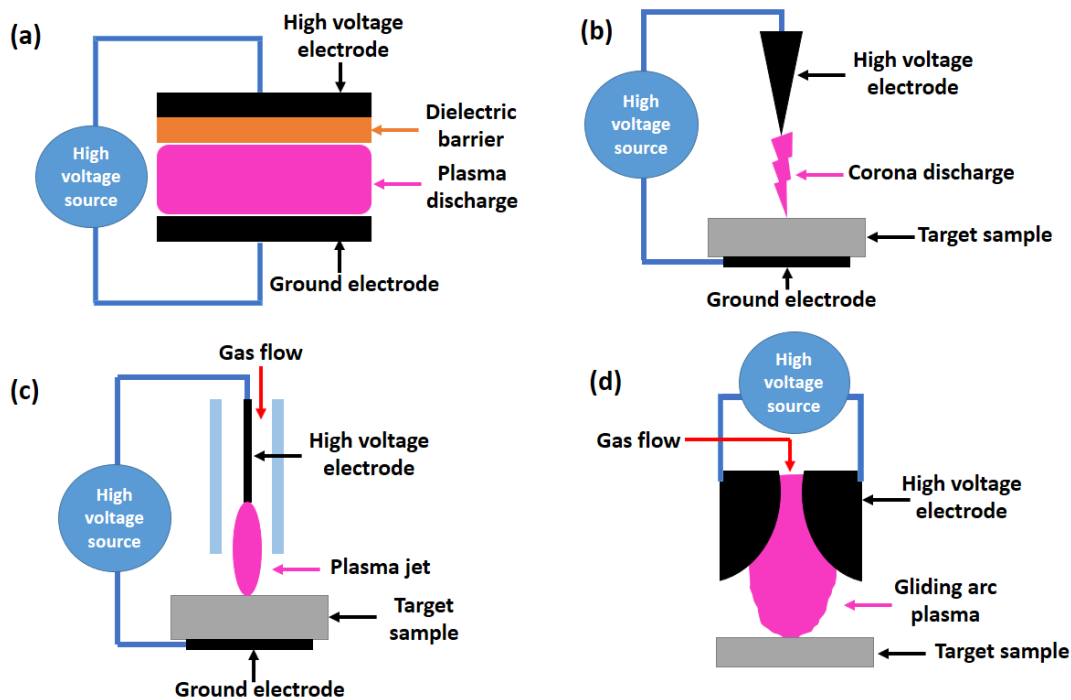
Figure 3.7. The most basic arrangement for various plasma discharges operated at atmospheric pressure (a) DBD, (b) corona discharge, (c) APPJ and (d) gliding arc.

Another kind of plasma discharge that can be produced under ambient conditions is APPJ. APPJ is gaining popularity due to its outstanding ability to generate high-velocity reactive species [88,112]. APPJ is operated by supplying a gas feed (for example, variable flow rates of argon, helium, and oxygen) to the limited reaction volume with an electrode (e.g. glass tube). In a variety of arrangements, coaxial cylindrical tubes with powered electrodes on either side and a powered central electrode inside the tube were used [68,126]. A rapidly flowing reactive species in a plasma jet reacts with its surroundings, resulting in a rich chemical environment. A gliding arc is another type of cold plasma that occurs under normal atmospheric conditions. Gliding arcs are non-stationary arc discharges induced by rapid gas movement between two divergent electrodes [127]. However, gas flow rates have an important effect on extending the arc. Gliding arc discharges allow the arc to expand until the input voltage is insufficient to sustain the discharge or form an arc at close electrode spacing.

3.4. Cold atmospheric plasma for wastewater treatment

The cold atmospheric plasma approach offers a strong oxidation capability, which is particularly useful for OMPs that are resistant to biodegradation [71,72,77,128]. The use of plasmas in water purification has grown in popularity due to their ease of use, effectiveness in removing hazardous OMPs in diverse water matrices and environmental friendliness.

Cold atmospheric plasma treatment of OMPs in water extensively began over ten to fifteen years ago and has since been tested on a variety of chemicals of different types [65,71]. There were a few studies where researchers reviewed already achieved data depending on the removal of a variety OMPs mixed with water (e.g. dyes, phenol, pharmaceuticals, pesticides, personal care products, perfluorinated compounds, etc) by plasma technique. The review by Magureanu et al. [119] discusses a summary of available information on the treatment of several pharmaceuticals by plasma from 1996 to 2013. In this

paper, the previous researchers evaluate alternative reactor setups and experimental variables and correlate their relevance to plasma system efficiency. It was discovered that plasma formation is mostly in the gas state above a thin liquid layer using DBD or corona sources for pharmaceutical elimination. Topolovec et al. [72] recently conducted a comprehensive review on the role of chemistry in the breakdown of many OMPs such as pharmaceuticals, perfluorinated chemicals and pesticides using cold atmospheric plasma sources. Hijosa-Valsero et al. [118] analyzed numerous plasma reactors and operational parameters utilized for the breakdown of several OMPs, including volatile hydrocarbons, phenols, dyes, pharmaceuticals and surfactants. Based on their study, plasma creation at the gas-liquid boundary for the destruction of OMPs was much more effective in terms of energy demand than plasma production inside the liquid domain. Malik [109] conducted one of the greatest reviews in 2010, demonstrating the energy yield necessary for the elimination of various hazardous dyes by various plasma sources. The production of pulsed corona discharge in small droplets and across a thin water layer was discovered to be the most successful method among all those investigated. The review carried out by Malik, 2010 gave a wealth of information for developing a highly efficient plasma device for water decontamination. The utilization of cold plasma reactors for the removal of phenolic substances was examined by Jiang et al. [129] and Locke [73] in 2006 and 2014, respectively. Investigators demonstrated that cold plasma may successfully destroy a variety of phenolic compounds at low concentrations. Another investigation on the combined influence of heterogeneous catalysts and cold plasmas for the removal and degradation of chemical pollutants from water is summarized in Russo et al. [130] review. They concluded that catalysts provided an important contribution to improving the productivity of plasma devices. A recent study (2021) from Barjasteh et al. [131] gives an outline of cold plasma for water purification, particularly an emphasis on bacterial deactivation and OMPs degradation.

A thorough examination was carried out utilizing published papers, primarily during the last ten to fifteen years. Each of the data obtained from the assessment was used to gain a thorough understanding of the efficient plasma source under various experimental conditions for the removal of three key OMPs (for example pesticides, pharmaceuticals and dyes). The following Tables 3.2, 3.3 and 3.4 provide an exhaustive list of plasma types used for dye, pharmaceutical and pesticide elimination, as well as working parameters and their impact on destruction. A range of various reactors categorized according to their discharge type (DBD, Corona, APPJ and gliding arc) are described. The quantity of degradation of different OMPs by plasma sources and with varied experimental conditions can be easily understood from the Tables. The same molecule was treated with several plasma sources, resulting in varied breakdown patterns. Furthermore, OMPs concentrations varying from a few milligrams to hundreds of milligrams, as well as different initial treatment volumes, have been treated and described.

Table 3.2. An overview of relevant publications on several types of plasma devices utilized for organic dye degradation.

Target compounds	Characteristics of plasma devices				T (min)	C_o (mg/L)	V_o (ml)	η (%)	Ref.
	Plasma source	Mode of discharge	Signal type	Operating conditions					
Methylene Blue	Corona	Discharge in bubbles	Pulsed	Voltage: 17 kV, pulse repetition rate: 72 Hz, gas: O_2 - 800 sccm, power: 10 W	20	150	100	90	[132]
Acid Orange 7	Corona	Discharge in bubbles	Pulsed	Voltage: 27 kV, repetitive frequency: 70 Hz, gas: air - 1.4 m^3/h,	45	20	600	83	[133]
	Corona + TiO_2							98	
Reactive Brilliant Blue	Corona	Discharge above liquid surface	DC	Voltage: 14 kV, gas: air - 2 L/min, discharge gap/electrode gap: 0.5	60	100	1000	~ 91	[134]
Methylene Blue	Corona	Discharge in bubbles	Pulsed/ DC	Voltage: 4 kV, gas: O_2 - 10 ml/min, power: 4 W	120	13.25	20	~ 100	[135]
Acid Orange 142	Corona	Discharge above liquid surface	DC	Voltage: 12.5 kV, gas: atmosphere air	90	20	100	~ 90	[136]
Rhodamie B, Methyl Orange, Chicago Sky Blue	Corona	Discharge in liquid	Pulsed	Voltage: 20 kV, frequency: 25 Hz	60	10 (each)	300	~ 77, 70, 91	[124]
Crystal Violet	DBD	Post-discharge	Pulsed	Voltage: 12 kV, frequency: 20 kHz, pulse width: ~50 ns, gas: O_2 - 700 ml/min, power: 5 W	1	4.08	250	100	[137]
Indigo Carmine	DBD	Discharge in bubbles	Pulsed	Voltage: 4kV, pulse frequency: 5 kHz, pulsed width: 750 ns, gas: mixture of Ar & O_2 - 250 sccm	3.2	50	200	99	[123]

Dye	Discharge	Configuration	Power	Parameters						Ref
Methyl Red	DBD	Discharge above liquid surface & post discharge	Pulsed	Voltage: 11 kV, pulse repetition rate: 76 Hz, gas: O_2 - 600 ml/min, power: 1 W	10	50	200	93		[138]
Methylene Blue	DBD	Discharge in bubbles	AC	Voltage: 6 - 8 kV, current: 30–50 mA, frequency: 9.7 kHz, gas: air - 1.5 L/min, power: 8.6 W	30	100	100	~98		[89]
Methylene Blue	Point-to-plate	Discharge above liquid surface and in bubbles	AC	Voltage: 2.57 kV, current: 27.7 mA, frequency: 60 Hz, Gas: N_2 - 0.1 L/min, power: 59.2 W	60	20	100	~100		[139]
Acid Red 88	DBD	Post discharge	AC	Voltage: 20 kV, gas: air - 7 L/min, power: 60 W	4, 5	25, 50	500	92, 91		[140]
				Voltage: 20 kV, gas: O_2 - 7 L/min, power: 60 W	1	25		95		
Methylene Blue, Methyl Orange, Congo Red	Indirect-APPJ	Discharge above liquid surface	AC	Voltage 0.7 kV, current 3 mA, frequency: 16 kHz, gas: Ar - 3 slm, power: 0.2 W	20	200		71, 81, 76		[141]
					30			87, 92, 84		
Methylene Blue, Methyl Orange, Congo Red	Direct-APPJ	Discharge above liquid surface	AC	Voltage: 1.2 kV: current: 5 mA, frequency: 16 kHz, gas: Ar - 3 slm, power: 0.4 W	20	200		95, 97, 86		
					30			97, 99, 90		
Orange I, Crystal Violet, Eriochrome Black T	Gliding arc	Discharge above liquid surface		Voltage: 10 kV, gas: air - 900 L/h	30, 60, 60	52.54, 53.03, 83.23		95, 89, 88.4		[127]
Acid Blue 25	Glow discharge	Discharge above	DC	Voltage: 15 kV, current: 0	60	20	500	78		[142]

Target compounds	Plasma sources	Mode of discharge	Signal type	Operating conditions	T (min)	C_o (mg/L)	V_o (ml)	η (%)	Ref.
		liquid surface		- 100 mA, gas: Ar - 1 slm					
	Glow discharge + TiO_2				60	20		90	
Methyl Orange	Gas discharge circulatory airtight configuran-ion	Discharge above liquid surface & post discharge	Pulsed	Voltage: 46 kV, pulses: 80 per second, gas: O_2 - 0.08 m^3/h, power: 5.67 W	20	60	400	92	[143]
Methyl Orange	Multi-needle configurat-ion	Discharge above liquid surface	Pulsed	Voltage: 22 kV, frequency: 50 Hz, gas: O_2	15	10	450	~90	[144]

T – Treatment time
C_o – Initial concentration
V_o – Volume
Ŋ – Removal efficiency

Table 3.3. Evaluation of chosen pharmaceutical degradation data by various plasma systems.

Target compounds	Characteristics of plasma devices				T (min)	C_o (mg/L)	V_o (ml)	η (%)	Ref.
	Plasma sources	Mode of discharge	Signal type	Operating conditions					
Tetracycline	Corona	Discharge in bubbles	AC	Gas: air - 0.06 m^3/h, power: 36 W	24	50	250	61.9	[145]
	Corona + TiO_2							85.1	
Sulfadiazine	Corona	Gas–liquid interface discharge	Pulsed	Gas: atmospheric air, power: 100 W	30	10	100	~100	[146]
Diclofenac	Corona	Discharge above liquid surface	Pulsed	Voltage: 20 kV, pulse frequency: 22 Hz, gas: O_2 - 1 L/min, power: ~24 W	15	50	55	100	[74]
Carbamazepine, Clofibric Acid, Iopromide	Corona	Discharge above liquid surface	AC	Voltage: 25 - 35 kV, frequency: 30 kHz, power: 500 W, gas: air	30	23.6, 21.5, 79.1	200	98, 100, 99	[147]
Diclofenac, Ethinylestradiol, Carbamazepine, Ibuprofen,	Corona	Discharge in liquid	Pulsed	Voltage: 80 kV, repetition rate: 20 Hz,	~60	0.5	300	45 - 99	[148]

Compound	Type	Configuration	Mode	Parameters					Ref
Trimethoprim, Diazepam, Diatrizoate				pulses duration 270 - 300 ns					
Diclofenac, Carbamazepine and Ciprofloxacin	Corona	Discharge above liquid surface	Pulsed	Voltage: 25 kV, frequency: 30 Hz, gas: ambient air, power: 101.5 W	4 - 8	1	50	~100	[115]
Tetracycline	DBD	Gas–liquid interface discharge	Pulsed	Voltage: 22 kV, frequency: 100 Hz, gas: air - 3.5 L/min	30	50	500	92.3	[149]
Paracetamol	DBD	Discharge above liquid surface	AC	Voltage: 13.6 kV, frequency: 500 Hz, gas: air - 10 sccm, power: 1 W	60	25	40	81	[150]
Nitrobenzene	DBD	Post discharge	AC	Voltage: 1.8 kV, frequency 50 Hz, gas: O_2 - 3 L/min, power: 0.53 W	60	20		75	[151]
Pentoxifylline	DBD	Discharge above water film & post discharge	Pulsed	Voltage: 12 kV, pulse frequency: 60 - 120 Hz, current: 50 A, gas: O_2- 600 sccm, power: 0.7 - 1.4 W	60	100	200	92	[152]
Amoxicillin, Oxacillin, Ampicillin	DBD	Discharge above water film & post discharge	Pulsed	Voltage: 17 kV, pulse repetition: 50 Hz, current 110 A, gas: O_2 - 600 sccm, power: ~2 W	10, 30, 20	100	200	>90	[153]

24

Compound	Type	Configuration	Mode	Parameters					Ref
Ampicillin	DBD	Discharge above liquid surface	Pulsed	Voltage: 11.2 kV, frequency: 690 Hz, pulse width: 1 - 10 ns, gas: atmospheric air	3	6988	1	100	[154]
Enalapril	DBD	Discharge above water film & post discharge	Pulsed	Voltage: 18 kV, pulse frequency: 50 Hz, current: 100 A, gas: O_2 - 600 sccm, power: 2 W	20	50	300	90	[155]
17β-Estradiol	DBD	Discharge above liquid surface	Pulsed	Voltage: 12 kV, pulse width: 22–36 μs, frequency: 14–22 kHz, current: 88 mA, gas: atmospheric air	30	0.1	500	100	[156]
Cyanide	DBD	Discharge over thin water film	Pulsed	Voltage: 12 kV, , repetition frequency: 94 kHz, power: 24 W, gas: He - 500 sccm	3	1	175	99	[157]
Telmisartan	APPJ	Discharge above liquid surface	AC	Voltage: 33 kV, frequency: 30 kHz, gas: Ar - 9000 sccm	20			63	[158]
Verapamil Hydrochloride	Gliding arc	Discharge above liquid surface		Power: 750 W, frequency: 50 Hz, gas: air - 0.86 m^3/h	80	2.45 - 24.45	25	37 - 97	[159]
Oxytetracycline Hydrochloride, Doxycycline Hyclate	Pin-to-water electrode	Discharge above liquid surface	AC	Voltage: 3 kV, current: 3 mA, frequency: 5 kHz, gas: ambient air	90	50	50	< 100	[160]

Water-electrode discharge	Discharge in bubbles	AC	Voltage: 3 kV, current: 3 mA, frequency: 5 kHz, gas: air - 1 L/min	~ 20	50	50	~100	

Table 3.4. An overview of the plasma systems utilized to remove pesticides in the literature.

Target compounds	Characteristics of plasma devices				T (min)	C$_o$ (mg/L)	V$_o$ (ml)	η (%)	Ref.
	Plasma source	Mode of discharge	Signal type	Operating conditions					
2,4-dichloropheno-xyacetic acid	Corona discharge + Ozonation	Discharge above liquid surface + Post discharge	DC/Pulsed	Voltage: 18 kV, Pulse repetition rate: 25 Hz, plasma gas: O$_2$ - 0.3 L/min, power: 11 W	30	25	330	~100	[161]
Atrazine	Corona + Fenton	Discharge in liquid	DC/Pulsed	Voltage: 45 kV, pulse frequency: 60 Hz, pulse width: 1 μS	10	5	400	100	[125]
Atrazine	DBD	Discharge above liquid surface	DC/Pulsed	Voltage: 23 kV, frequency: 300 Hz, pulse duration: 400 ns, gas - air 0.5 SLM, power: 1.7 W	45	0.03	100	61	[162]
	DBD + Nanofiber membrane							85	
Dichlorvos, Malathion, Endosulfan	DBD	Discharge above liquid surface	DC/Pulsed	Voltage: 80 kV, frequency: 50 Hz, gas: atmospheric air	8	2	20	78.98, 69.62, 57.71	[76]
Atrazine	DBD	Discharge above liquid surface	AC	Voltage: 20 kV, frequency: 100 kHz, gas: Helium - 5 L/min,	5	5	4	93	[163]

				power: 30 W					
Chlorfenvinphoos						5		94	
Dichlorvos	DBD	Discharge above liquid surface	AC	Voltage: 0 - 250 V, frequency: 5 - 35 kHz, current: 0 - 1.2 A, gas: air, power: 85 W	6	60	40	~100	[164]
Dimethoate					6	10	40	~100	
Nitenpyram	DBD	Discharge above liquid surface	AC	Voltage: 80 V, current: 1 - 2.5 A, power: 200 W	180	100		~83	[165]
Acetamiprid	DBD	Discharge above liquid surface	AC	Voltage: 250 V, current: 0 - 4 A, power: 170 W	200	50		~83	[166]
Alachlor	DBD	Discharge in bubbles	AC	Voltage: 8 kV, frequency: 50 kHz, gas: O_2 - 1 L/min, power: 40 W	30	1	500	~100	[122]
	DBD + Ozonation	Discharge in bubbles and post-discharge			15			~100	

As seen in the above tables, numerous plasma sources, reactor design, and operating parameters in water treatment have been investigated. Plasma sources such as Corona discharge, APPJs, DBDs, and others have been briefly mentioned in earlier studies. Corona discharges are produced with various electrode geometries: pin-to-pin, pin-to-plate, or multi-pin electrode, and are driven by high voltage pulses [65,70,129]. These electrode designs were utilized to induce corona discharge in either gas or liquid phases. To generate corona discharge in the liquid phase, a powered electrode was typically put into the liquid, and discharge was produced within the bubbles or directly in the liquid.

The pin electrode design is widely used because it produces an intense electric field at the tip of the electrode [73,109]. In the case of a single-pin electrode setup, plasma confines in a limited volume. In order to overcome this, previous researchers developed multi-pin electrode plasma systems that can treat wide surfaces of polluted water.

The APPJ is particularly effective at transporting highly concentrated reactive species from the gaseous to the liquid phases via gas flow in the jet. It is very useful for the treatment of pollutants that stay mostly

at the liquid surface (e.g. surfactants). The geometry of the APPJs can also have an impact on the plasma chemistry and pollution treatment. For example, in the case of a pin-type APPJ, less applied power is required to maintain the discharge than for a DBD-type APPJ (where the electrode is placed around the glass tube). It was found that pulsed corona and DBD above the thin water film are the most effective in terms of better elimination rates, owing to their increased surface area to volume ratio [65,109,146,148,167]. The larger the plasma-solution contact area, the longer the residence period and the stronger the interaction of reactive species with contaminants [168]. Researchers also developed pulsed corona discharge with a wetted-wall reactor and coaxial design to improve the plasma liquid contact surface [148]. It was also revealed that plasma reactors with continuously mixing liquids produced impressive outcomes [161].

In the majority of cases published in the literature, treatment was carried out either with plasma in interaction with water or in bubbles. In such instances, plasma-generated short and long-lived reactive species react with the contaminated water. However, there are cases where only long-lived species generated in plasma are used and exposed to polluted water directly. Researchers, for example, used the post-discharge setup (sometimes called "plasma-ozonation"), which was successfully investigated for dye removal [137]. This type of arrangement improves mass transfer across the gas and liquid phases.

In terms of reactor design, the Researcher asserted that continuous circulation flow, thin-film, and multi-electrode configurations can provide significant interactions between reactive species and liquid, making them suitable for large-scale applications.

Overall, when we look at all of the reactor configurations, we can see that other researchers have also identified multi-electrode type plasma sources where the plasma interacts with a broad surface of dirty water. The plasma generated at the flowing or recalculated contaminated water solutions type arrangement has also gained a lot of attention. Overall, these plasma sources and reactor configurations offer a high scalability potential.

Several experimental operating parameters, including applied voltage and power, feed gas, water matrix, catalysts and pH, were tested for their impact on degradation [65,72]. The contaminants treated in the literature have substantially higher concentrations than those reported in environmental or wastewater samples. Higher concentrations minimize complications in the analysis of degradation intermediates. Researchers have noted that the initial concentration of the OMPs has a significant impact on the deterioration, as described in numerous papers [68,143]. In general, it was found that decrease in elimination and an increase in OMPs concentration. On the one hand, an increase in OMPs concentration is expected to enhance the oxidation speed till the creation of active species reaches the limiting stage in the mechanism [65,70]. For example, reactive species produced in plasma progressively break down the target chemical, resulting in the creation of many intermediates. The intermediate products may quench the fresh plasma-generated reactive species, resulting in a decrease in the rate of pollutant degradation.

The water matrix also played a significant role in the degradation of OMPs [156]. For example, investigators reported that the destruction of pollutants is better in pure water than in tap water and other water samples. The reason for this is that impurities in tap or actual water samples might reduce the concentration of available reactive chemical species in the solution. However, the solution's conductivity was also considered [124]. If the conductivity of the treated solution exceeds the optimal value, fewer reactive species can be formed. For instance, it has been noted that increased conductivity led to the development of a weaker electric field and the generation of fewer oxidizing substances in the solution, both of which had a detrimental effect on degradation [156].

Input voltage/power provided in discharge is critical in pollutant degradation [76,136,140]. For example, increasing the input power increases the percentage of removal. The quantity of extremely reactive chemical species and the intensity of UV radiation improve with increasing power. Higher power could raise the electric field, resulting in more high-energy electrons colliding with gas molecules, increasing the formation of reactive species. The power is adjustable by altering both the frequency and the magnitude of the applied voltage.

The plasma treatment was performed in a variety of gas environments, as indicated in Tables 3.2–3.4, and feed gas played an essential role in the degradation of OMPs by influencing plasma chemistry. Molecular gases, such as oxygen, nitrogen, and air, are commonly incorporated. Noble gases and their combinations with molecular gases have also been investigated in various OMPs treatments. The Researcher discovered that using pure oxygen as a feed gas (as compared to nitrogen or air) resulted in the development of a rich short and long-lived ROS environment, which is highly efficient in water purification. As indicated in the Paschen curve (Figure 3.2), one of the challenges with molecular gases is the need for high voltage for a breakdown under ambient circumstances. These issues can be resolved by adding noble gases (argon and helium) to the system. The drawback of employing noble gases is their high cost. According to previous researchers, employing argon (or mixing with molecular gases) and recirculating within the system, which is less expensive than helium, is still conceivable for use in the treatment.

In many circumstances, pH affects the pollutant degradation rate, which is of course related to molecule structure [115,124]. The greater reactivity of ROS at lower solution pH appears to accelerate the breakdown of OMPs almost proportionately. Many investigations have found frequently that plasma treatment solutions are promptly acidified due to the generation of RNS (nitric acid and nitrous acid) in the liquid. Lower pH, on the other hand, is especially advantageous for the decomposition of most pollutants.

Several researchers combined cold atmospheric plasma with heterogeneous catalysis to accelerate pollutant removal [142,169]. It was investigated as additional novel way to improve the degradation rate. TiO_2 nanoparticles were the most often utilized catalyst. TiO_2 and plasma functioned better together than plasma alone. The addition of TiO_2 results in the formation of extra ROS as a result of photocatalytic reactions on the surface triggered by UV radiation generated by the plasma. More catalysts have been investigated, including graphene oxide, silver phosphate and others. However, there are various constraints to exploring catalysts in plasma reactors, such as separating the catalyst from water for regulatory concerns.

It has been recognized that comparing the various kinds of plasma sources is not simple. There are numerous aspects of the plasma that can influence degradation and they are not limited to the type of plasma source employed. Corona discharges, for example, have the benefit of not needing additional working gas but require greater input energy for gas breakdown, whereas APPJs and DBD plasma systems generally work with gases. As previously indicated, that is an obstacle that can be overcome. Similar to APPJs, treatment with recirculation employing a set of settings and working gas (e.g. argon) can accomplish efficiency while keeping the overall price low. Furthermore, the construction of APPJ is fairly straightforward, and discharge can occur at lower applied voltages when noble gas is used. APPJ can provide a plasma-rich chemical environment that facilitates OMPs elimination, and it is well known that due to its design the APPJ produces significant convection of reactive species into liquids.

The major purpose of this thesis was to build, describe, and use a cold atmospheric plasma generator to degrade multiple OMPs in water. The previous study has not thoroughly investigated the APPJ type of

plasma supply for organic pollution remediation. There have been a few investigations, but for the most part, a single electrode-APPJ was used to treat smaller amounts of water. In this work, a three-pin APPJ was built, electrically and optically examined, and demonstrated for water purification. A method was also tested in which contaminants were treated with a plasma recirculation system, proving the scalability of the plasma-based water treatment process.

CHAPTER 4

4.   Materials and methods

This chapter contains thorough information about the chemicals, instruments and plasma reactor setup used in the experiments. The techniques for preparing samples are addressed first, followed by an explanation of the reactor setup and experimental protocols.

4.1. Target compounds

Four different chemical compounds were chosen and treated with plasma. These include two organic dyes (Acid Blue 25 and Disperse Red 1), one pharmaceutical (Diclofenac) and one industrial chemical (4-Chlorobenzoic). Each compound has unique properties, such as various functional groups, solubility and reactivity with oxidizing agents. They have previously been identified in the environment.
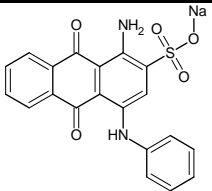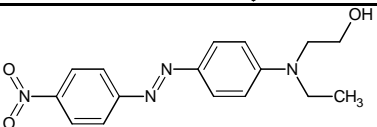
4.1.1.   Organic dyes (Acid Blue 25 and Disperse Red 1)

AB25 is an anthraquinonic dye-containing three merged aromatic rings [142]. Anthraquinonic dyes are the second most widely known class of industrial dyes, primarily used for dyeing wool, polyamide and leather [36,68]. AB25 is frequently used as a model chemical for removing anthraquinonic dyes from water solutions.

The second dye chosen was DR1, which is the first red dye in the disperse class and belongs to the azo (-N=N-) group. DR1 is widely used in the textile industry to color polyester materials [170]. Anthraquinone and azo dyes together make up higher than half of all dyes used in the textile industry worldwide [68]. These dyes are resistant to degradation in biological WWTPs due to their chemically complicated structure.

Sigma Aldrich provided AB25 (purity: 45 %; CAS: 6408-78-2) and DR1 (purity: 95 %, CAS number: 2872-52-8) for this study. Table 4.1 shows the differences between AB25 and DR1. By dissolving a suitable amount of analytical grade of AB25 in distilled water, a dye-containing solution with a greater concentration was created. To make a stock solution, DR1 was dissolved in ethanol and the solution (DR1 + ethanol) was blended with distilled water. Before the beginning of the plasma treatment in both cases, a stock was diluted with distilled water to produce a lower concentration.

Table 4.1. Shows the characteristics of organic dyes.

	Chemical structure	Chemical formula	M.W (g/mol)	Types
AB25		$C_{20}H_{13}N_2NaO_5S$	416.38	Anthraquinone
DR1		$C_{16}H_{18}N_4O_3$	314.34	Azo
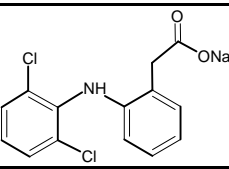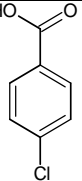
4.1.2. Pharmaceutical and industrial chemical (Diclofenac Sodium and 4-Chlorobenzoic Acid)

DCF is a kind of nonsteroidal anti-inflammatory medication (NSAID) that is used to relieve mild to severe pain [42,74]. It is predicted that a large amount of DCF (>1000 tons) is used globally each year. DCF is stable in the aquatic environment, which is why it is commonly found in freshwater habitats [171]. DCF can be hazardous to aquatic life, vegetation and people's health. The consumption of DCF resulted in an extraordinary reduction in vulture populations in India. To avoid additional vulture population declines, various governments (including India, Nepal and Bangladesh) have banned the use of DCF [172]. Based on the survey, WWTPs remove approximately 30-70 % of DCF [171].

The pCBA was selected as a target chemical for the treatment. The pCBA is an industrial chemical that is utilized in the synthesis of a wide range of chemical compounds. It is also used commercially in the pharmaceutical industry [173]. Due to its strong reactivity with HO·, it was also utilized as a probe compound in several water treatment processes to assess HO· content [174].

Sigma Aldrich supplied DCF (purity 98%, CAS number: 15307-79-6) and pCBA (purity 98%, CAS number: 74-11-3) A stock solution of each component was made by dissolving it in distilled water. Distilled water was added and diluted to obtain a lower-concentration solution. Table 4.2 lists the features of DCF and pCBA.

Table 4.2. Pharmaceutical and industrial chemical characteristics.

	Chemical structure	Chemical formula	M.W (g/mol)
Diclofenac sodium		$C_{14}H_{10}Cl_2NNaO_2$	318.13
Para-Chlorobenzoic acid		$C_7H_5ClO_2$	156.57

4.2. Reactor configuration

The treatment of OMPs was carried out with the help of two cold atmospheric plasma sources. The following sections provide a comprehensive overview of the plasma reactors.

4.2.1. Atmospheric pressure plasma jet with pin-electrode geometry

Figure 4.1 depicts a schematic representation of the experimental setup. The pin-APPJ is constructed using glass and ceramic tubes as well as a stainless steel electrode (powered electrode). The powered electrode is a 1 mm diameter stainless steel wire with a sharpened edge inserted axially inside a ceramic tube. The glass tube has an outer diameter of 6 mm and an inside diameter of 4 mm. The inner powered electrode is linked to the high voltage (HV) source. A copper tape was put on the bottom side of the sample vessel and a 1 kΩ resistor was used to ground it. The powered electrode's tip is positioned 10 mm away from the liquid sample's surface. Argon (5.0 purity) was utilized as the input gas, with a flow rate of 1 slm (standard liters per minute) regulated by a mass flow monitor (OMEGA, FMA5800/5500). Argon was introduced into a glass tube. In this setup, 5 mL of solution was treated by pin-APPJ for various treatment times.
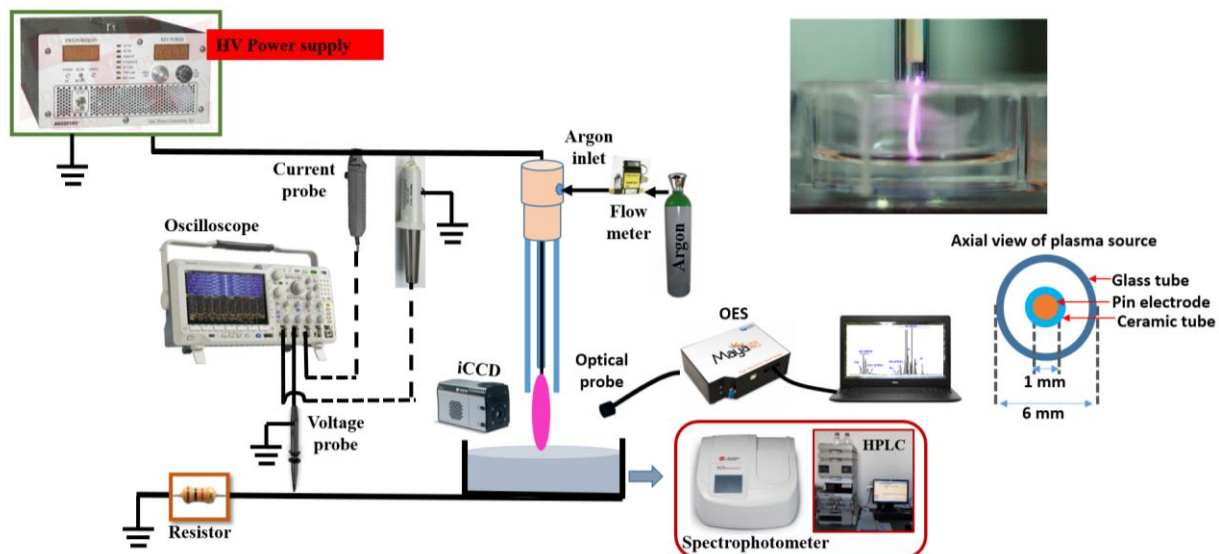
Figure 4.1. Schematic diagram of the pin-APPJ arrangement.

4.2.2. Atmospheric pressure plasma jet with multi-needle electrodes geometry

Figure 4.2 depicts a schematic representation of the experimental setup with multi-needle electrodes-APPJ. Three syringe needle electrodes had inner and outer diameters of 1 mm and 1.8 mm, respectively. The needles were placed coaxially inside the glass tubes, which had inner diameters of 3.7 mm, exterior diameters of 5 mm, and lengths of 45 mm. The needle tip was retracted 7 mm with respect to the end of each tube thus making completely the same electrode geometry for all three jets. The jets were distanced 20 mm apart by using a teflon casing that also allowed support for electrical and gas connections. Figure 4.3 shows the detailed picture of the casing of multi-needle electrodes-APPJ. In all experiments, 15 ml and 30 ml of sample were placed in a plastic Petry dish and treated with plasma. The distance between the tip of the needle and the sample was fixed to 15 mm for each needle. The spacing was not constant during the treatment because of the small evaporation of the liquid. The evaporated volume was

estimated to be between 0.5 ml and 2 ml and the variation in the length of the gap was not more than 1-2 mm. The copper tape was used as a ground electrode by wrapping it around the bottom of the sample vessel. In all studies, argon gas with a total flow rate of 2 slm was employed as feed gas to the gas distribution system which was designed to spread the flow equally among the jets.
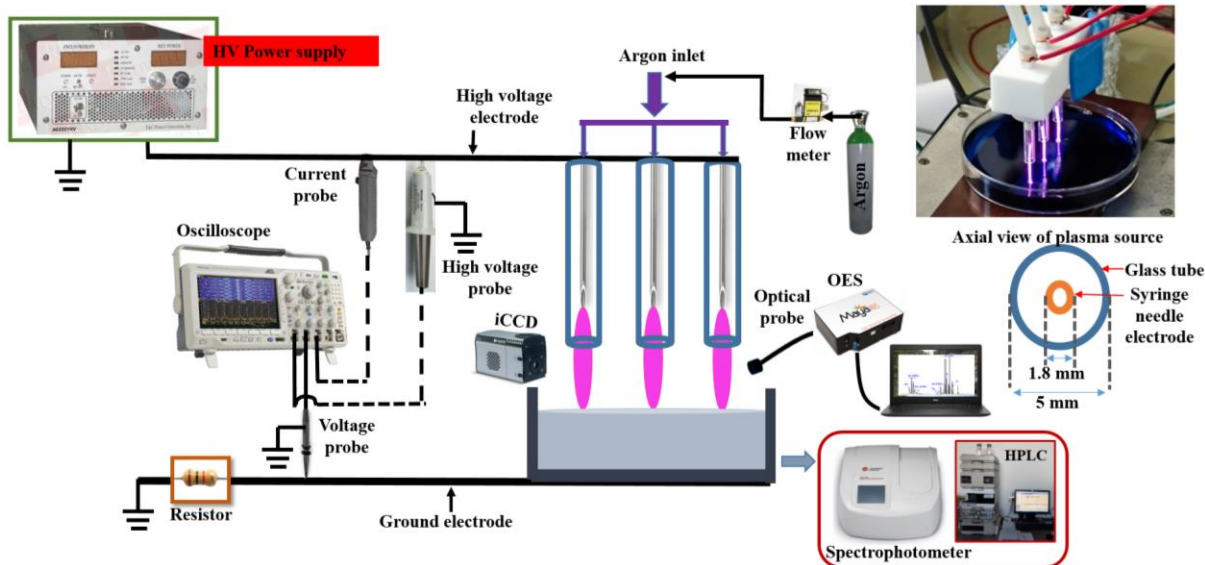
Figure 4.2. Schematic of multi-needle electrodes-APPJ configuration, operating without flow.
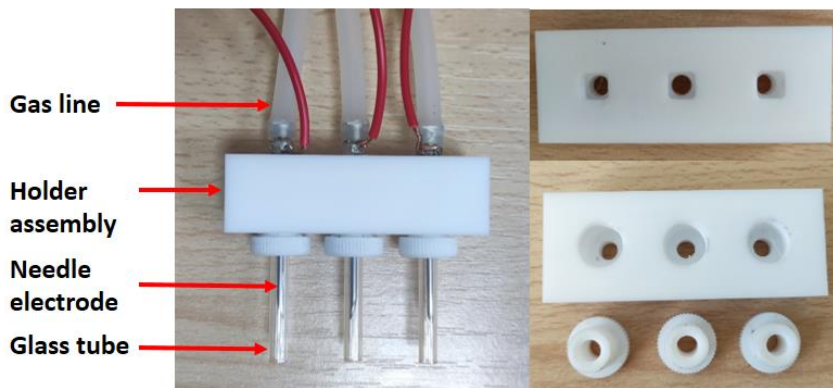
Figure 4.3. Assembly of multi-needle electrodes-APPJ.

In another experimental setup, the APPJ was positioned over the flowing liquid surface during flow system assembly (Figure 4.4) using a multi-syringe needle electrode type setup. In this scenario, a 250 mL solution was treated, with approximately 12 % of the solution in contact with the treatment area at all times. The solution was continually recycled by a pump (located inside the solution reservoir) at a flow rate of 300 ml/min, with a Reynolds number of 1349. The Reynolds number suggested a laminar flow. The tests were run for varied treatment periods, with 2 ml samples collected at various intervals for analysis.
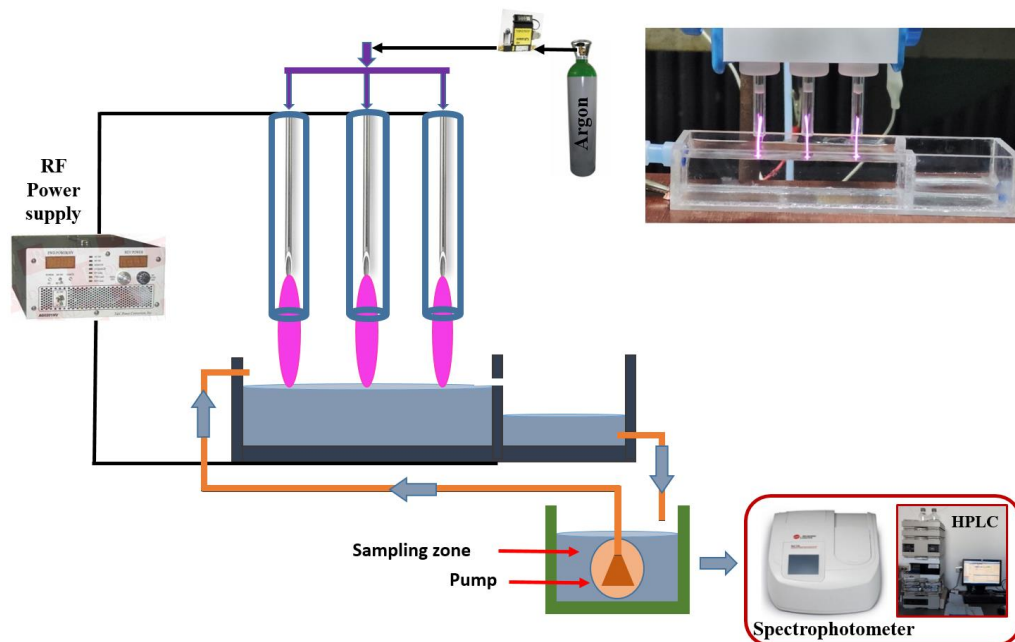
Figure 4.4. Diagram of a multi-needle electrodes-APPJ arrangement in use with a recirculation system.

4.3. High voltage power supply

For all experiments, plasma was ignited using a commercial RF high voltage power source (T&C Power Conversion AG0201HV) that generates sine signals over a different frequency range. The power supply displays the power (forward and reverse power) in Watts sent to the plasma source. For both plasma systems, frequency tuning was done in order to minimize the reflected power. Therefore, the pin-APPJ and multi-needle electrodes-APPJ working frequencies were 333 kHz and 350 kHz, respectively.

4.4. Electrical measurement

The primary discharge parameters such as voltage, current and power deposition were computed under various operating conditions. The voltage and current waveforms were measured at the pin-electrode that was connected to a high voltage source and, also, in the ground branch of the electrical circuit where the plasma plume is in contact with treated liquid. The electrical schematics of the experiment is given in Figure 4.2. A high voltage probe was used to measure the voltage at the powered electrode (Tektronix 6015A). A current probe was used to measure the current flowing through the cable to the powered electrode (Agilent N2783B). A voltage probe was utilized to capture the voltage drop across the 1 kΩ resistor in the grounded section (Agilent 10073C). A four-channel digital oscilloscope (Tektronix MDO3024) with a maximum frequency of 200 MHz was used to observe the time-varying voltage and current waveforms. Simultaneously, the oscilloscope data was transmitted to a laptop for storage and additional processing. The power given to the plasma source from the power supply and the power in the grounded line, i.e. the power transferred from the plasma passing through the sample, were determined and details of the procedure are given in Chapter 5.

4.5. Optical emission spectroscopy

Optical emission spectroscopy (OES) is a versatile method that has been used in a variety of plasma studies. OES enables to keep track of the various excited species that emerge from the plasma jet.

35

Maya2000 Pro-UV-NIR (Ocean Insight-High Sensitive Spectrometer) with an optical resolution of 0.18 nm FWHM was used in this research. To collect the emission from the entire region of the plasma jet, an optical fiber (M114L02) with a length of 2 m and a core diameter of 600 m was put perpendicular to it. The distance between the active plasma volume (streamer) and the fiber end was around 10 cm. This enabled to gather of light from a wide spatial angle, containing emissions from the whole active region. The recorded spectra was uploaded to a laptop. The emission of plasma is evaluated both with and without plasma (background). To obtain the accurate spectrum, the background spectra were subtracted from the plasma emission spectra. The spectrum intensity was normalized to account for the performance of the optical system. OES was performed on both plasma sources. Figure 4.5 depicts the OES with multiple needle electrodes - APPJ arrangement.
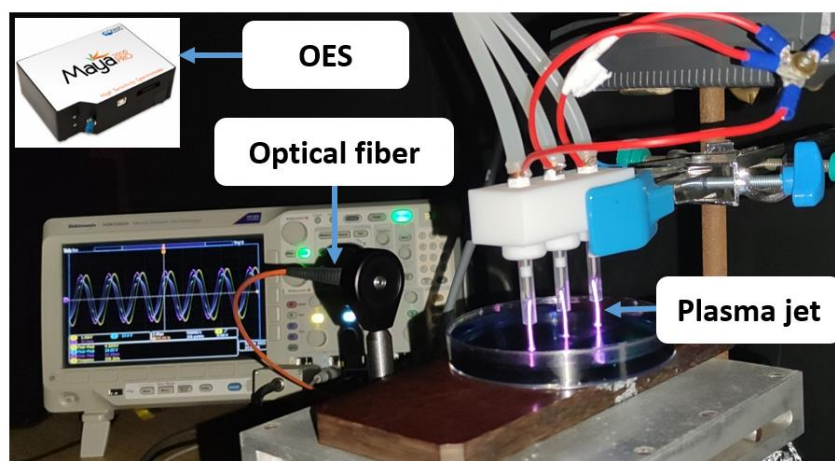
Figure 4.5. OES configuration for multi-needle electrodes-APPJ.

4.6. Plasma imaging

For plasma imaging, a gated intensified charge-coupled device (ICCD) was used to obtain the necessary temporal and spatial resolution for imaging the plasma jet. Non-invasive technologies such as imaging systems can be used to evaluate plasma profiles as well as capture time-resolved development. An iCCD camera is widely employed to investigate the dynamical characteristics of plasma discharge. Images of specific reactive species with plasma discharge are typically recorded using an iCCD camera and various band pass filters.

In this study, the plasma emission was recorded employing an Andor iStar DH734I iCCD camera with different acquisition conditions (e.g. gain, exposure time and gate pulse width). Two distinct lenses were employed for imaging. In the case of pin-APPJ, for example, the emissions were collected using a Micro-NIKKOR 105 mm f/2.8 lens with an auto extension ring. The Nikon UV-105 mm f/4.5 lens was attached to the camera for imaging of multi-needle electrodes-APPJ. The iCCD camera's lens was positioned perpendicular to and in front of the plasma jet. Band pass filters (BPF) were placed in front of the objective in order to record the spatial emission pattern at selected wavelengths, i.e. coming from different excited species (e.g. HO·, O·, H·, N_2, Ar*). A MATLAB script was used for batch processing of the data. Figures 4.6 and 4.7 show the iCCD in pin-APPJ and multi-needle electrodes-APPJ configurations, respectively.
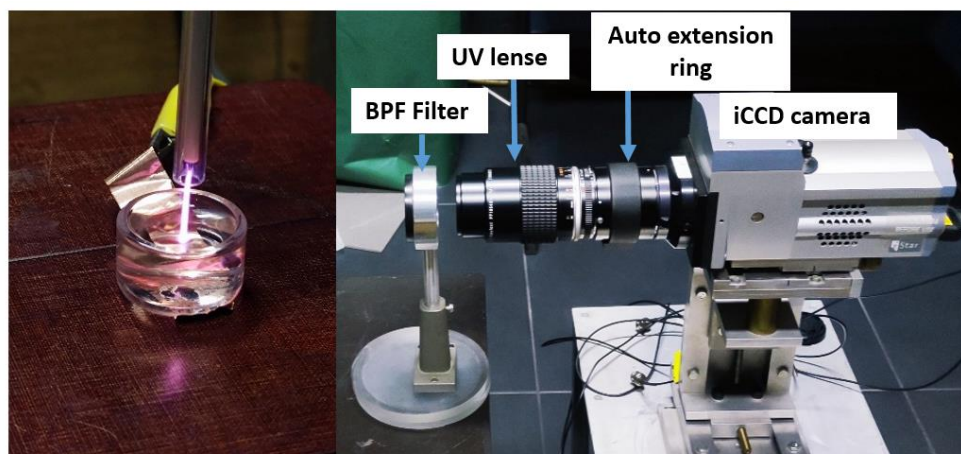
Figure 4.6. Experimental setup for pin-APPJ imaging with an iCCD camera.
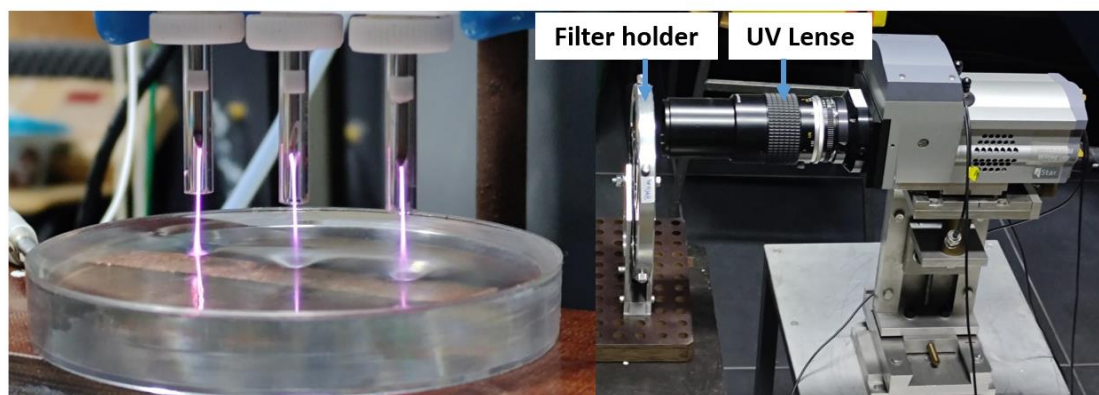
Figure 4.7. Experimental setup for multi-needle electrodes-APPJ imaging with an iCCD.

The band-pass filters were selected in such a way to allow to scan of the emission from plasma belonging to excited species involved in water purification. The transmittance % of each filter at a specific wavelength was determined using a spectrophotometer. Table 4.3 displays the filter's center wavelength, bandwidth, line of interest, and filter transmission in percentage at the line of interest. Each filter has a bandwidth of approximately $\pm$ 10 nm.

Table 4.3. Filters for ICCD imaging.

Type of filters, central wavelength	Line of interest	Max. transmission %	Transmission % at line of interest
310 nm	HO·	76	65 % at 309 nm
780 nm	O·	97	96 % at 777 nm
840 nm	O·	57	57 % at 844 nm
425 nm	N_2 (SPS & FNS)	17	14 % at 425 nm & 15 % at 426 nm
430 nm	N_2 (SPS & FNS)	97	22 % at 425 & 86 % at 426 nm
660 nm	H_α	98	95 % at 656 nm
710 nm	Ar*	64	26 % at 706 nm

4.7. Analytical methods

4.7.1. Spectrophotometer for organic dyes analysis

For the evaluation of AB25 and DR1 dye degradation, a spectrophotometer (Beckman Coulter DU 720 UV/Visible, shown in Figure 4.8) was employed.

Figure 4.8. Spectrophotometer for sample analysis.

Measurements of solution absorbance were performed in the wavelength range between 200 nm and 700 nm. The maximal intensity of AB25 absorbance occurs in the visible area at 602 nm and this wavelength was employed to monitor dye removal by plasma. The greatest intensity of DR1 was measured at a wavelength of 502 nm. The calibration curves for DR1 (a) and AB25 (b) are shown in Figure 4.9.
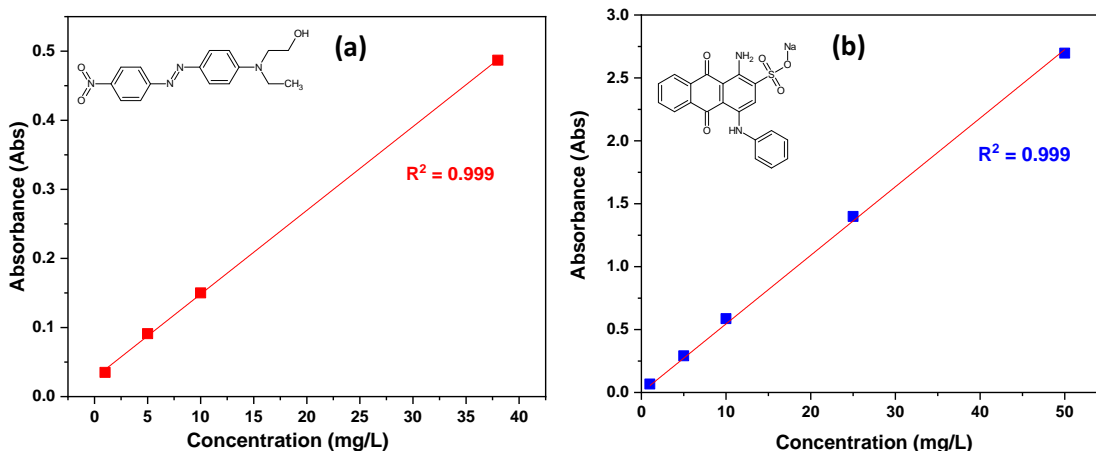
Figure 4.9. AB25 (**a**) and DR1 (**b**) calibration curves.

The adsorption of the light passing through a colored solution is described by Beer-Lambert's Law. The law expresses the linear correlation (absorbance $\propto$ concentration) between absorbance and concentration of the absorbing sample [175]. The more dye there is in the sample, the more light it absorbs and the less light it transmits. It is envisaged that the color-contributing chemical component of the AB25 and DR1 will be altered throughout the chemical oxidation process, hence reducing the molecule's ability to absorb light in the visual domain [68].

4.7.2. HPLC-DAD for pharmaceutical and industrial chemical analysis

HPLC or High-Pressure Liquid Chromatography (shown in Figure 4.10), is one of the most essential analytical tools for determining the characteristics of liquids. HPLC can separate, identify and quantify elements in even the most complex mixtures. The separation of an analyte (sample) between a mobile phase (eluent) and a stationary phase is the foundation of the HPLC differentiation idea. The molecules travel slowly within the stationary phase (column) due to the analyte's chemical characteristics and the duration spent on a certain column is governed by the unique intermolecular interactions between the molecules of a sample and the packing substance. Detectors used in HPLC have varying degrees of attainable sensitivity. The most common type of detector is a UV or UV-VIS detector. The reason behind this is that the bulk of chemicals produced by industries may absorb UV light.
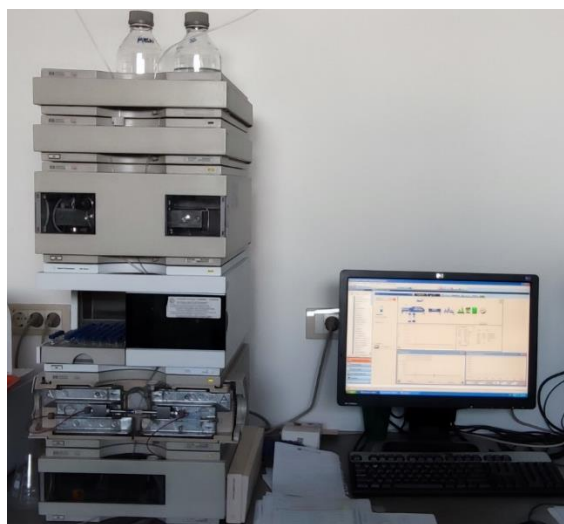
Figure 4.10. HPLC for sample analysis.

HPLC measurements were performed at the Institute for biological research "Sinoša Stanović", University of Belgrade. DCF and pCBA contents were determined using HPLC (Agilent Technologies, Waldronn, Germany, 1100 series,) coupled with a UV-DAD detector and a cartridge column (Hypersil BDS-C18, 3 μm, 2.0 mm x 125 mm). The column temperature was maintained at 30 ^{o}C, with a flow rate of 0.5 ml/min and an injection volume of 10 μL. Before injection, the solution was screened with a regenerated 0.22 µm cellulose syringe filter (Agilent technologies, Santa Clara, CA, USA). Acetonitrile (HPLC gradient grade) and deionized water (with 1% orthophosphoric acid analytical reagent grade) comprise the mobile phase. Ultra-pure water was generated by using the Water Purification System (New Human Power Integrate, Human Corporation, Seoul, and Republic of Korea).

At time 0, the mobile phase in DCF is composed of acetonitrile/water (20:80, v:v%) and the proportion was changed as follows: 70:30 to 7 minutes and 20:80 to 12 minutes. In the case of pCBA, identical solvents were utilized, with a ratio of 20:80 at time 0 to 40:60 at 8 minutes and to 20:80 at 12 minutes. In both situations, the maximum retention time was set to 12 minutes. The detection wavelength was tuned to 276 nm for DCF and 240 nm for pCBA. Figure 4.11 depicts the calibration graph for DCF (a) and pCBA (b).
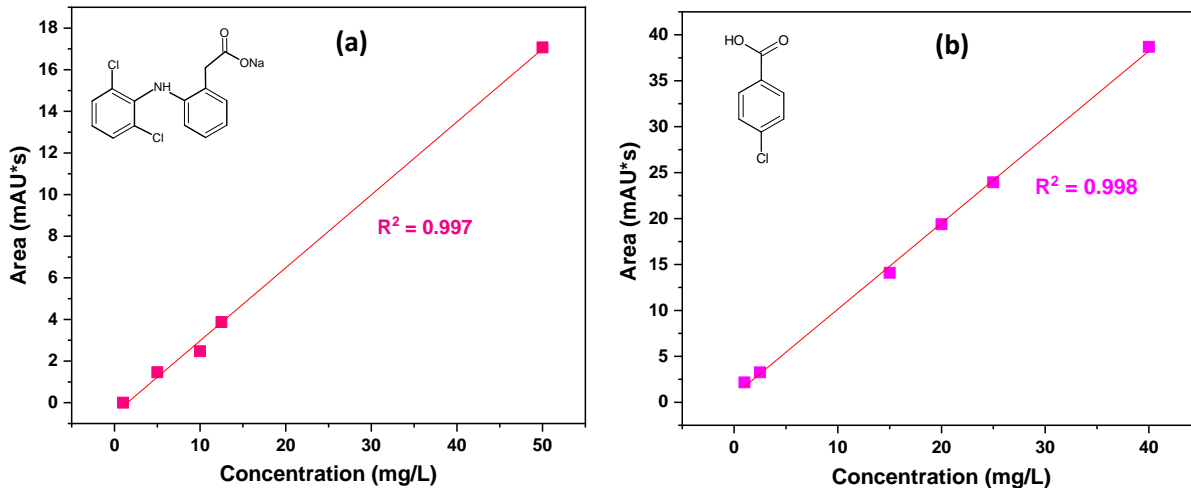
Figure 4.11. Calibration curves for (a) DCF and (b) pCBA.

Figure 4.12 depicts the HPLC chromatogram for DCF and pCBA. The peak of DCF and pCBA appeared at 6.5 minutes and 4.5 minutes of retention time, respectively. Several previous researchers have also provided HPLC analytical techniques for DCF and pCBA, which can be found in the following journals: [176–178].
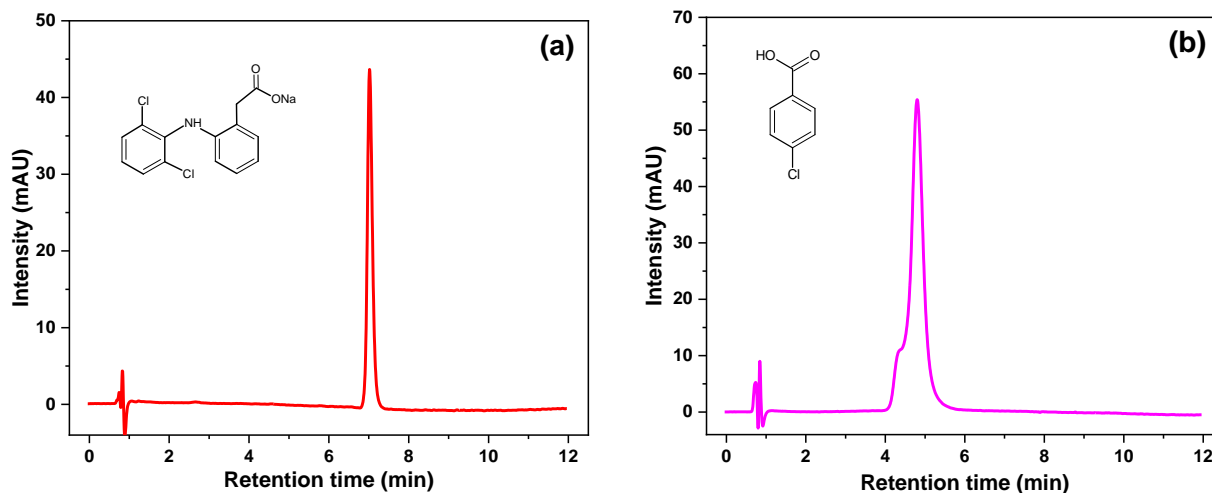
Figure 4.12. HPLC chromatogram for (a) DCF and (b) pCBA, at 25 mg/L.

The following equation was used to calculate the removal efficiency of all the target compounds (AB25. DR1, DCF and pCBA):

$$Removal\ (\%) = \frac{C_o - C \times d}{C_o} \times 100 \qquad (4.1)$$

Where C_o (mg/L) represents the initial concentration, C (mg/L) represents the final concentration after treatment and d represents the evaporation coefficient.

The provided equation was used to calculate the energy yield (Y), which is defined as the amount of target compounds removed per unit of power deposited on the sample:

$$Y\left(\frac{mg}{kWh}\right) = \frac{C_o\left(\frac{mg}{L}\right) \times V_o(L) \times \frac{1}{100} \times Removal(\%)}{P_{mean} \; at \; the \; sample \; (kW) \times t(h)} \quad (4.2)$$

Where V_o denotes the initial volume of solution (in liters), P_{mean} is the average power deposition at the sample (in kW) and t denotes the treatment period (in h).

The energy yield at 50 % elimination of a certain pollutant was calculated using the equation below for a comparison of various OMPs treatments:

$$Y_{50}\left(\frac{mg}{kWh}\right) = \frac{C_o\left(\frac{mg}{L}\right) \times V_o(L) \times \frac{1}{100} \times Removal(50\%)}{P(kW) \times t_{50}(h)} \quad (4.3)$$

4.7.3. LC-MS-Orbitrap for determining pharmaceutical transformation products

The Orbitrap analytical tool (shown in Figure 4.13) is widely employed in a wide range of applications to reveal trace-level substances in complicated mixtures, such as agriculture, clinical research, food, forensic toxicology and so on. The Orbitrap-LC-MS device has been used effectively to detect organic pollutants in wastewater. Orbitrap offers the highest possible resolution. These high-resolution accurate-mass sensors detect a wide range of compounds and small molecules during screening while preserving optimal selectivity and sensitivity.
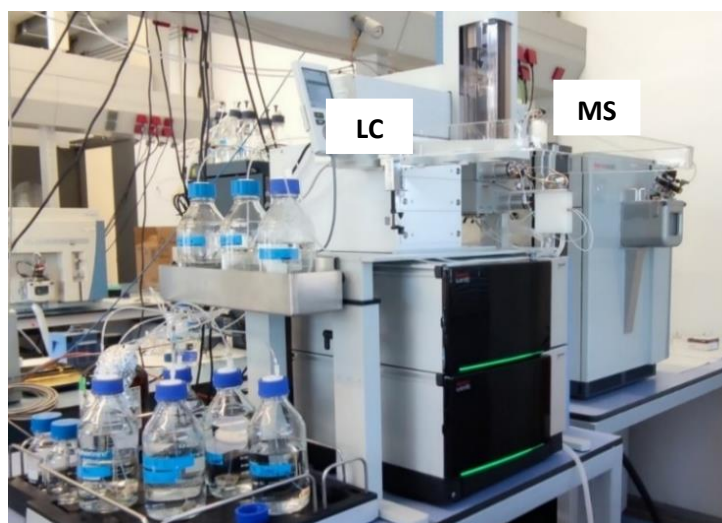
Figure 4.13. Orbitrap Exploris 120 high-resolution liquid chromatography-mass spectrometer (Thermo Fisher Scientific).

In this study, the byproducts of DCF breakdown were examined using an Orbitrap Exploris 120 high-resolution liquid chromatography-mass spectrometer (Thermo Fisher Scientific). The component in the sample was separated using a reverse-phase column (Hypersil GOLD-Selectivity C18, 3 μm, 2.1 mm x 50 mm). The column temperature was fixed to 30 ºC. The injection volume and flow rates were both 10 μL and 0.4 ml/min. The experiments were conducted in negative ion and positive ion modes, with ionization voltages of 2500 V and 3500 V, respectively. An ionization source was chosen using heated electrospray ionization (H-ESI) device. In the mass range of 40 to 5000, the mass spectra were obtained in full scan mode.

The mobile phase composition in the positive ion mode was HPLC water with 0.1 % formic acid and methanol. The mobile phase in the negative mode was HPLC water containing 5 mM ammonium acetate (at pH 8) and methanol. Composition variation began with 98:2 %, climbed to 2:98 in 4.7 minutes, remained steady until 6 minutes, and then reduced to 98:2 % in 9 minutes. The extracted data was then sent to Thermo Fisher Scientific's chemical discoverer software and processed [179,180]. The software also includes an excel-based report with chemical data, isotopes, retention period, m/z, fragment ion, intensity, mass error (ppm), and other information. ChemSketch (ACD/ChemSketch Freeware, [181]) was used to depict the chemical structure and fragmentation pattern of each probable transformation product. Figure 4.14 shows the mass spectra for DCF in the positive ion mode (m/z: 296.0237) at a concentration of 50 mg/L.
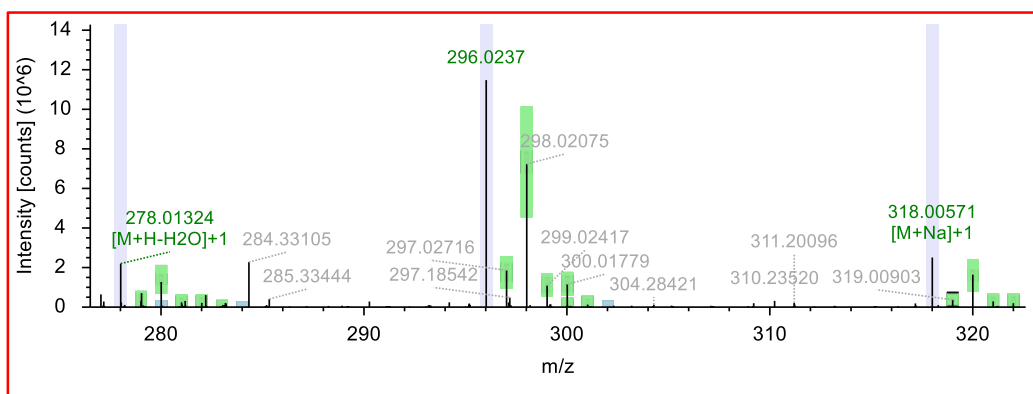
Figure 4.14. MS spectra for DCF.

4.7.4. The pH and conductivity analysis

A conductivity (HANNA-HI76312) and a pH (HANNA-HI1330) meter are used in all treatment operations to determine the solution conductivity and pH. Both probes were connected to a measurement device (HANNA-HI5521). The measuring unit was adjustable, with a wide color display, capacitive touchscreen keys, and a USB connector for computer connection, and it enables parallel assessment of pH on one channel and conductivity on another. Figure 4.15 depicts the measuring monitor as well as both probes.
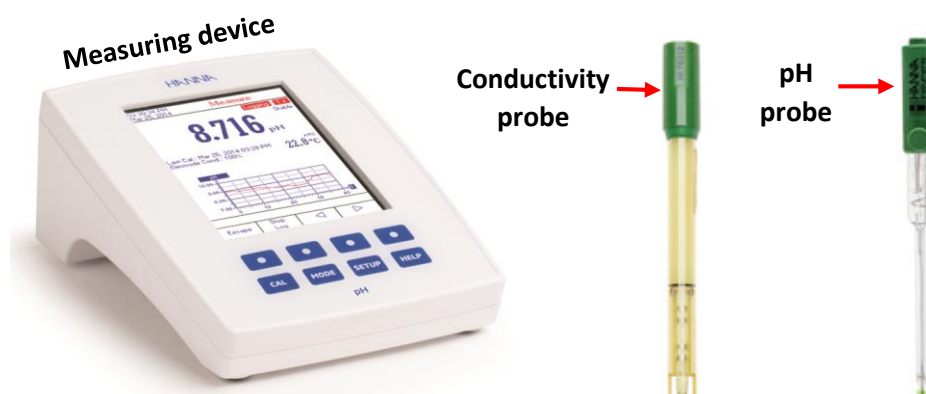
Figure 4.15. Conductivity probe, pH probe and measuring unit.

4.7.5. Temperature measurement

The bulk liquid temperature was also vital to know during plasma liquid interactions. An Opsens Solutions TempMonitor (TMM-G2-10-100ST-D.N.V.L) paired with a fiber optic temperature sensor was used in this investigation, which was ideal for and offers precise temperature measurements of liquid during plasma liquid interaction.

The optical fiber was linked to a sensing GaAs (Gallium Arsenide) crystal at the fiber's tip. The tip of the optical fiber was placed at the plasma liquid contact during the measurement. The working temperature range of the fiber optic temperature sensor was -40 °C to +250 °C. The temperature monitor was attached to an optical fiber, and the tip of the fiber was put at the plasma-liquid interface of the 3 pin-APPJ, as illustrated in Figure 4.16 (a & b).
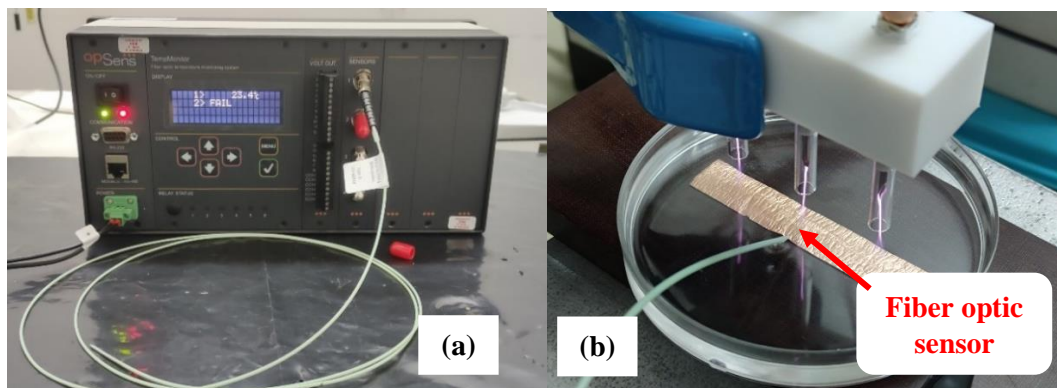
Figure 4.16. (a) Temperature monitor, **(b)** fiber optic temperature sensor placed under APPJ.

The temperature of the target liquid was measured before and during plasma treatment. Table 4.4 depicts the comparative outcomes in both scenarios. First, the initial temperature was measured when the plasma was turned off; in both cases, the temperature stayed rather steady. Both plasma sources warmed the samples with plasma exposure time, although one pin-APPJ warmed the samples significantly faster, which can be attributed to the difference in liquid volume. It can be shown that after 10 minutes of continuous exposure of plasma to liquid, the temperature rose to 94 °C for pin-APPJ and 29 °C for 3 pin-APPJ. In the case of the 3 pin-APPJ, the initial volume was larger, which played an essential role in counterbalancing the warming impact and allowing heat to disperse within the liquid via convection. As a result, the increased volume of treatment can keep the liquid at a lower temperature.

Table 4.4. Temperature measurement in case of both plasma sources during the treatment.

Treatment time (min)	Temperature (°C)	
	1 pin-APPJ, V_o = 5 ml	3 pin-APPJ, V_o = 30 ml
0	22	20
1	45	21
3	59	22
5	64	22
10	94	29

4.8. Experimental design

The investigations on the treatment of specific pollutants (AB25, DR1, DCF, and pCBA) employing both plasma sources, as well as the experimental conditions and parameters, are summarized in Table 4.5. The collected results from all experimental conditions are briefly presented in Chapters 5 and 6.

Table 4.5. Treatment conditions for each of the chosen OMPs using both plasma sources.

OMPs	Plasma source	Power (W)	Ar flow (slm)	Gap (mm)	V_o (ml)	C_o (mg/L)	Treatment time (min)
AB25	1-pin	11	1	10	5	25 & 50	1, 3, 5, 7, 10
AB25	1-pin	8, 9, 11, 12	1	10	5	50	5
AB25	1-pin	11	1	5,10,15	5	50	5
DCF	1-pin	10	1	10	5	25 & 50	1, 3, 5, 7, 10
pCBA	1-pin	10	1	10	5	25 & 40	1, 3, 5, 7, 10
DR1	1-pin	10	1	10	5	38	1, 3, 5, 7, 10
AB25	3-pin	14	2	15	15 & 30	25 & 50	3, 5, 10, 15, 20
AB25	3-pin	11	2	15	250	25	10, 20, 30, 40, 50, 60
DCF	3-pin	6	2	15	250	25 & 50	10, 20, 30, 40
pCBA	3-pin	9	2	15	250	25	20, 50

In the instance of 1 pin-APPJ, treatments were carried out while taking into account several experimental factors to determine their impact on pollutant degradation, such as treatment time, initial pollutant concentration, power deposition, and discharge gap. The role of each parameter was thoroughly examined. Throughout the treatment with 1 pin-APPJ, the initial volume and argon flow were fixed.

In one case, DR1 was treated with 1 pin-APPJ at an initial concentration of 39 mg/L to compare treatment results with AB25 at a concentration of 50 mg/L. The molar ratio for DR1 at 39 mg/L and AB25 at 50 mg/L was the same, equal to 0.12 mM.

In case of 3 pin, the experiments were carried out while taking into account the effect of treatment time, initial pollutant concentration, and initial solution volume. The 3 pin-APPJ-recirculation was also implemented, and in this case, the solution volume, solution flow rate, argon flow, initial concentration (excluding DCF), discharge gap were all fixed and only the plasma treatment period was varied.

The degradation of OMPs was monitored by using appropriate analytical approaches. A spectrophotometer, for example, was used to evaluate the characteristics of plasma-treated and untreated dye-containing solutions. HPLC was used to analyze the DCF and pCBA-containing solution. A DCF-containing solution treated with a three-pin APPJ-recirculation system was examined using Orbitrap-LC-MS.

The treatment of AB25 dye was also done with plasma activated water (PAW). In this case, PAW was produced during the interaction of 1 pin-APPJ with distilled water (V_o = 5 ml). The PAW was characterized in order to detect plasma-induced RONS in the liquid. After that, PAW was mixed with AB25 solution and the mixture was evaluated for a longer period of time to determine the influence of long-lived RONS on AB25 oxidation. The details of the treatment technique and the obtained results are briefly covered in Chapter 5.

CHAPTER 5

5. Treatment of contaminated water by using Pin-electrode atmospheric pressure plasma jet

This chapter focuses on the electrical and optical characterization of pin-APPJ, as well as the treatment of chosen OMPs with varying operational characteristics. Electrical and optical characterization was performed before testing the performance of the pin-APPJ source in the treatment of OMPs. Characterization of plasmas is an important step since it offers information on discharge characteristics and the presence of reactive species in the plasma. In this chapter, the degradation pattern of each pollutant was studied and remarked on and the corresponding energy yield was determined. The influencing parameters on the degradation of selected OMPs, as well as diagnostic processes, gave a wealth of data for the development of a multi-pin APPJ plasma source.

5.1. Electrical and optical characterization

Electrical measurement

A typical time variable voltage and current waveform collected during treatment is depicted in Figure 5.1. It can be seen that the voltage and current are both sinusoidal. The detailed electrical measurement approach is described in Chapter 4.
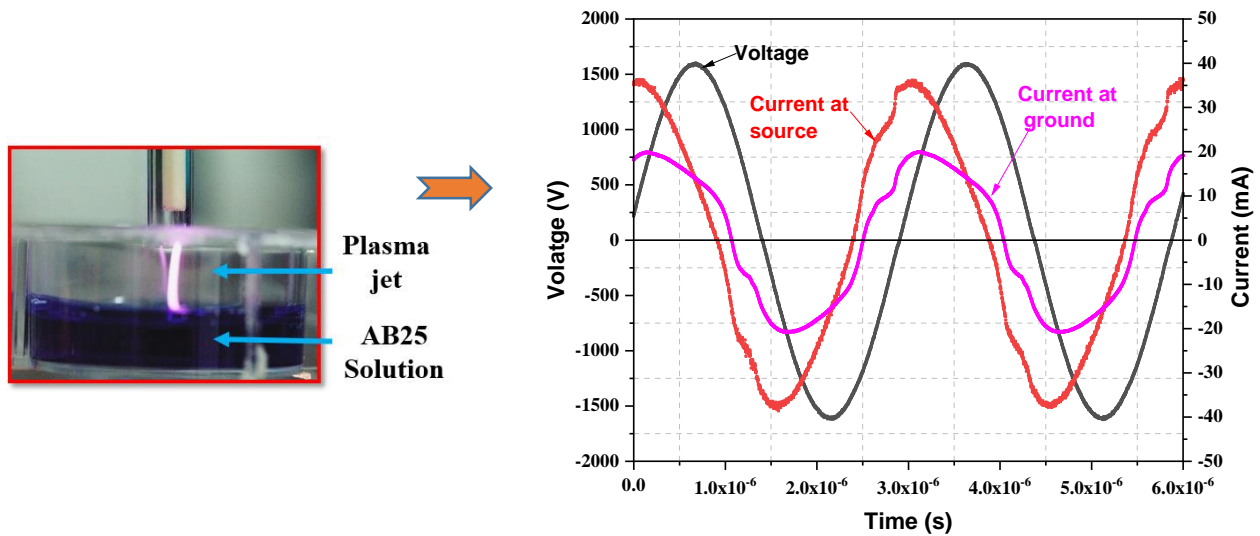
Figure 5.1. Pin-APPJ in contact with dye solution (b) a typical voltage (source) and current (source & ground) waveform was captured during treatment by pin-APPJ, working gas argon 1 slm.

The discharge parameters were estimated by using collected voltage and current waveforms. For example, the mean power deposition to the plasma system was determined over a 6-period timeframe by averaging the instantaneous power, which is the product of recorded voltage and current. The mean power was calculated using equation 5.1.

$$P_{mean\ at\ source} = \frac{1}{nT} \int_{T1}^{T2} v(t) \times i_s(t) \times dt \qquad (5.1)$$

Where P_{mean} denotes mean power at the source, $v(t)$ denotes voltage signal at the source and $i_s(t)$ denotes current at the source and $nT = T_2 - T_1$.

The mean power provided at the ground (in contact with the sample) was determined in the same way, as shown in equation 5.2.

$$P_{mean\ at\ ground} = \frac{1}{nT} \int_{T1}^{T2} v(t) \times i_g(t) \times dt \quad (5.2)$$

Where P_{mean} is mean power at the sample *and* $i_g(t)$ is the current in the grounded branch of the circuit.

The current in contact with the sample $i_g(t)$ was calculated using equation 5.3, as a voltage drop ($v_R(t)$) over the resistor ($R=1k\Omega$).

$$i_g(t) = v_R(t)/R \quad (5.3)$$

The RMS (RMS: root mean square) voltage and current were determined using waveforms and utilized to study the behavior of the plasma system's V-I characteristics. The V_{rms} and current I_{rms} are determined using the provided equations (5.4 to 5.6).

$$V_{rms} = \sqrt{\frac{1}{nT} \int_{T1}^{T2} (v(t))^2 dt} \quad (5.4)$$

$$I_{rms\ at\ source} = \sqrt{\frac{1}{nT} \int_{T1}^{T2} (i_s(t))^2 dt} \quad (5.5)$$

$$I_{rms\ at\ ground} = \sqrt{\frac{1}{nT} \int_{T1}^{T2} (i_g(t))^2 dt} \quad (5.6)$$

The electrical characterization results are shown in Figure 5.2. Figure 5.2 (a) shows V-A at the source, while Figure 5.2 (b) shows V-A in contact with the sample (ground). The characterization was carried out in two modes: without plasma and after plasma ignition. When there was no plasma, the relationship between voltage and current changed linearly. However, when plasma was ignited, the voltage dropped significantly. After ignition, the voltage barely changed and became almost constant as the power from the RF power supply was increased. It was found that after plasma ignition, the current delivered to the source was approximately twice as high as it was at the sample.
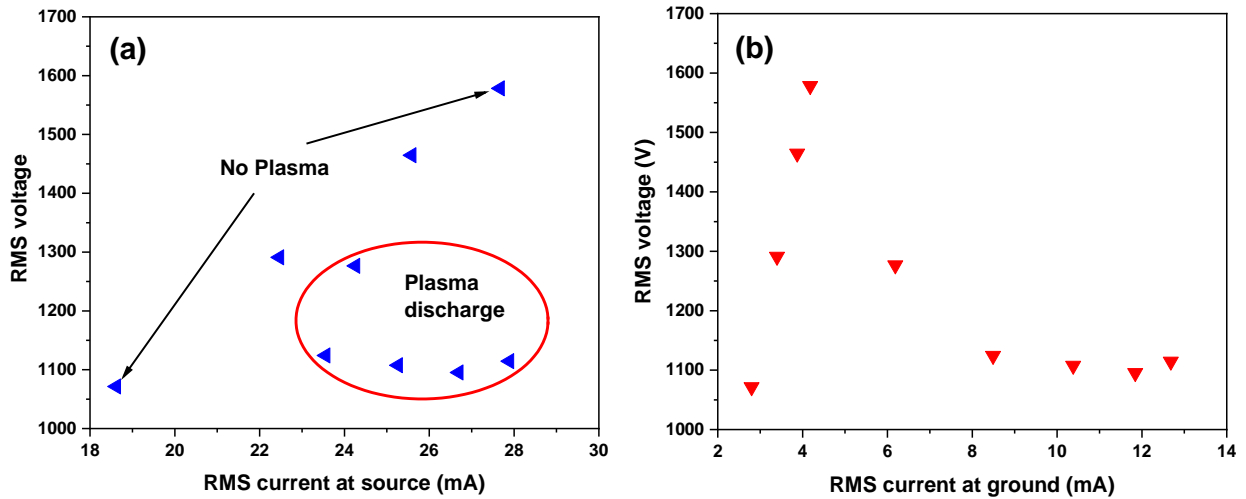
Figure 5.2. The V-A characteristics indicate (a) RMS voltage as a function of RMS current at the source and (b) RMS current in contact with the sample, working gas argon 1 slm.

One of the most important parameters for plasma-based treatment processes is the power supplied to the plasma system, which is used to calculate the system's energy efficiency. The power deposition was estimated and Figure 5.3 depicts the power transferred in both circuits, at the source and in contact with the sample. When there was no plasma ignition, there was power deposition in the system due to parasitic resistance in the electrical circuits. After the ignition, power deposition increased instantly while voltage was reduced. The increase in power at constant voltage is mostly owing to a significant increase in the current delivered to the source and in contact with the sample. The power delivered to the sample was evaluated in this investigation and it ranged from 5 W to 11 W.
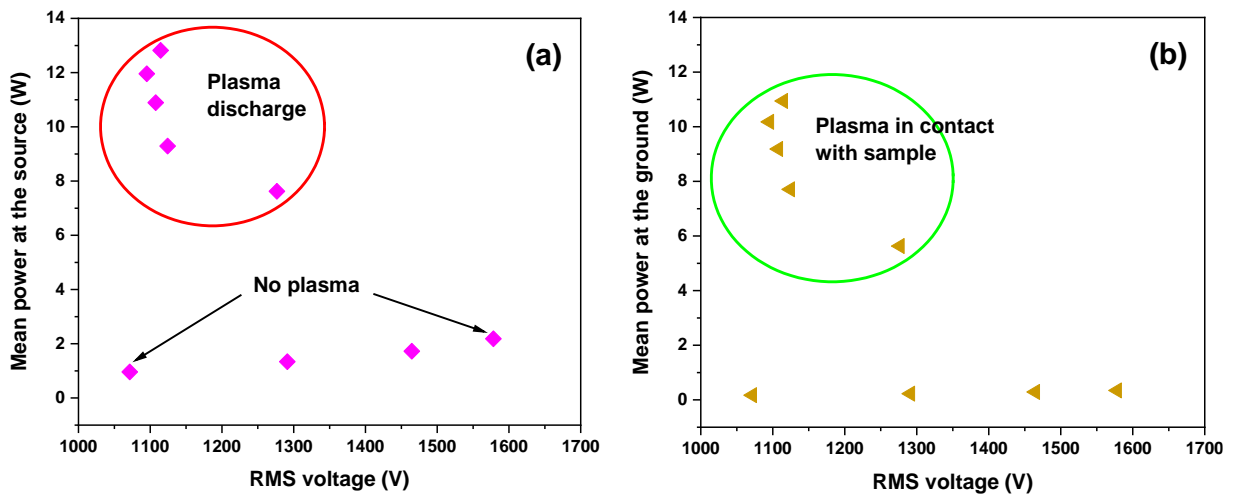
Figure 5.3. (a) Plasma mean power deposition at the source as a function of RMS voltage (b) mean power at ground vs RMS voltage. Experimental conditions, target: AB25 dye sample and working gas argon 1 slm.

Optical measurement by OES

OES is a non-intrusive optical measurement technique that provides an overview and insight into plasma gas phase chemistry. In this investigation, OES was used to characterize the reactive species produced by the open-air argon plasma discharge. OES has identified and characterized a number of plasma-induced reactive species that may contribute to the degradation of OMPs.

OES spectra confirmed several radicals, excited molecular and molecular ion species, the emission intensity of each species are shown in Figure 5.4. The chemical species corresponding to their wavelength and atomic-molecular transitions are given in Table 5.1. The spectra were captured in the wavelength range of 200 to 1100 nm. HO·, O·, N_2 (SPS), N_2 (FNS), N_2 (FPS), H_α and excited atomic argon were found in spectra obtained from 200 to 1100 nm.

The HO· band occurred at 309 nm. N_2 (SPS) was identified throughout a wide range of wavelengths, with the maximum intensity recorded at 337 nm. Monoatomic oxygen lines were discovered at two distinct wavelengths, with the strongest emission occurring at 844.6 nm. The excited nitrogen molecular ion N_2^+ (FNS) between 391.4 and 428 nm as well as a weaker intensity of N_2 (FPS) are also present for the molecular nitrogen ions. Argon lines were detected at a variety of wavelengths, with the greatest emission strength measured between 773.5 and 811.5 nm.
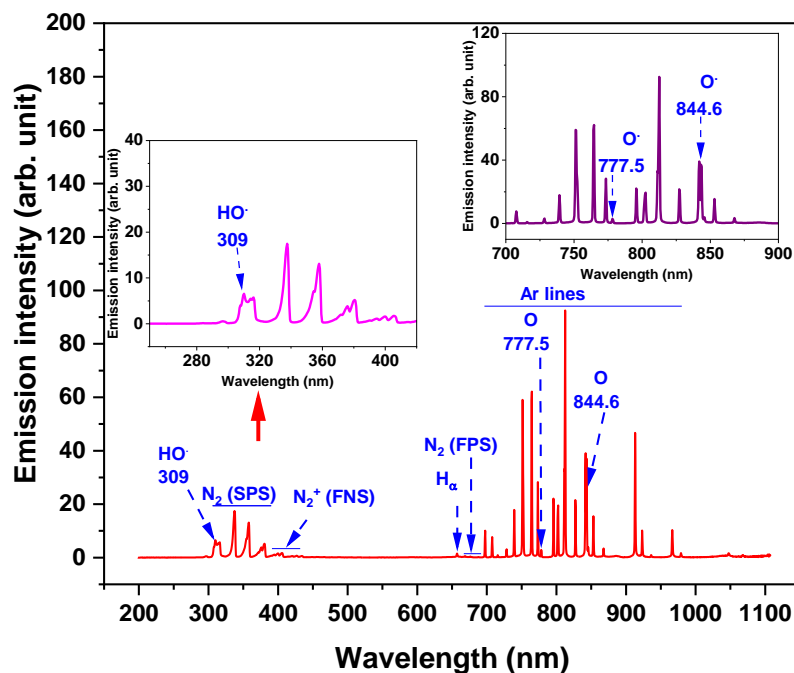
Figure 5.4. The optical emission spectra of argon-APPJ in open air. Sample AB25 dye solution, $V_o = 5$ ml, argon flow 1 slm, P_{mean} at the sample 11 W.

Table 5.1. The plasma produced reactive species and transitions.

Chemical species	Wavelength (nm)	Corresponding atomic & molecular transition
HO·	309	$A^2\Sigma^+ \rightarrow X^2\pi$
N_2 (SPS: Second positive system)	297.6 - 380.4	$C^3\pi_u \rightarrow B^3\pi_g$
N_2^+ (FNS: First negative system)	391.4 & 428	$B^2\Sigma_u^+ \rightarrow X^2\Sigma_g^+$
H_α (Balmer line)	656.5	$3p \rightarrow 2q$
N_2 (FPS: First positive system)	661 - 676	$B^3\pi_g \rightarrow A^3\Sigma_u^+$
O·	777.5	$O\ (3p^5P \rightarrow 3s^5S)$
O·	844.6	$O\ (3p^3P \rightarrow 3s^3S)$
Argon	690 - 912	$4p \rightarrow 4s$

The vast majority of the energy in cold atmospheric plasma is transferred to the formation of excited species, metastables and dissociation of chemical species. Several researchers have thoroughly investigated the argon-air gas phase plasma chemistry and studied energy levels diagrams for various emission spectrum profiles, as illustrated in Figure 5.5 [182]. The energy level diagram shows the link between the energy requirements of different reactive species for electronic transitions from one state to another. Figure 5.5 shows that each species has a different energy level. Argon plasma species that are excited to higher energy states can excite and form a diverse range of reactive species when they come into contact with liquid and ambient air.

Figure 5.5. Energy diagram for exciting species in an argon-air mixture [182].

The primary sources of excited species and ions in argon-air plasma are electrons and argon metastables. As indicated in equations 5.8 and 5.9, HO radicals can form in the gaseous phase of plasma, primarily as a result of dissociative excitation of water molecules caused by the collision of argon metastables, but

they can also form as a result of high-energy electrons. The presence of water molecules in the gas phase of plasma is due mostly to humid air mixing with argon gas flow.

$$e^- + H_2O \rightarrow HO^. + H^. + e^- \quad (5.8)$$

$$Ar^* + H_2O \rightarrow HO^. + H^. + Ar^* \quad (5.9)$$
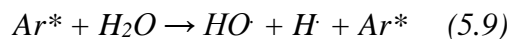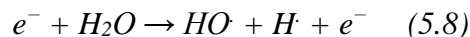
Generally, argon species (metastables) have energies level above 11 eV (can be seen in Figure 5.5) and oxygen and nitrogen have energy levels lower than argon metastables. Therefore, argon metastables have high enough energy for the excitation of molecular nitrogen [183] and dissociation of molecular oxygen via collisional dissociation, which can be explained by the following reactions 5.10 and 5.11.

$$Ar^* + N_2 \rightarrow N_2^* + Ar \quad (5.10)$$

$$Ar^* + O_2 \rightarrow O^. + O^. + Ar \quad (5.11)$$
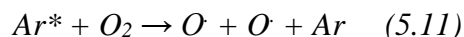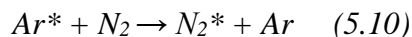
Atomic oxygen can also originate after the dissociation of molecular oxygen by energetic electrons, described by reaction 5.12.

$$e^- + O_2 \rightarrow O^. + O^. + e^- \quad (5.12)$$
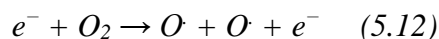
The generation of molecular nitrogen ions could be caused primarily by electron impact excitation and ionization of molecular nitrogen. Figure 5.5 shows that ionization reactions demand a considerable amount of energy and that ions can be created by electrons with enough energy. APPJ is also a source of UV radiation, which can at some extent contribute to the formation of reactive species such as HO· and O· by photolysis of water molecules and molecular oxygen.

It was investigated that plasma-produced HO· and O· to be the primary group of short ROS contributing to the degradation of OMPs in water. Other plasma-induced reactive species have also been linked to water purification.

The OES was carried out at various input powers, as shown in Figure 5.6. (a). It was revealed that the intensity of reactive species emission increased with input power, with some of them increasing significantly and others only a little. The intensity ratio at higher and lower power levels was also examined to determine the highest fluctuation in reactive species intensity, as shown in Figure 5.6. (b). The intensity of all detected reactive species emissions increased, with argon, hydrogen and HO· emissions being the most affected. The shift in emission intensity with power can be linked to the formation of more energetic species, which can help to increase the plasma-rich chemical environment. Since more reactive species were created at greater power levels and they also function on the degradation of OMPs, as indicated in the next section.
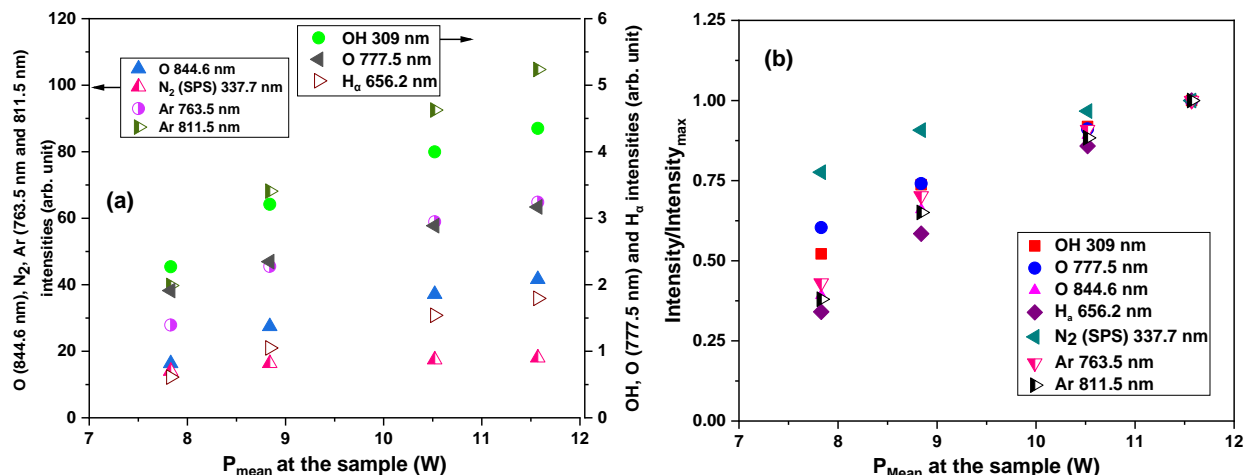
Figure 5.6. (a) The intensity of excited species emission versus input power **(b)** and intensity ratio versus input power. Experimental conditions, $V_o = 5$ ml and argon flow 1 slm.

Optical measurement by iCCD

The pin-APPJ iCCD was performed to gain more understanding of the optical properties of plasma. The measurements were taken with and without optical filters. To investigate the unique spatial evolution of reactive species ((HO·, O·, H$_\alpha$, Ar*, N$_2$ SPS and N$_2^+$ FNS) in plasma, band-pass filters with variable transmission % were placed in front of an iCCD camera attached to a lense. The filters were chosen based on the reactive species observed in the gaseous phase of plasma at various wavelengths as revealed by the OES spectra.

Andor Solis software was used for imaging and all essential input data was given to the software to collect the photographs. First, as shown in Figure 5.7, iCCD was taken without plasma by placing a scale near the plasma source and a liquid sample beneath it. Images captured without plasma revealed the electrode tip coordinates as well as the location of the liquid surface during image processing. To process the iCCD images, MATLAB software with written scripts was utilized, for example, to create the geometry of the electrode and liquid surface, as well as to generate the emission profile.
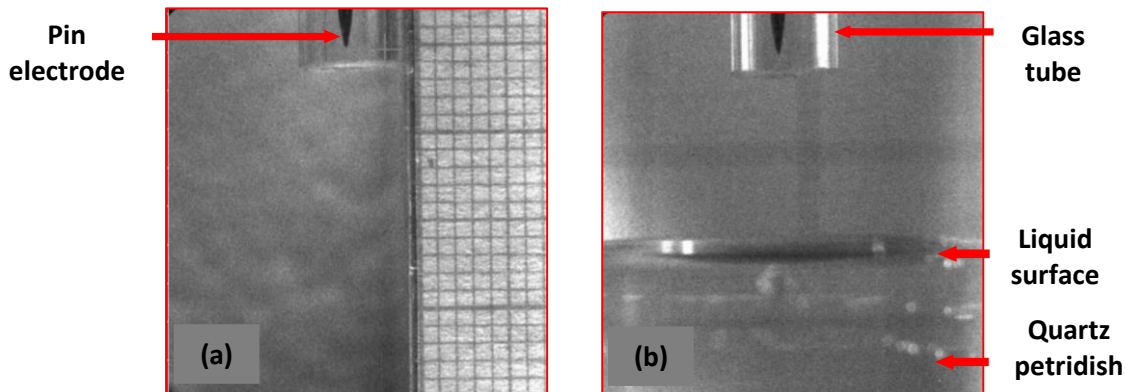
Figure 5.7. The iCCD images without plasma, (a) with scale and (b) with a liquid sample. Acquisition parameters gain 0, exposure time 100 ms, gate pulse width 75 ms.

Plasma imaging was investigated utilizing various acquisition parameters. An appropriate set of acquisition parameters was established and used to produce the images. Initially, a background image

was captured without plasma and then the background noise was eliminated in Andor solis software to extract the effective images in the count.

Figure 5.8 (a) depicts plasma interaction with distilled water containing quartz perti dish but without iCCD camera under the same operating conditions (sample volume, discharge gap, argon flow, etc.) as when iCCD data were taken. The iCCD images associated with pin-APPJ at two distinct input power levels are shown in Figure 5.8 (b). As shown in Figure 5.8 (b), the intense emission are broadly dispersed in the entire active plasma with both input powers, although brighter light emissions along the jet occurred with a higher power. The existence of brighter intensity regions indicates that there is more excitation of reactive species in certain parts of the streamer.
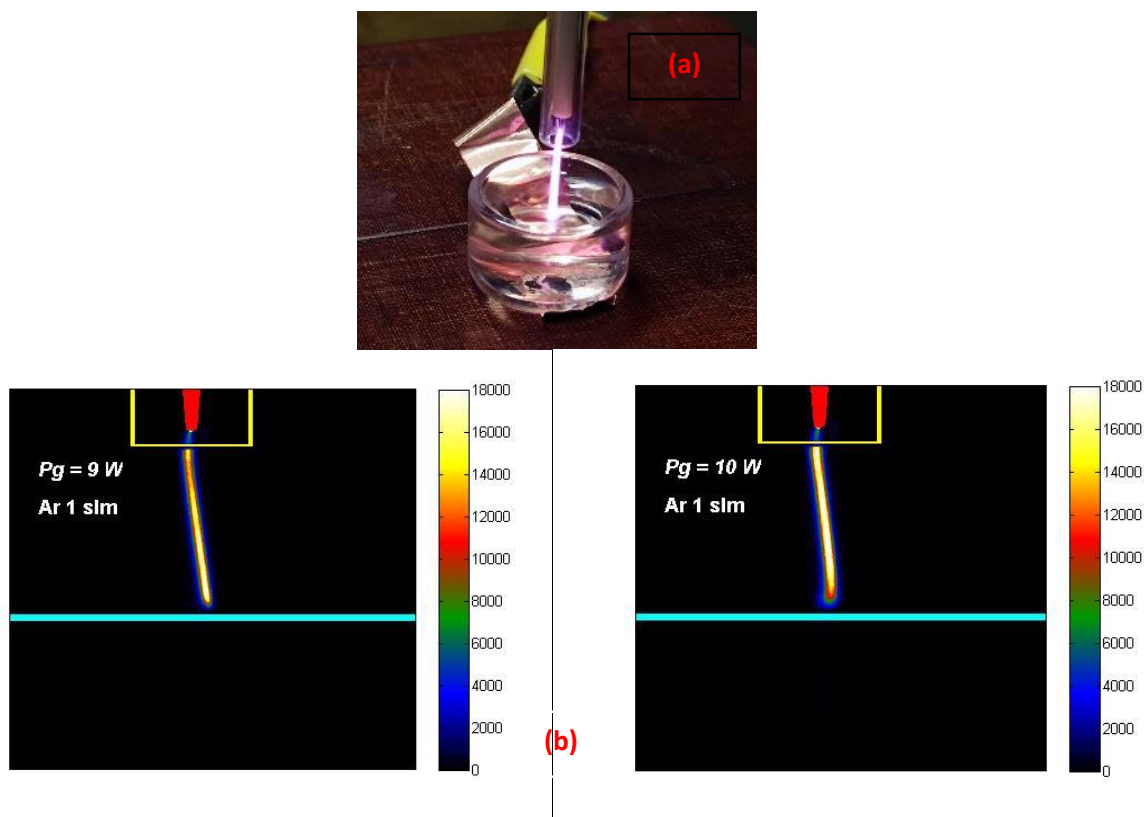
Figure 5.8. (a) Pin-APPJ in contact with liquid, **(b)** iCCD images of plasma jet emission for two mean powers deposited to the discharge. Acquisition parameters, gain 0, exposure time 20 ms, gate width 1 ms.

Various optical filters (310 nm, 780 nm, 660 nm, and 425 nm) were utilized to capture the spatial emission of various lines/bands inside the discharge. Each filter had a bandwidth of roughly 10 nm. When the filters were applied, less light reached the iCCD camera detector and the iCCD gain was increased from 0 to 50. During image processing, the filter specifications (transmission efficiency) and photocathode efficiency of camera were taken into account.

Image taken with filter at 310 nm shown in Figure 5.9 was primarily employed to track and collect the excitation spatial emission of HO· radicals. It was observed that HO· emission detected along the whole streamer similarly to the plasma channel recorded without a filter. Intensity of the image was brighter with greater input power, which could be attributed to the presence of more excited HO· radicals. Due to the band width of the filter, reduced transmission efficiency was also in the 315 nm area enabling the

vibrationally excited bandhead of molecule N_2 SPS (315.8 nm) to be also recorded within the 310 nm filter's transmission window.
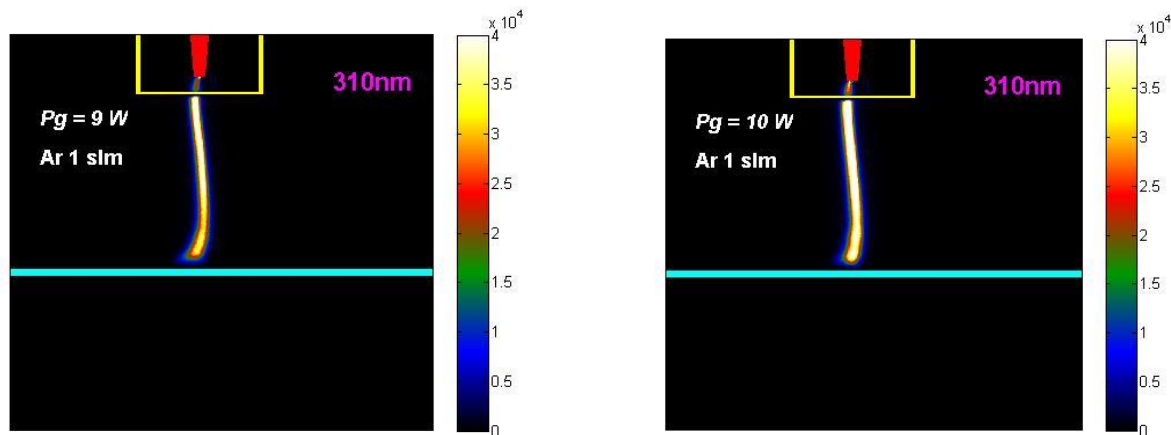
Figure 5.9. iCCD images with filters (310 nm) for two mean powers deposited to the discharge. Acquisition parameters, gain 50, exposure time 20 ms, gate pulse width 5 ms.

Figure 5.10 depicts the emission observed by applying the following filters: 780 nm, 425 nm, and 660 nm at two different input powers. The filter at 780 nm was transparent for primarily $O^{\cdot}$ emission at 777.5 nm, as well as the argon line, because argon emission is located near the peak of the atomic oxygen at around 772 nm. The filter at 660 nm was used for observing of H_α with a wavelength of 656 nm and a filter with a central wavelength of 425 nm was employed to track ionic nitrogen N_2^+ (FNS) and N_2 (SPS). The emission distribution profile was nearly the same at both powers when employing a 425 nm filter, but there was somewhat more emission from N_2^+ (FNS) and N_2 (SPS) species at higher power. The emission was lower in the case of the 660 nm filter at both powers, although the intensity of the emission was not significantly higher at higher power.
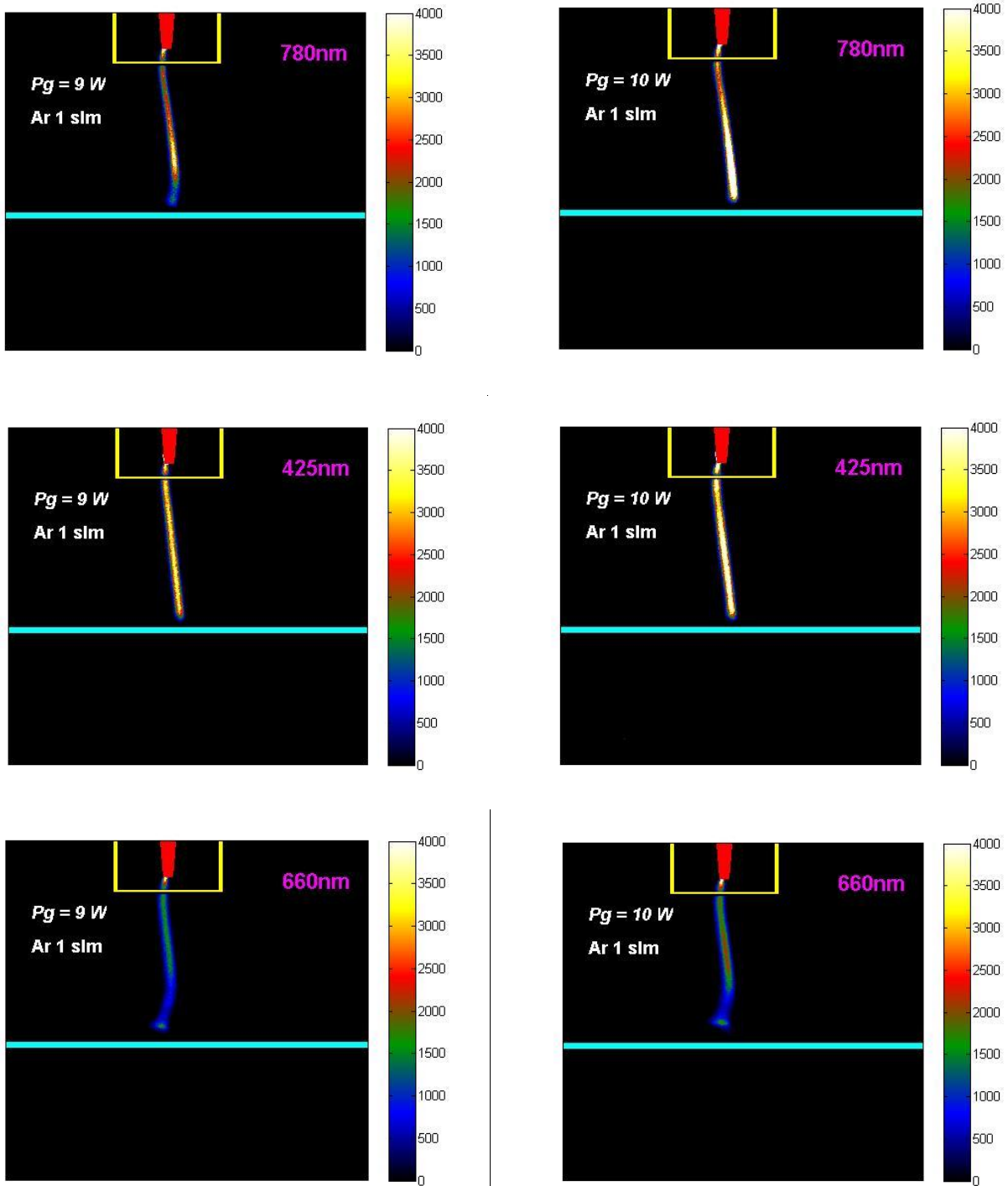
Figure 5.10. iCCD images with filters (780 nm, 425 nm, and 660 nm) for two mean powers deposited to the discharge. Acquisition parameters, gain 50, exposure time 20 ms, gate pulse width 5 ms.

5.2. Removal of Acid Blue 25 dye

The experiments on the treatment of the AB25 dye were done by two approaches. The first one is known as a direct treatment, where dye solution was directly exposed to plasma jet and most plasma created short and long lived reactive species as well as electrons, UV emission and electric field can engage in dye degradation, as shown in Figure 5.11. The majority of previous research on the treatment of various OMPs by cold atmospheric plasma has been conducted by direct exposure of polluted water solution to plasma.

Another method was indirect - the dye solution was not held under plasma jet; rather, the dye was treated with plasma-generated plasma-activated water (PAW). PAW, a chemically rich solution, was generated by exposing distilled water to a plasma jet and then PAW was mixed with a dye solution. As a result, long-lived RONS created by plasma can linger in the PAW and oxidize dye molecules. There has been limited investigation into the use of PAW to treat organic compound-containing contaminated water. The results of both treatment approaches with a large number of experimental factors are described and elaborated on in the following sections. Several experimental parameters in the direct treatment of AB25 were investigated to assess their influence on dye degradation.
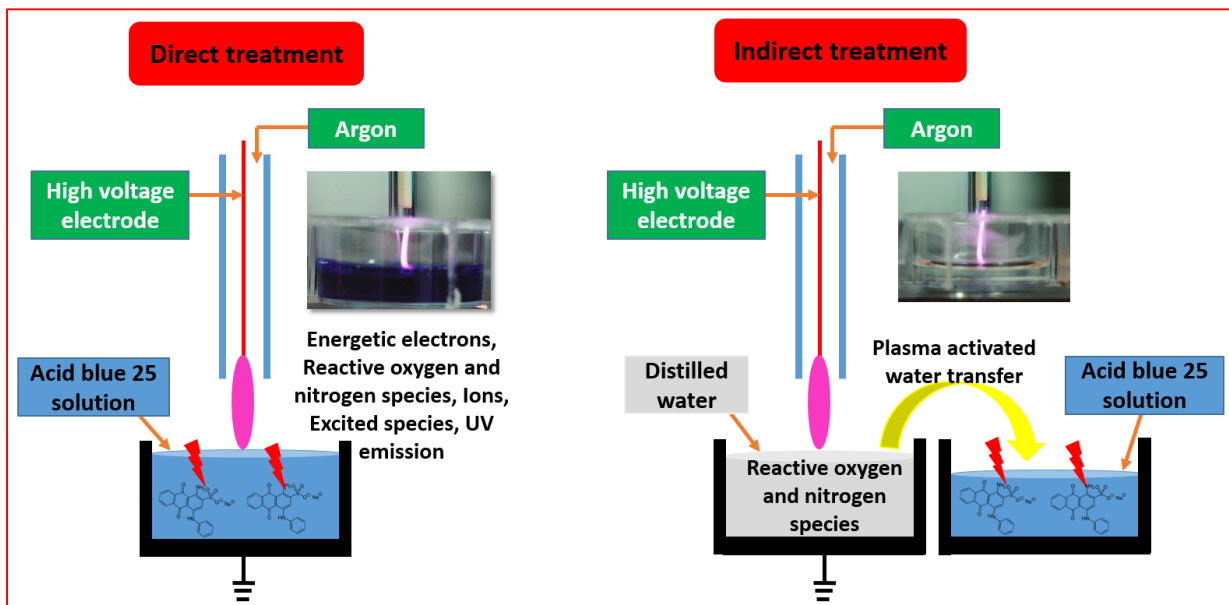
Figure 5.11. Schematics for treating dye solutions directly and indirectly [68].

5.2.1. Effect of experimental parameters (initial concentration, input power, treatment time, discharge gap)

Effect of initial dye concentration

The effect of two initial dye concentrations (25 mg/L and 50 mg/L) on the degradation rate was explored. Figure 5.12 (a) depicts the results of a study in which the dye concentration was held constant while the treatment period was varied and the degradation trend was investigated. Table 4.5 provides information regarding the specifics of the experimentation.

When the dye solution was exposed to plasma, the dye concentration in water rapidly decreased. It was discovered that lowering the dye concentration aided in rapid degradation. Figure 5.12 (b) shows that more than half of the dye was removed in both cases during the first three minutes of plasma treatment. Degradation removal of up to 87 % for 25 mg/L and 73 % for 50 mg/L were measured after 5 minutes. It was found that at concentration of 25 mg/L, total dye elimination was achieved, whereas at double the concentration, removal was approximately 93 % within 10 minutes. The quick degradation during the initial plasma exposure can be attributed to the fact that the majority of plasma-induced reactive species were consumed by dye molecules. However, after a longer treatment, remaining dye molecules may react with reactive species as well as intermediates formed by dye degradation, thereby slowing elimination.
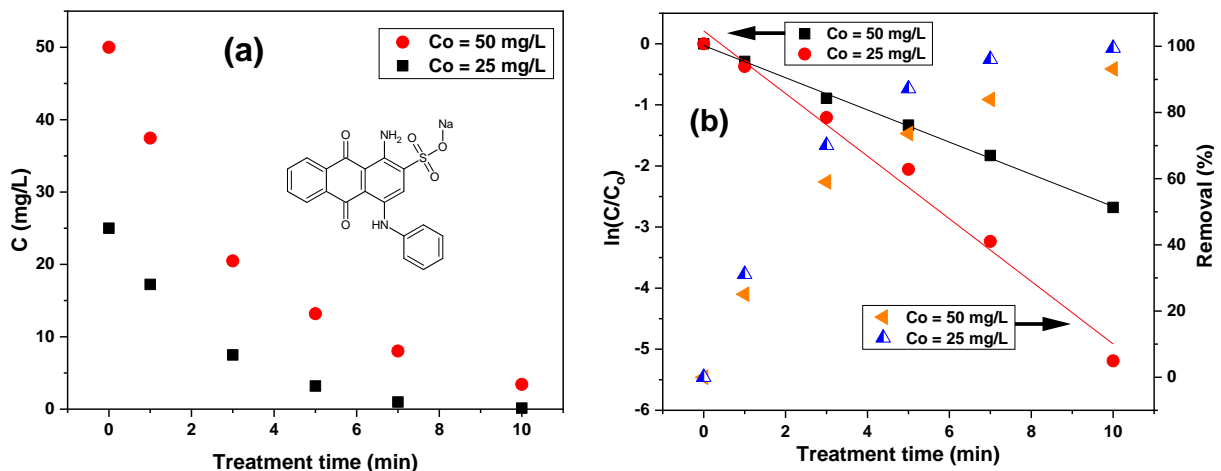
Figure 5.12. Drop in AB25 concentration (C) with treatment time **(a)** and logarithmic decrease in AB25 concentration and removal % with treatment time **(b)** at $V_o = 5$ ml, argon flow 1 slm and P_{mean} at the sample 11 W.

When dye-treated solutions were compared visually, it was determined that when the initial dye concentration was lower, the dye faded after a longer treatment time, as depicted visually in Figure 5.13. However, in higher initial dye concentration solutions, the dye molecules were retained and the solution appeared colorless even after prolonged plasma contact.
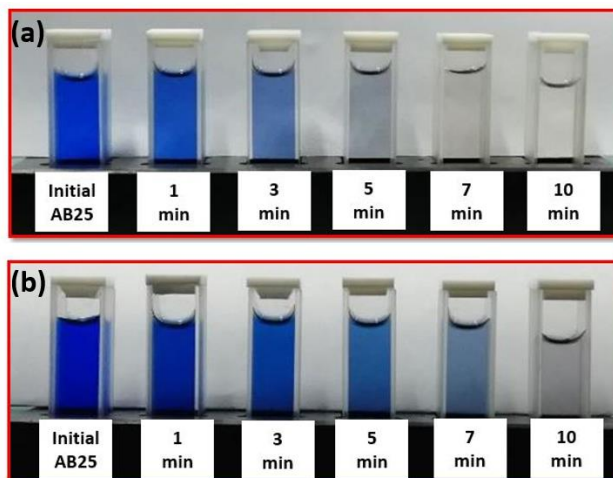
Figure 5.13. The color of AB25 samples changed upon direct treatment with APPJ **(a)** $C_o = 25$ mg/L **(b)** $C_o = 50$ mg/L, experimental conditions, $V_o = 5$ ml, argon flow 1 slm and P_{mean} power at the sample 11 W.

Some authors researched the degradation processes for AB25 dye and studied the role of reactive species, their effect and reactivity at various positions of AB25 molecules. Ghodbane et al. [184], for example, examined the chemistry involved in the breakdown of AB25 by reactive species produced by air plasma. They discovered that plasma-induced reactive species can attack dye molecules in a variety of locations, including the amino, sulfonic and vinylsulfonyl functional groups, which are located far from anthraquinone (one of the most resistive and stable groups having fused aromatic ring). It was revealed that several hydroxylation processes can occur, resulting in the degradation of the quinone group and the production of low molecular weight molecules.

The degradation kinetics study was performed to assess the rate of elimination of AB25. Because the treatment was carried out at different periods, the degradation kinetics patterns were simply predicted. The degradation of AB25 dye at both concentrations was found to be well fitted with a first-order kinetic model and to be in good agreement with the regression coefficient, as shown in Table 5.2. The first-order kinetic is defined by equation (5.12), where k is the rate constant and t is the treatment duration.

$$\frac{C}{C_o} = e^{-kt} \quad (5.12)$$

The time required to remove 50 % of the AB25 dye from water was determined as the half-life ($t_{1/2}$), as described in equation 5.13.

$$t_{1/2} = \frac{0.693}{k} \quad (5.13)$$

According to Table 5.2, the rate constant was high for lower initial concentrations and the treatment time required for 50 % elimination was around two times less than for higher concentrations. It is feasible to suppose that plasma-induced reactive species were present in the same quantity for both initial dye concentrations, but a lower rate constant for higher concentrations suggests that formed intermediates products may quench the plasma-generated reactive species that were responsible for dye degradation. The researchers [142] found almost identical AB25 degradation characteristics when using air plasma discharge; however, the rate of degradation was different since the operating conditions were different than in our investigation.

Table 5.2. Removal rate constants and half-life at two distinct AB25 concentrations.

AB25 concentration (mg/L)	First-order rate constant k (min^{-1})	R^2	$t_{1/2}$ (min)
25	0.512	0.98	1.35
50	0.263	0.99	2.63

* R^2: Regression coefficient

Another important parameter, energy yield, was determined in order to quantify the cost-effectiveness of the plasma system. Because the plasma experiments were conducted in a laboratory, they cannot be directly compared to industrial or commercial scales. The energy yield in terms of energy required (kWh) to remove mg of pollutants was determined in this work and the effect of experimental conditions on energy yield was investigated. The energy yield as a function of AB25 dye elimination is depicted in Figure 5.14 for both initial concentrations. It was discovered that lower removal supported better energy yield, owing to shorter treatment time. The maximum energy yield was 342 mg/kWh for 25 % removal

and 127 mg/kWh for more than 90 % removal at 50 mg/L concentration and 212 mg/kWh for 31 % removal and 68 mg/kWh for complete removal of dye at 2 times lower dye concentration.
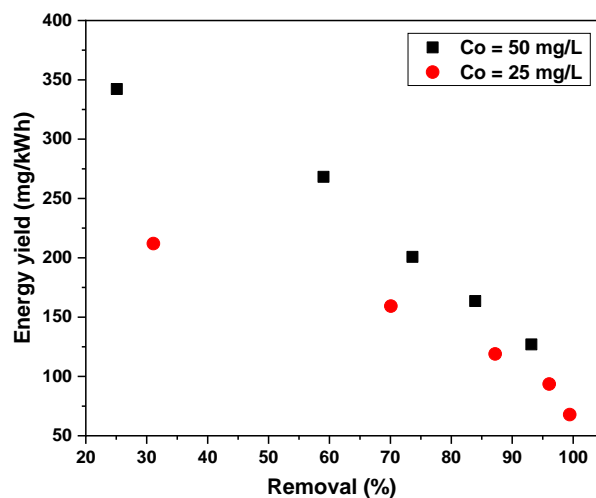
Figure 5.14. Energy yield with removal %, experimental conditions, $V_o = 5$ ml, argon flow 1 slm and P_{mean} at the sample 11 W.

The energy yield for 50 % dye removal was estimated so that the treatment of other selected compounds could be compared. In this study, it was discovered that while the dye removal was held constant (50 %), the energy yield did not vary considerably for both concentrations, for example, the energy yield was about 259 mg/kWh for 50 mg/L and 252 mg/kWh for 25 mg/L at 50 % removal, respectively. The energy yield comparison with other pollutants is explored at the end of this chapter.

The pH and conductivity of plasma-treated solutions were also determined. The pH value for all the plasma-treated samples decreased drastically, as can be seen in Figure 5.15 (a). Lower pH in some way helps to enhance the reactivity of reactive species for dye degradation. Since argon plasma was generated in contact with surrounding air so mainly nitrogen-based species can be formed in the gas phase as well as at the liquid interface, however, these chemical species can be transferred in the liquid and changed their characteristics. Therefore, change in pH is mainly caused by the formation of acidic molecules (such as nitric and nitrous acid) and hydrogen ions (H^+) inside the solution. The concentration of H^+ was also calculated based on the measured pH value, it can be seen that as pH decreased the concentration of H^+ increased almost linearly, as illustrated in Figure 5.15 (a). The conductivity value grew by an order of magnitude throughout the treatment. Smaller ions, such H^+ ions and their abundance in the liquid may increase conductivity. The relationship between conductivity and H^+ ion concentration is depicted in Figure 5.15 (b).
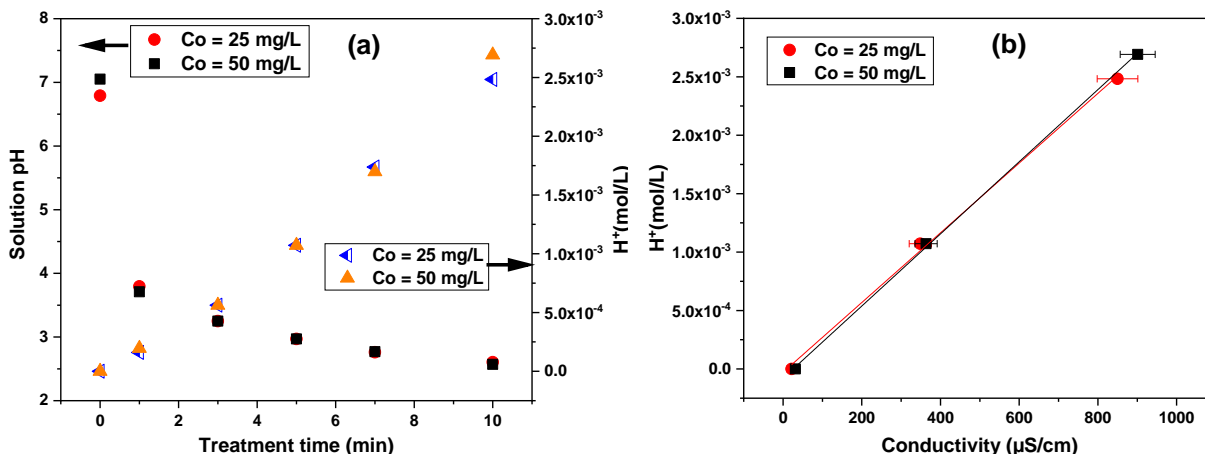
Figure 5.15. The relationship between (**a**) pH and H^+ concentration and treatment duration and (**b**) H^+ concentration and conductivity.

Effect of power deposition

The effect of input power on the degradation of AB25 dye was also examined. The experiment was carried out with a fixed treatment and dye concentration while the input power was varied to assess the effect. More power provided to plasma, as expected, can improve dye degradation. More energy may be delivered to the plasma at higher powers, leading to the formation of more chemically rich reactive species. As previously established by OES experiments, increasing power resulted in a greater intensity of reactive species, meaning a greater quantity of reactive species, which resulted in a favorable influence on degradation. Figure 5.16 displays the effect of input power on dye removal, illustrating that power is critical in removing AB25 dye.
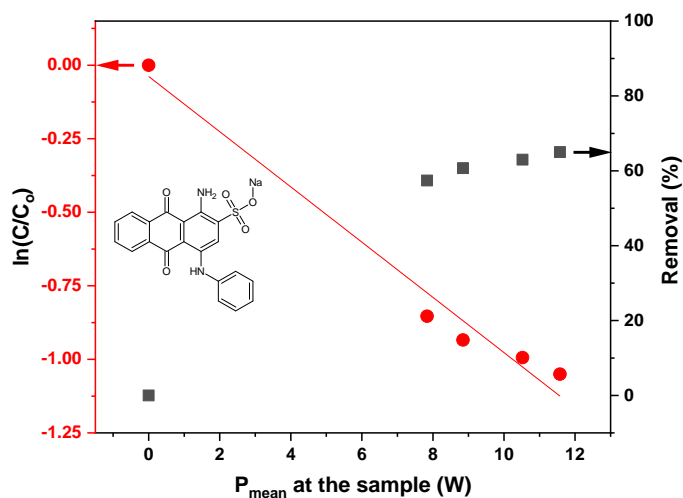
Figure 5.16. The normalized logarithmic decline in AB25 concentration and removal % with power deposition to the sample. Experimental conditions, $C_o = 50$ mg /L, treatment time 5 min, $V_o = 5$ ml, argon flow 1 slm.

The degradation kinetics of AB25 dye with relation to power were investigated while maintaining the treatment time constant. The first-order kinetic reaction was adjusted (as shown in equation 5.14) and instead of time, the power value was taken into account. The goal was to determine whether it was

preferable to increase treatment duration or input power; the rate is shown in Table 5.3. It was discovered that the degradation rate was lower when the input power was adjusted as opposed to the treatment period.

$$\frac{C}{C_o} = e^{-k\prime P} \qquad (5.14)$$

The same half-life formula was used to compute the power required ($P'_{1/2}$) to remove 50 % of the dye; however, in the equation, treatment time was replaced with power, as shown in equation 5.15. It was observed that around 7 W of power was required to remove 50 % of the dye.

$$P'_{1/2} = \frac{0.693}{k\prime} \qquad (5.15)$$

Table 5.3. Removal rate constant and half-life in plasma at varied input powers.

AB25 concentration (mg/L)	Treatment time (min)	First-order rate constant k' (W⁻¹)	R²	P'₁/₂ (W)
50	5	0.093	0.97	7.38

The energy yield was calculated using the amount of input power required to remove 50 % of the dye while keeping the treatment period constant. It was revealed that the energy yield achieved was roughly 203 mg/kWh, which declined when the treatment period was varied. With the obtained energy yield, it can be inferred that 50 % dye removal at variable power during a specific treatment interval is not a good idea. It might be more cost-effective to treat the samples at lower power and for a shorter period.

Effect of the discharge gap

The discharge gap is the distance between the powered electrode's tip and the liquid surface and it indicates how close or distant the electrode can be placed to generate a plasma discharge. The experiment was carried out with three different spacing and plasma was produced in each case, although with varying intensities. It was determined that dye degradation was more evident at 10 mm of a gap, which is why, in the case of pin-APPJ, the entire experiment was carried out at the gap where significant dye removal occurred. The dye removal was not considerably affected by the various discharge gaps, as shown in Figure 5.17, but it was slightly higher at 10 mm than it was at the other two gaps.
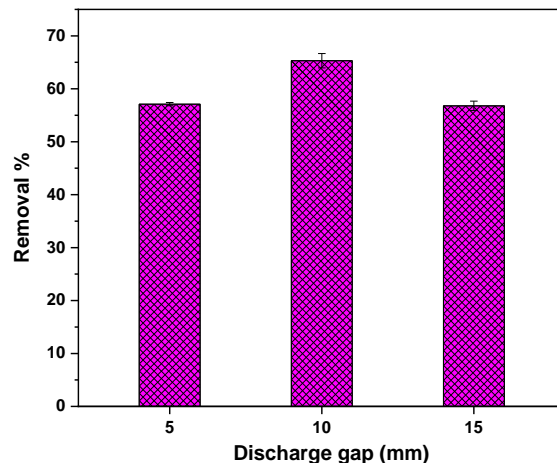
Figure 5.17. The percentage of AB25 removed varies with the discharge gap. Experimental conditions, $V_o = 5$ ml, argon flow 1 slm, $C_o = 50$ mg/L, treatment time 5 min and P_{mean} at the sample 11 W.

5.3. Effect of Plasma activated water on Acid Blue 25 dye removal

Water purification using PAW is a new and exciting area of study; PAW can be particularly effective in the treatment of water used in agricultural applications [68]. Organic pollutants, for example, have been found in natural water bodies as a result of their widespread use in industry and agriculture; as a result, many contaminants found in agricultural water can impair crop productivity while eroding soil quality. PAW contains several reactive species that can aid in the degradation of organic contaminants and pathogens [185]. Furthermore, the presence of various reactive species in PAW, particularly RNS, can act as a fertilizer to promote plant development and protect it against disease [186]. PAW can also help remove organic contaminants created by plant roots, which can be harmful to plant growth.

PAW was created by using pin-APPJ for the treatment of distilled water at a different treatment times. The main idea was to investigate the influence of long-lived RONS on dye degradation. The PAW was analyzed using colorimetric techniques in order to quantify the RONS. A UV/Visible spectrophotometer was used to determine the quantities of NO_3^-, NO_2^- and H_2O_2 in PAW and the reagents specified in Table 5.4 were used to compute RONS. For example, to quantify the amount of H_2O_2, titanium oxysulfate ($TiOSO_4$) reagent was added to PAW, where H_2O_2 in PAW can interact with $TiOSO_4$ to form a yellow color, which was recorded at the absorbance of 407 nm. NO_3^- and NO_2^- levels, on the other hand, were determined using Griess assay kits (NO_3^- test: 1.09713.0002, NO_2^- test: 1.14776.0002, Merck). In the case of NO_3^-, sulphuric acid (H_2SO_4) and nitrate reagent were used and the absorbance of the resulting complexes was measured at 357 nm. For NO_2^- concentration detection, H_2SO_4 and a nitrite reagent were used and absorbance was quantified at 525 nm.

Table 5.4. Reagents for RONS measurement in PAW.

Chemical species	Reagent	Absorbance wavelength (nm)
H_2O_2	$TiOSO_4$	407
NO_3^-	H_2SO_4 & nitrate reagent	357
NO_2^-	H_2SO_4 & nitrite reagent	525

After the characterization of PAW, it was determined that each species had a specific quantity; for example, Table 5.5 reveals that H_2O_2 had a higher concentration than the other two chemical species. Probes were also used to measure the pH and conductivity of PAW; it was revealed that PAW became acidic as the pH decreased and conductivity increased.

Table 5.5. PAW physicochemical properties after 10-minute plasma treatment. Experimental conditions, $V_o = 5$ ml, argon flow 1 slm, P_{mean} at the sample 11 W.

pH	Conductivity (μS/cm)	H_2O_2 (mg/L)	NO_3^- (mg/L)	NO_2^- (mg/L)
2.62	708.4	255	222	0.06

Many reactive species can be created in the gas phase, transferred to the region where plasma-liquid interaction take place, and those reactive species can combine to make other reactive species. However, Henry's law provides an estimation when analyzing the transfer of reactive species (for example, H_2O_2, HNO_3, HNO_2, O_3 and so on) from the gas-liquid interface to bulk liquid. H_2O_2 is considered to have the greatest Henry's constants by at least an order of magnitude greater than other RONS, allowing for quicker diffusion in liquid. H_2O_2 is a typical reactive species that is formed in PAW and has an oxidation potential of 1.77 V. It can also react with contaminants and breakdown them in water.

The creation of H_2O_2 can be attributed mostly to the dominating recombination reaction of short-lived species $HO^\cdot$ radicals in gas-phase during plasma-liquid interaction. The formation of H_2O_2 is also a good indication of $HO^\cdot$ formation in plasma-based liquid treatment.

Various RNS (HNO_3 & HNO_2) considered hydrophilic species can form in the gas phase as well as at the plasma liquid interface. These species, which may diffuse through liquids, may contribute to NO_2^- and NO_3^- generation in the PAW and lower the pH. According to the literature, peroxynitrous acid (ONOOH) can also be generated in the presence of H_2O_2, NO_2 and H^+ and at lower pH levels and it is a highly reactive oxidizing species with an oxidation potential of 2.0 V [68]. Of course, a broad variety of chemical reactions can be involved in the prediction of those RONS in the liquid phase; for example, the aqueous chemistry of various plasma-induced reactive species can change the concentration of each RONS and produce new RONS.

PAW was created and then mixed with an AB25 dye-containing solution to investigate degradation. More experiments were carried out depending on the measured value of each chemical species in PAW. For example, individual solutions of (I) H_2O_2, (II) NO_3^-, (III) NO_2^- and (IV) $H_2O_2 + NO_3^- + NO_2^-$ were

mixed with AB25 dye solution. PAW and chemical species (I)-(IV) containing AB25 dye solutions were kept and evaluated using a spectrophotometer regularly for up to 17 days to determine the contribution of PAW and individual reactive species in dye degradation.

The effect of PAW and specific chemical species on dye removal is shown in Figure 5.18 (a). No dye elimination was identified on the day that PAW and chemical ((I)-(IV)) were mixed, indicating that dye concentration remained constant. Within a few days, the color started to disappear.

The largest effect of degradation was associated with PAW and H_2O_2 solutions in 17 days. The chemical solutions such as (II)-NO_3^- or (III)-NO_2^- have a negligible effect on dye removal for up to 17 days. The degradation of AB25 in solution (I)-H_2O_2 was rapid after 8 days, reaching close to 50 % in 17 days. The removal of AB25 was higher with a mixture of all three reagents (IV) in the first 10 days, but both cases (I & IV) had roughly the same influence between 14 and 17 days. These effects could be attributed to the creation of extra reactive species in the solution in the presence of H_2O_2 + NO_3^- + NO_2^-, which could have contributed to the dye's rapid degradation in the first 10 days. Figure 5.18 (b) displays the dye color change in the (I)-(IV) chemical solution after 17 days.
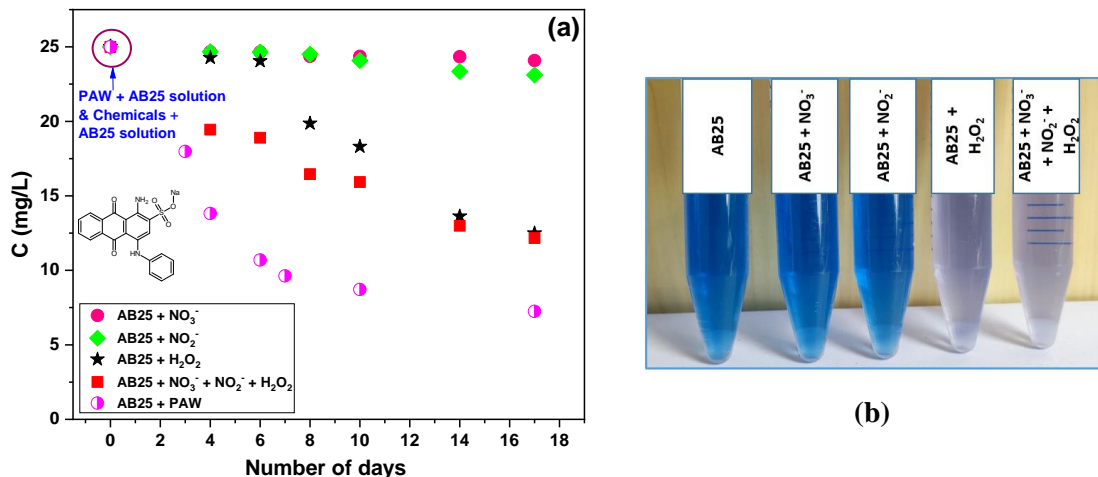
Figure 5.18. (a) Effect of PAW and prepared RONS solutions on the degradation of AB25. The initial concentration of AB25 was 25 mg/L. The concentration of AB25 was intermittently measured for 17 days.

The most efficient dye removal was identified when PAW was mixed with dye solution, with approximately 71 % elimination in 17 days, which was greater than with individual and combinations of chemical species. As previously stated, PAW is a source of a wide variety of reactive species; it is possible that other reactive species that have not yet been identified may play a significant role in dye removal. On the subject of reactive species, ONOOH in PAW may participate in dye degradation; other articles have also demonstrated this [187,188].

An additional experiment was carried out in which dye was held for several days under acidic conditions to test if dye removal may occur by hydrolysis at low pH. The pH of the dye-containing solution was decreased using hydrochloric acid (HCl); the pH was kept around 3. The results of the investigation showed that no dye was removed after 17 days in acidic conditions.

Another experiment was performed to assess indirect treatment and the contribution of long-lived reactive species, in which the direct plasma treated dye solution was analyzed both immediately and after being kept and examined for 17 days. The purpose was to investigate the role of plasma-generated long-lived reactive species in the removal of leftover dye in the solution after direct treatment. The first dye solution was subjected to a plasma jet for 5 minutes at two concentrations (25 mg/L and 50 mg/L). After the treatment, the final dye concentrations in both solutions were determined to be 16 mg/L for 50 mg/L and 3 mg/L for 25 mg/L, as indicated in Figure 5.19 by the circle. The concentration of both plasma-treated dye solutions was then monitored for 17 days. There was a minimal reduction in dye concentration for both concentrations over the 17-day timeframe.
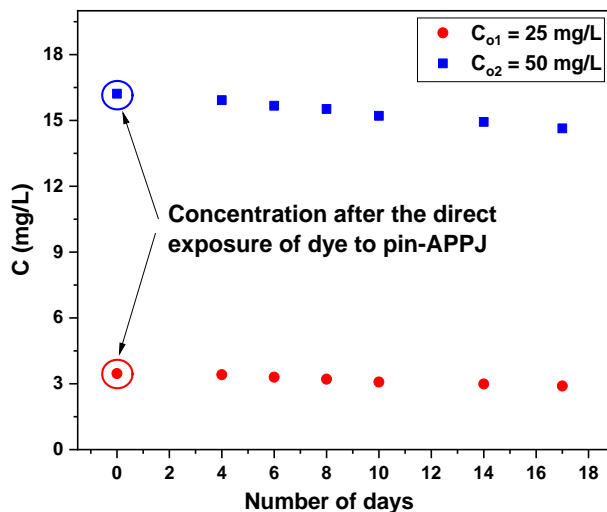
Figure 5.19. The extended effect of long-lived species on AB25 decomposition after direct plasma treatment. Experimental conditions, C_{o1} = 25 mg/L and C_{o2} = 50 mg/L, treatment time 5 min, argon flow 1 slm, V_0 = 5 ml, P_{mean} at the sample 11 W. AB25 concentrations were measured immediately after direct plasma treatment and then on regular basis for the next 17 days.

It was revealed that H_2O_2 was more dominant in the removal of dye during indirect treatment with PAW and individual chemical solutions. After the case of dye solution treated with direct plasma, virtually little removal in 17 days could indicate insufficient H_2O_2 production. One hypothesis is that in the presence of dye, most plasma-induced $HO \cdot$ radicals at the liquid interface react with dye molecules, resulting in a decreased contribution to H_2O_2 generation. Another hypothesis is that H_2O_2 was generated but dissociated as soon as it was produced because plasma is a source of UV radiation and UV light may dissociate H_2O_2 into $HO \cdot$.

5.4. Removal of Disperse Red 1 dye

DR1 has different properties than AB25 and it was the second dye chosen as a model compound for the treatment by pin-APPJ. It was revealed that this type of dye was treated with cold atmospheric plasma for the first time. Because of their low solubility in bulk water solutions, disperse dyes tend to enrich on the liquid surface, resulting in a higher average concentration at the liquid surface than in the bulk solution.

The degradation pattern for DR1 differed from that of AB25; the concentration of DR1 was considered 38 mg/L for comparative reasons based on molar ratio; the molar ratio for 38 mg/L of DR1 and 50 mg/L

of AB25 was the same 0.12 mM. Figure 5.20 (a) demonstrates that after exposing plasma to DR1 dye-containing solution, the concentration decreased with treatment time. As expected, a longer treatment time favored higher degradation since the DR1 solution was exposed to reactive species for a longer period. The degradation was the fastest within the first 3 minutes after plasma treatment. Because DR1 is a non-ionic molecule, it preferentially accumulates at the surface. As a result, rapid degradation after initial plasma exposure can be explained by the rapid oxidation of surface-enriched DR1 molecules by diverse reactive species during plasma-liquid interaction.

Although no study on the removal of DR1 by plasma was done, the researchers explored the Photo-Fenton-AOP treatment of DR1 and the degradation mechanism based on HO· radicals generated by the Fenton procedure [170]. According to studies, HO· can react with DR1 via an electrophilic addition reaction to the aromatic ring, as well as attack the azo bond in DR1, resulting in degradation and the formation of smaller molecules.
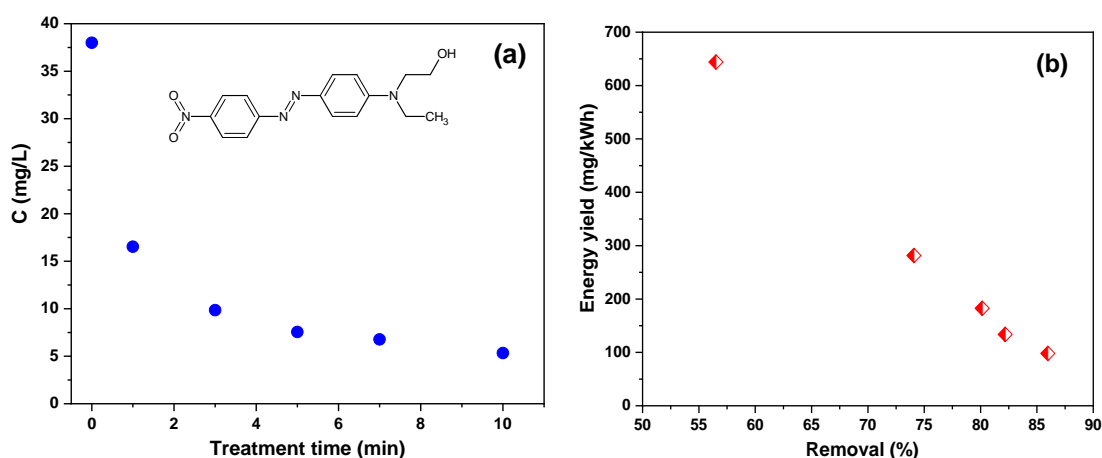
Figure 5.20. (a) The change in DR1 concentration as a function of treatment time (b) energy yield as a function of removal %. Experimental conditions, $C_0 = 38$ mg/L, $V_0 = 5$ ml, argon flow 1 slm and P_{mean} at the sample 10 W.

Because this form of plasma source can generate a significant number of reactive species at the liquid surface and most dye molecules can come into contact with these reactive species, plasma can be very energy efficient for these types of compounds where the concentration of target molecules is higher at the liquid surface (e.g. Disperse dyes, PFOS, surfactants, etc). For example, after calculating the energy yield, it was found that after 1 minute of treatment, the elimination rate was 56 % and the energy yield was 644 mg/kWh (shown in Figure 5.20 (b)). However, after 10 minutes of treatment, the elimination rate increased to 86 %, despite the fact that the energy output was around six times lower.

The pH was also examined and it was found that the pH of plasma-treated solutions was lowered; after 10 minutes of treatment, the pH dropped from 7.9 to 3.0. The pH change, as previously noted, can be attributed to the formation and diffusion of RNS in the solution as a result of argon plasma contact with ambient air.

5.5. Removal of pharmaceutical and industrial chemical

The pin-APPJ was used to treat pCBA and DCF-containing water solutions under almost identical experimental conditions as dye removal and the findings were discussed briefly. The degradation pattern

for compounds was explored and it was observed that the oxidation of both compounds varies significantly, as discussed below.

5.5.1. Effect of initial concentration and treatment time

Treatment studies with pCBA and DCF were conducted and the obtained results are discussed. Figure 5.21 displays the degradation pattern of plasma degradation of pCBA in distilled water solution. The pCBA molecule is made up of a single aromatic ring with a hydroxyl-carboxyl group and a chlorine atom attached at the para position. It only reacts with a few and specialized substances, particularly with highly oxidative chemical oxidants. In this investigation, the concentration of pCBA decreased considerably with treatment time for both initial concentrations. The reduction was more noticeable in the first 3 minutes, with more than half of the pCBA disappearing, which is connected to the number of reactive species that interacted with a high concentration of pCBA. Longer plasma exposure may allow the transition product created just after pCBA breakdown to become more noticeable, quenching the newly formed reactive species in the plasma. Overall, the data imply that pCBA is destroyed after a longer treatment period.
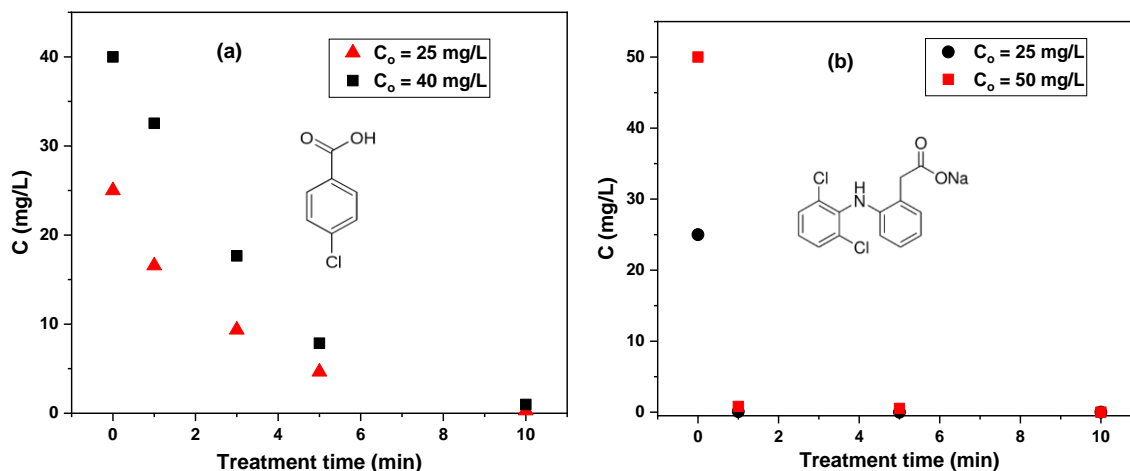
Figure 5.21. Concentration variation with treatment time, **(a)** pCBA (C_o = 25 mg/L and C_o = 40 mg/L) and **(b)** DCF (C_o = 25 mg/L and C_o = 50 mg/L). Experimental conditions, V_o = 5 ml, argon flow 1 slm, P_{mean} at the sample 10 W.

Some papers investigated the degrading behavior of pCBA in various AOPs, primarily using HO· radical attack [178,189]. Because there was evidence of HO· generation by pin-APPJ in this study, the degradation of pCBA associated with HO· radicals can be interpreted similarly to the literature. It has been demonstrated that continuous HO· attack on pCBA molecules leads to pCBA disintegration via the hydroxylation process. For example, the presence of a C-Cl bond in pCBA can be first cleaved by chloro-aromatic degradation, but HO· can attack the carboxyl group of the aromatic ring, which is likely to undergo additional degradation. Overall, this leads to ring breakage and subsequent degradation into small fragments, as well as mineralization into H_2O, CO_2 and HCl. As plasma contains a large number of reactive species; additional reactive species could speed up the decomposition of pCBA during the plasma treatment. However, determining the role of individual species in pCBA or other chemical degradation is out of the scope of this thesis.

The kinetics of pCBA elimination was investigated and the results are shown in Table 5.6. The degradation pattern was well explained by a first-order kinetic model. At lower concentrations, the rate constant was greater. The pCBA degrades similarly to AB25 dye (as previously observed with AB25), however, the rate of removal differs, with pCBA removing at a slower rate than AB25. Of course, the chemical structures and reactivity of these substances differ, resulting in a varied decomposition rate. The predicted half-life for pCBA elimination is shown in Table 5.6, which was lower for lower initial concentrations.

Table 5.6. Degradation rate constants and half-life at two distinct pCBA concentrations.

pCBA concentration (mg/L)	First-order rate constant k (min^{-1})	R^2	$t_{1/2}$ (min)
25	0.438	0.98	1.58
40	0.377	0.99	1.83

During the plasma treatment of DCF solution, we observed that DFC decomposed faster compared to pCBA, as seen in Figure 5.21 (b), with nearly total removal occurring within the first 1 minute of treatment. The reason could be that DCF reacted with the bulk of plasma-generated reactive species, resulting in fast elimination. Several papers have claimed that DCF can react with HO· as well as other long-lived reactive species, such as O_3, at a high rate, which could explain the quicker decomposition. Of course, additional reactive species produced by plasma could also contribute to DCF degradation. The degradation mechanism of DCF compound has been briefly investigated in the subsequent chapter.

The pH was determined in both situations and the calculated pH, as well as the H$^+$ values, are shown in Table 5.7. The pH was much lower after 10 minutes of treatment, but the initial concentration did not play a significant effect on the final pH, as both substances and concentrations had about the same final pH. The concentration of H$^+$ rose as the pH decreased, owing to the transport of RNS from the gaseous phase to the liquid medium.

Table 5.7. Changes in pH and concentration of H$^+$ for pCBA and DCF samples with treatment time.

	Concentration (mg/L)	pH		H$^+$ (mol/L)	
		Control	After 10 min	Initial	After 10 min
pCBA	25	4	2.57	9.77×10^{-5}	2.69×10^{-3}
	40	4	2.65	9.77×10^{-5}	2.24×10^{-3}
DCF	25	6	2.66	10^{-6}	2.19×10^{-3}
	50	6	2.69	10^{-6}	2.04×10^{-3}

Figure 5.22 depicts the energy yield as a function of elimination percent for both compounds. At a pCBA concentration of 40 mg/L, the maximum energy yield was 269 mg/kWh for 34 % removal, while the lowest was 79 mg/kWh for 95 % elimination. However, at a starting concentration of 50 mg/L, the energy yield for DCF elimination climbed to 1776 mg/kWh for 98 % removal, which is much higher than pCBA.
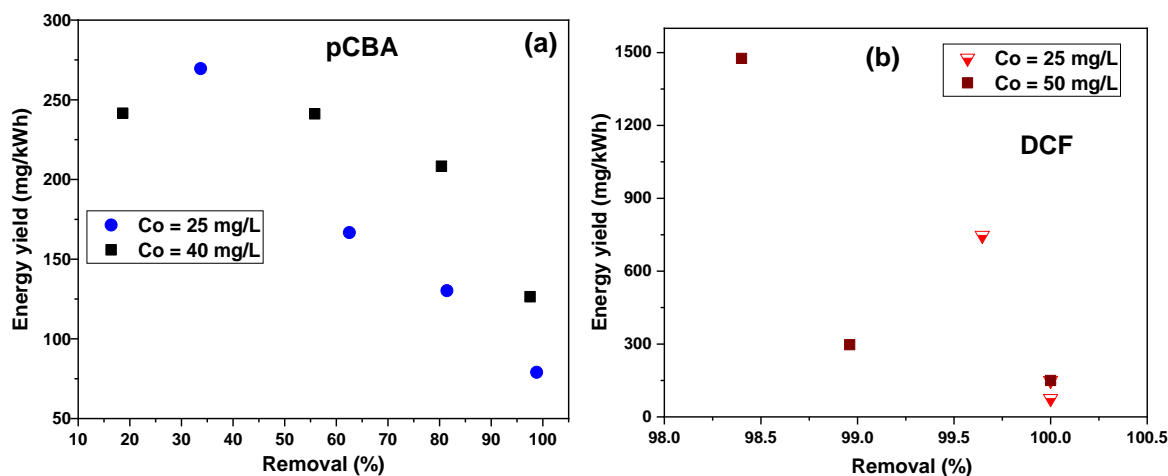
Figure 5.22. Energy yield function of removal **%** for **(a)** pCBA (C_o = 25 mg/L & 40 mg/L) and **(b)** DCF (C_o = 25 mg/L & 50 mg/L). Experimental conditions, V_o = 5 ml, argon flow 1 slm, P_{mean} at the sample 10 W.

5.5.2. Comparison between energy yields for different compounds

Table 5.8 compares and displays the energy yield at 50 % for all selected substances. The key reason for considering the 50 % removal criteria was to compare pollutants because in all cases, at least more than 50 % removal was detected. As the results reveal, each molecule has a varied removal rate under plasma and the energy yield was dependent on numerous experimental conditions such as the nature of the pollutants and their concentrations. The result indicates a difference in order of magnitudes concerning energy yield. The energy yield for DCF was found to be around 2 to 6 times that of the other pollutants studied. After DCF, DR1 elimination resulted in a high energy yield, at least double that of AB25 and pCBA. At low concentrations, the energy yield of AB25 and pCBA was nearly identical, but it differed at higher concentrations. Overall, taking into account all of the data, the highest energy yield was obtained as follows: DCF > DR1 > pCBA > AB25, showing that plasma can be more energy efficient for pollutants like DCF and DR1.

Table 5.8. Comparison of energy yields for each compound (excluding DCF) based on 50 % removal.

Compounds	C_o (mg/L)	Removal %	Energy yield (mg/kWh)
DCF	25	99	747
	50	98	1476
pCBA	25	50	253
	40	50	354
AB25	25	50	252
	50	50	259
DR1	38	~50	644

CHAPTER 6

6. Treatment of contaminated water by using Multi-needle electrodes atmospheric pressure plasma jet

The findings of the pin-APPJ treatment revealed the influence of parametric variables on the degrading behavior of selected OMPs. Although plasma can nearly eliminate most OMPs, the single pin-APPJ, due to its limited interaction volume, is inadequate for treating large amounts of water. A new plasma source is known as multi-needle electrodes (3 jets)-APPJ was designed and constructed, and plasma was created over the liquid surface. The new plasma source created a wide contact interface between plasma and liquid, allowing chemically rich reactive species to interact with polluted water efficiently. Plasma was also produced over the recirculated liquid surface to enhance the plasma liquid contact area and mixing, allowing more OMPs to come into contact with the plasma. This chapter explores the newly developed plasma source, first the electrical and optical characterization, and then the treatment of OMPs with and without a recirculation system, taking into account a wide range of degradation-influencing experimental parameters.

6.1. Electrical and optical characterization

The electrical and optical properties of the multi-needle electrodes-APPJ system were measured. The outcomes of both investigations are discussed below.

Electrical measurement

The electrical characterization was carried out under various conditions to confirm that the plasma device can be operated efficiently at varied input voltages, currents, and power deposition. The electrical characteristics of this plasma source were likewise comparable to pin-APPJ in general, but the electrical discharge parameters changed quantitatively due to different operating conditions.

The electrical characterization was performed when AB25 dye-containing solution was placed under a plasma jet, as shown in Figure 6.1 (a). Figure 6.1 (b) depicts the recorded voltage and current waveforms when the sample's power deposition is adjusted. Varying the power from the RF power supply distorts and alters the amplitude of the voltage and current, resulting in changes in power deposition to the sample.
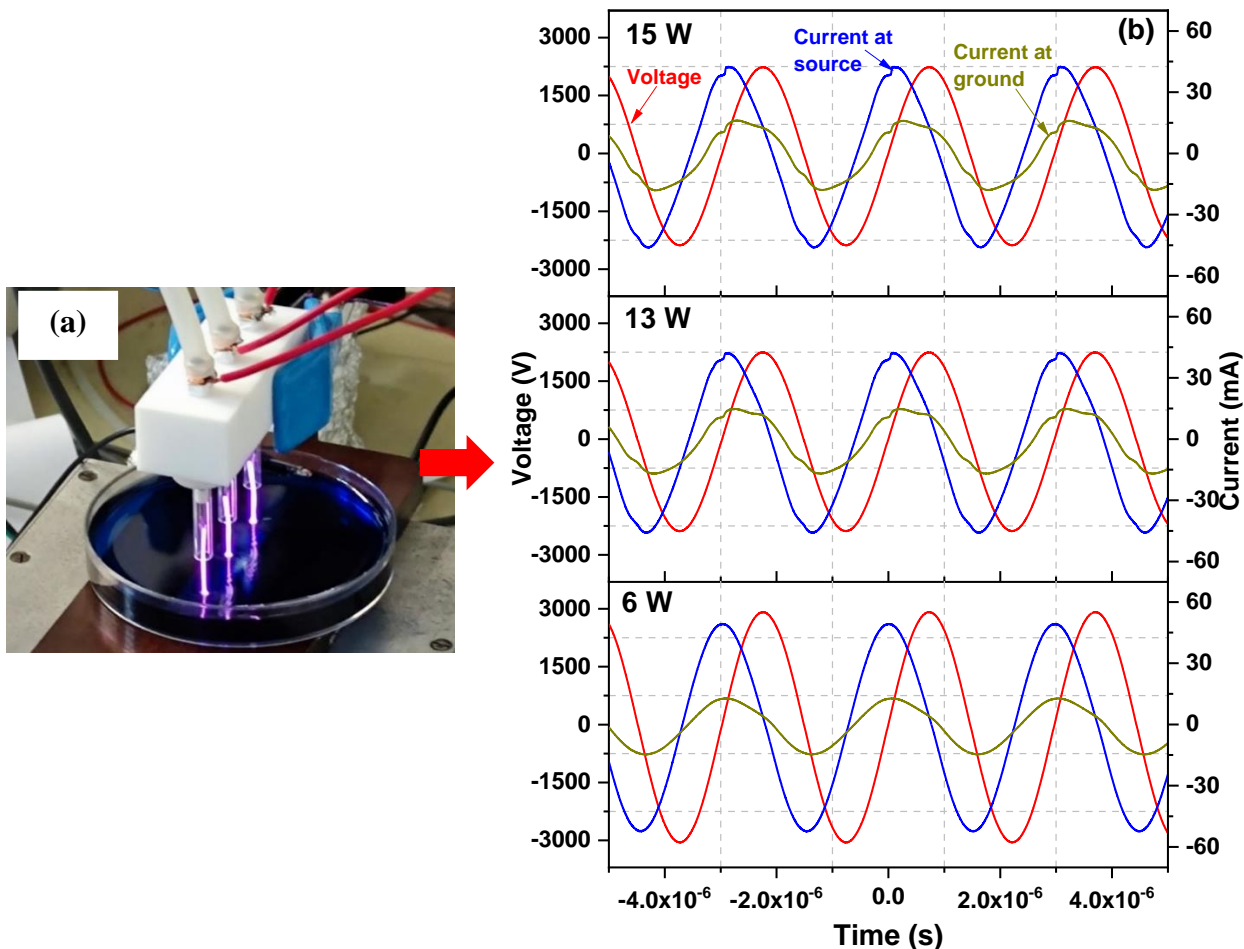
Figure 6.1. (a) Plasma (3-jets) in contact with AB25 dye solution, **(b)** recorded waveforms utilized to determine three distinct powers deposited to the sample. Experimental conditions, $V_o = 30$ ml, argon flow 2 slm.

Figure 6.2 (a & b) depicts the outcomes of the experiment in the V-I characteristics of a plasma system. The RMS voltage and current values varied linearly before plasma ignition. The greater voltage was achieved by progressively increasing the power supplied by the RF power supply. When the discharge was ignited, the voltage was significantly reduced because the voltage required to maintain the plasma was lower than the initially ignited voltage. It should be noted that the RMS voltage given is not necessarily identical to the breakdown voltage. The current delivered to the source was significantly higher than the current at the ground after plasma ignition. Overall, after plasma ignition, as the power from the RF power supply increased, the plasma remained ignited even when the voltages at the source were not considerably changed and the current at the sample rose above the values at which the plasma was first ignited.

71
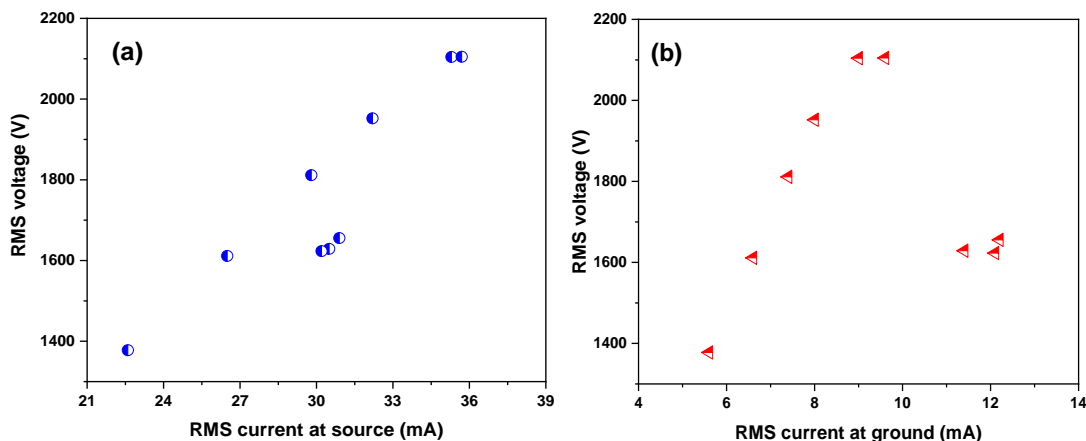
Figure 6.2. V-A characteristics reflect RMS voltage as a function of RMS current at **(a)** the source **(b)** the sample. Experimental conditions, V_o = 30 ml, argon 2 slm.

The power delivered in two distinct circuits (at the source and the sample) was measured. After ignition, the power delivered to the source was approximately 6 W-18 W and the power delivered to the sample was 5.8 W-16 W. The power deposited in the sample was regarded as the power consumed during OMPs oxidation.
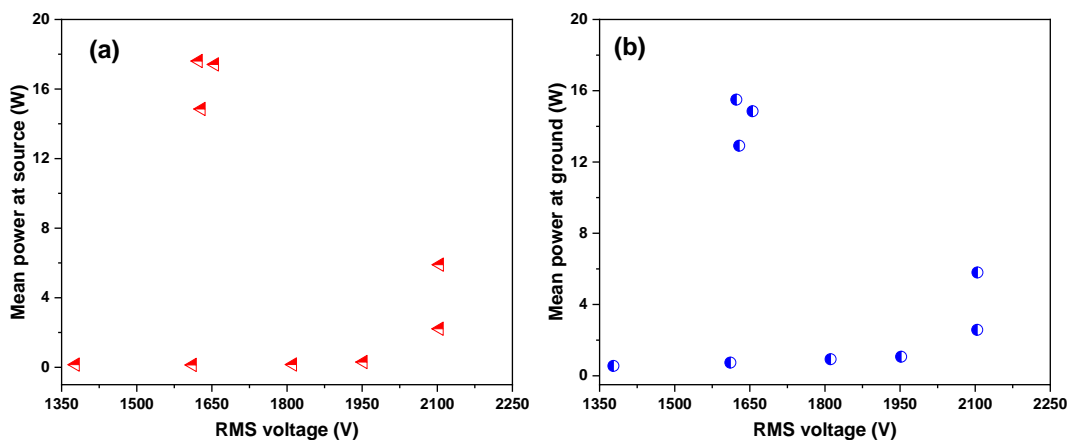
Figure 6.3. Variation of mean power (delivered in two distinct circuits of a plasma system) as a function of RMS voltage **(a)** mean power at the source **(b)** mean power at the sample. Experimental conditions, V_o = 30 ml, argon 2 slm.

Optical measurement by OES

The generation of reactive species during plasma interaction with AB25 dye solution was studied using OES. The recorded emission spectra, shown in Figure 6.4, clearly demonstrate distinct RONS and excited argon lines inside the discharge. It was revealed that the emission intensity of HO· and N_2 (SPS) was greater than that of NO and N_2 (FNS) in the spectral region from 200 nm to 450 nm. From 700 nm to 1000 nm, primarily argon lines and two atomic oxygen lines (O·) occurred. The chemical events involved in the production of each reactive species, as well as information about the band and line electronic transitions, are briefly reviewed in Chapter 5. It was also discovered that the optical properties, in this case, were nearly identical to pin-APPJ, but the emission intensities differed. Overall, OES spectra demonstrated that the production of HO· and O· mostly facilitates the decomposition of OMPs in water.
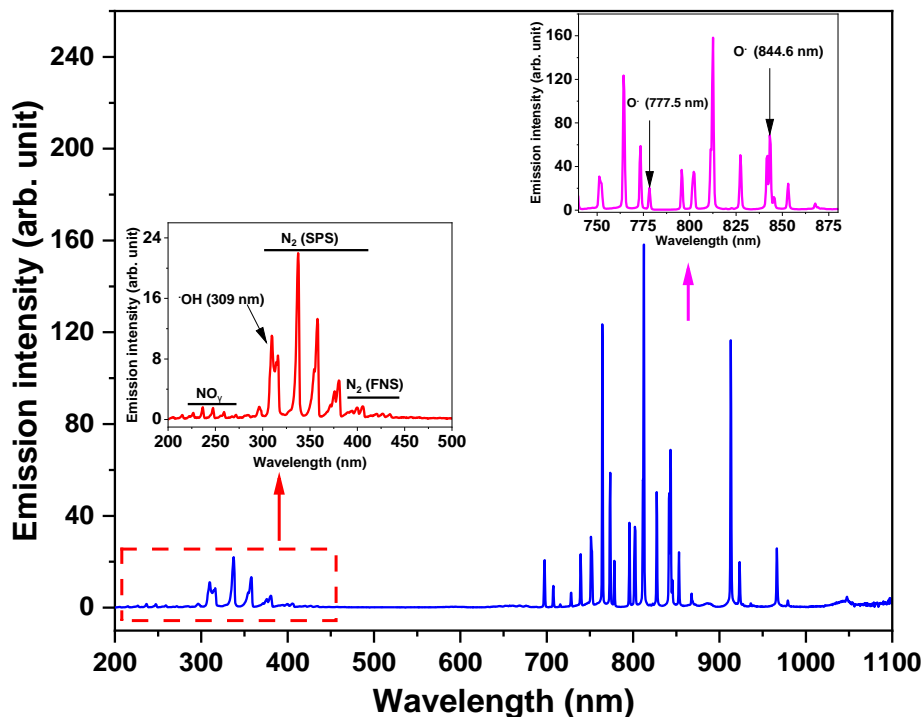
Figure 6.4. The emission spectra of argon - APPJ when it comes into contact with ambient air and a liquid surface. Experimental conditions, V_o = 30 ml, argon flow 2 slm, P_{mean} at the sample 15 W, and integration time 100 ms.

The effect of power deposition on the emission intensities of RONS and argon lines has also been studied; the results are given in Figure 6.5 (a). Except for certain argon lines, most reactive species' emissions grew with power increased. The intensity of the emission at greater power was divided by the intensity at the other power levels (i.e. intensities/intensities at maximum power), as shown in Figure 6.5 (b), to determine which reactive species was more influenced by the provision of input power. Among all created reactive species, the emission intensity of HO· and O· (777.5 nm) rose significantly with power. In contrast, the intensity of argon lines at 763.5 nm was increasing and then decreasing with power increase.
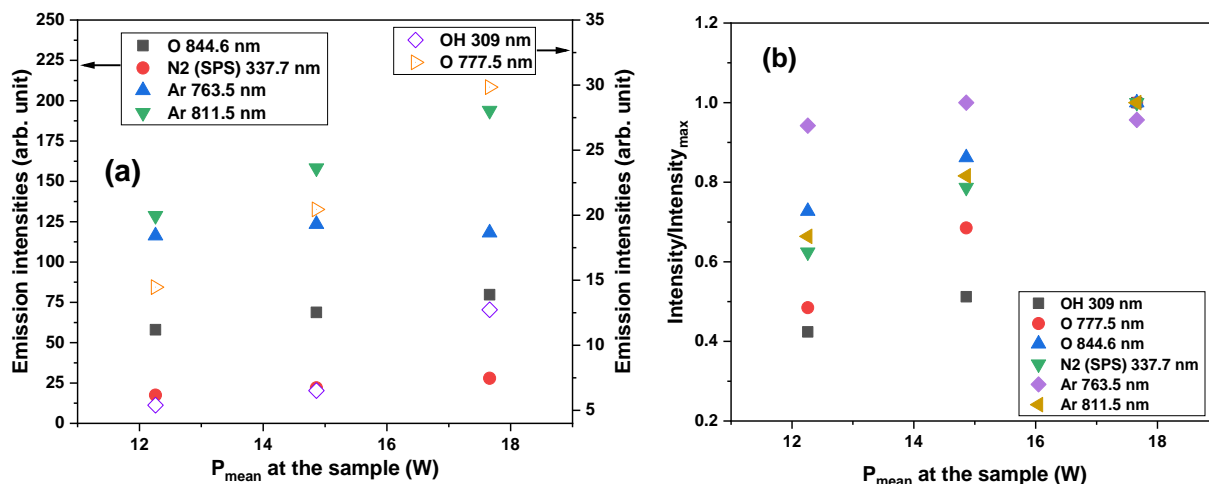
Figure 6.5. **(a)** The intensity of excited species emission, and **(b)** intensity ratio as a function of various input powers (power in contact with the sample). Experimental conditions, $V_o = 30$ ml, and argon flow 2 slm.

Optical measurement by iCCD

The 3 pin-APPJ iCCD imaging was performed to record the emission from all three jets with and without filters. During the imaging, a petri dish entirely filled with 60 ml of distilled water was placed beneath the plasma jet. The flow rate of argon was adjusted from 2 slm to 3 slm. First, images were gathered without plasma to determine the locations or coordinates of the glass tubes, needle electrodes, and liquid surface, and geometry could be sketched in MATLAB during image processing after the plasma was ignited. The images without plasma are shown in Figure 6.6.
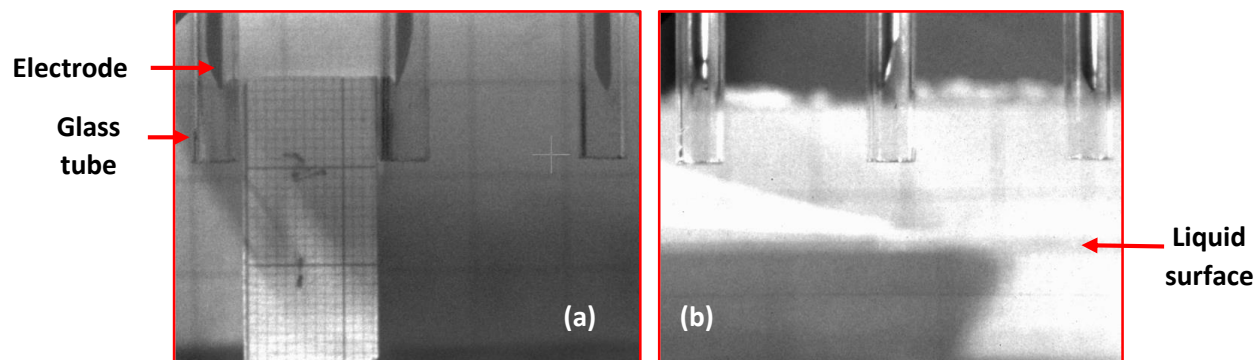
Figure 6.6. The iCCD images without plasma, **(a)** with scale, and **(b)** with a liquid sample. Acquisition parameters, gain 0, exposure time 100 ms, gate pulse width 75 ms.

Figure 6.7 illustrates images captured with plasma at both argon flow rates. The brighter emission was dispersed all along the jets in both cases, although the intensity of the emission was slightly lower downstream of the jet in the case of 3 slm.
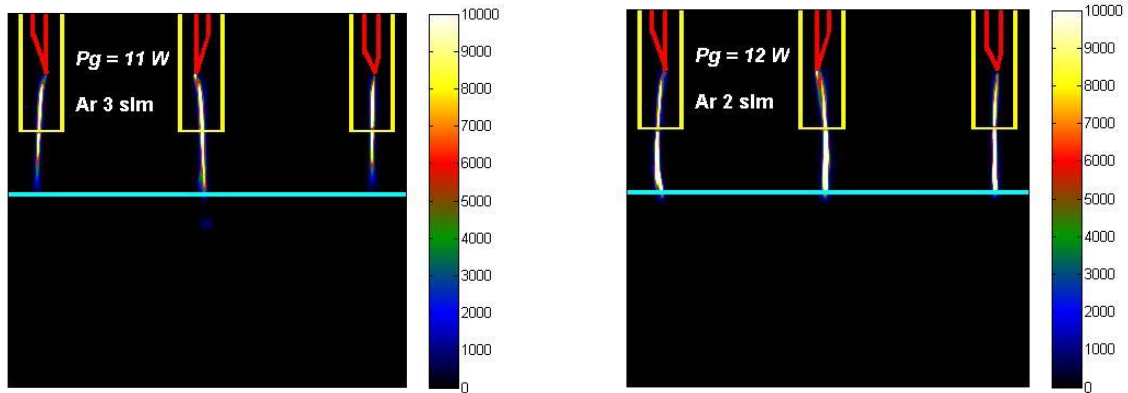
Figure 6.7. The iCCD images of 3 pin-APPJ. Acquisition parameters, gain 0, exposure time 20 ms, gate pulse width 3 ms.

The images were captured using bandpass filters in order to determine the spatial distribution of various reactive species in plasma jets, which are critical in water treatment. During image processing, the properties of selected filters (transmission characteristic) and camera specifications (photocathode quantum efficiency) were also taken into account. The intensity scale of the images was kept unchanged in some instances so that the recorded images with filters could be compared. The specification of each selected band bass filter with appropriate transmission percentage at the line of interest can be found in detail in Chapter 4.

Figure 6.8 depicts the images obtained with the 310 nm and 780 nm filters. A filter with a central wavelength of 310 nm was employed to see spatially resolved emissions of HO· in combination with (SPS). The highest HO· and N_2 (SPS) emission occurred closest to the liquid surface in the case of 2 slm, while the emission was less intense and the emission profile was thinner in all three jets at 3 slm. A 780 nm filter was utilized to collect spatially resolved emissions from O· and excited argon. Both species were detected at both flow rates, but their emission intensities were lower than those of HO· and N_2 (SPS). The brighter intensity of O· and excited argon was particularly visible in the center of jets. The stronger emission intensity ascribed to the may be more excitation occurs in that area.
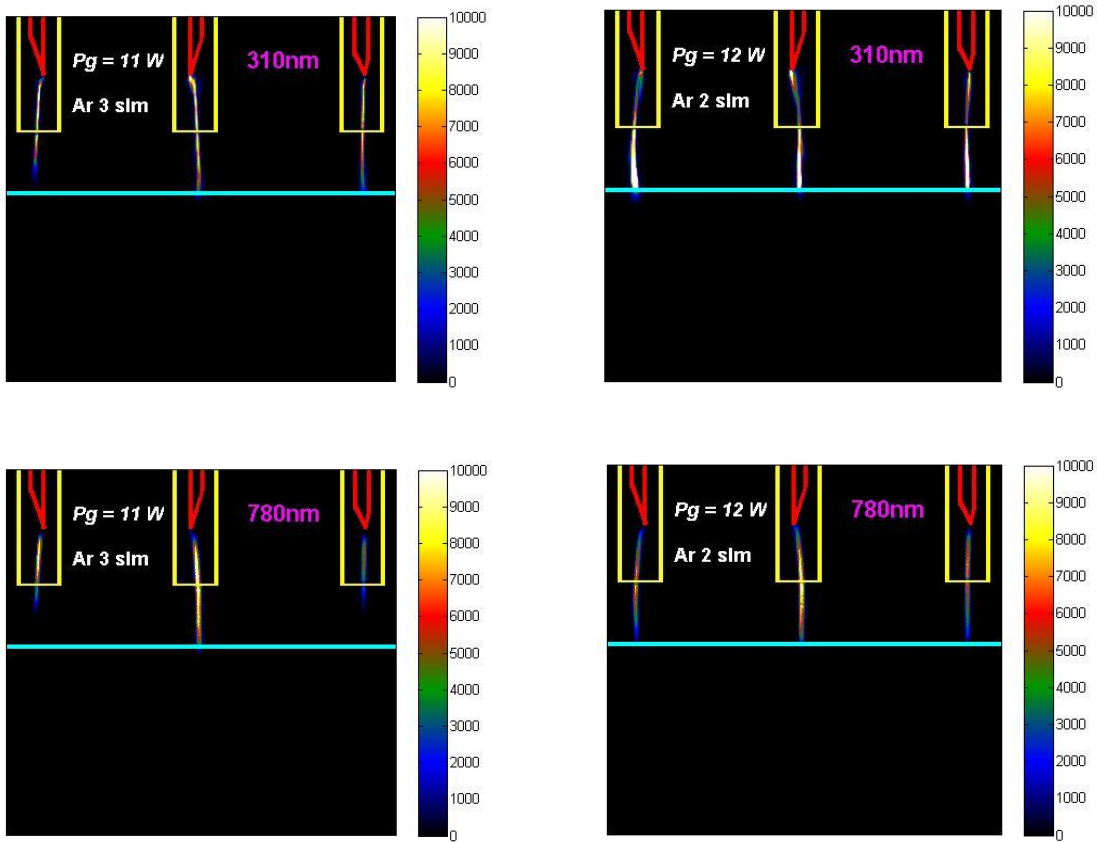
Figure 6.8. The iCCD images with filters (310 nm and 780 nm). Acquisition parameters, gain 80, exposure time 20 ms, gate pulse width 3 ms.

The spatial distribution emissions of H_α, N_2 (SPS)+N_2 (FNS), and excited argon were monitored with 660 nm, 425 nm, and 710 nm filters, and their intensity levels are shown in Figure 6.9. The emission from H_α was more visible at low 2 slm, especially downstream of all three jets, and it became less intense at high argon flow rates. The 430 nm filters show that the emission was caused by N_2 (SPS)+N_2 (FNS), and that both appeared at both flow rates, but at lower intensities. In the case of 710 nm filters, the emission profile of excited argon appeared highest in the vicinity of the needle electrode tip and the middle of the jets, and the emission was dramatically reduced close to the liquid surface for both flow rates.

Figure 6.9. The iCCD images with filters (660 nm, 430 nm and 710 nm). Acquisition parameters, gain 80, exposure time 20 ms, gate pulse width 3 ms.

The 840 nm filter was utilized to determine the presence of O· emission as well as excited argon in the discharge, which can be seen in Figure 6.10. It is apparent that emission increases at the top and middle of jets and then decreases significantly downstream of the jets. It appears that the excited argon was quenched near the liquid surface.
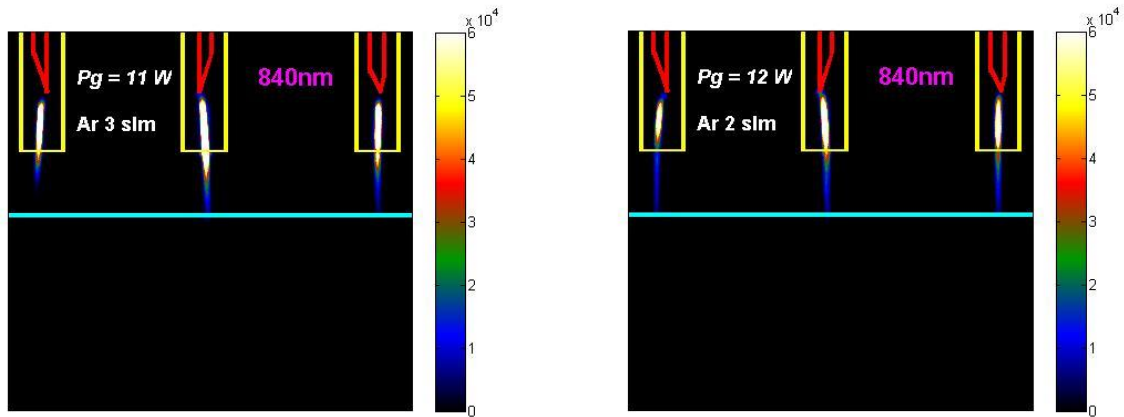
Figure 6.10. The iCCD images with filter (840 nm). Acquisition parameters, gain 80, exposure time 20 ms, gate pulse width 3 ms.

Focused imaging of a 3 pin-APPJ system

The iCCD imaging was performed using a 3 pin-APPJ system, but the camera was focused on the middle jet. The images were obtained using identical acquisition conditions for all three jets. The goal was to collect and view the plasma emission profile with higher resolution in order to examine the details of plasma emission. Again, the imaging was done without filters, and filters were utilized to capture the emission from key reactive species. Figure 6.11 shows images taken of the middle jet at two distinct argon flow rates. It was observed that a broader and sharper intensity of plasma emission appears throughout the discharge.
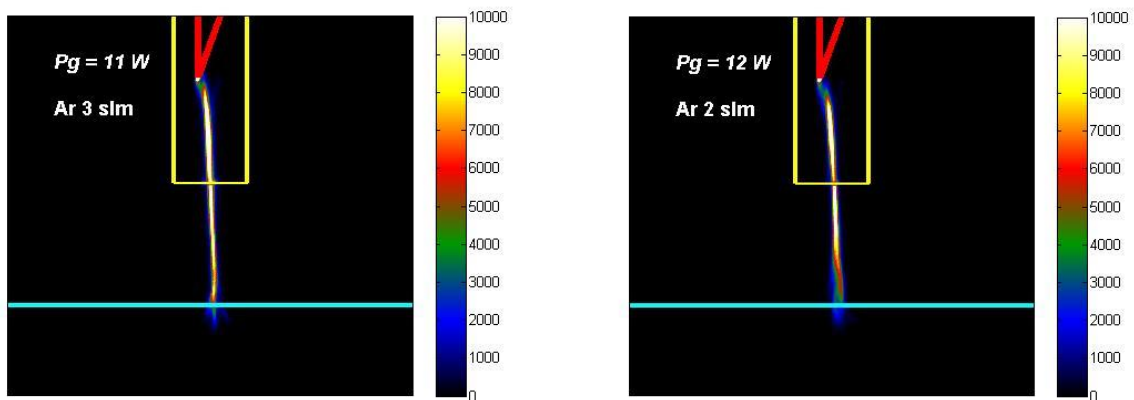
Figure 6.11. The iCCD images (focused on the middle jet) of 3 jet-APPJ. Acquisition parameters, gain 0, exposure time 20 ms, gate pulse width 3 ms.

Figure 6.12 shows the spatially resolved emissions obtained using 310 nm and 780 nm filters at two different argon flow rates. According to the 310 nm filtered image, the HO· + N_2 (SPS) emission was consistent throughout the discharge at both flow rates. In the case of O· and excited argon, which were recorded at 780 nm, they appeared at a higher intensity predominantly in the top stream of the jet, and emission was almost totally quenched at lower flow rates, but at higher flow rates, a significant amount of emission also appeared downstream of the jet. Overall, the emission collected by 310 nm filters was more intense than that captured by 780 nm filters.
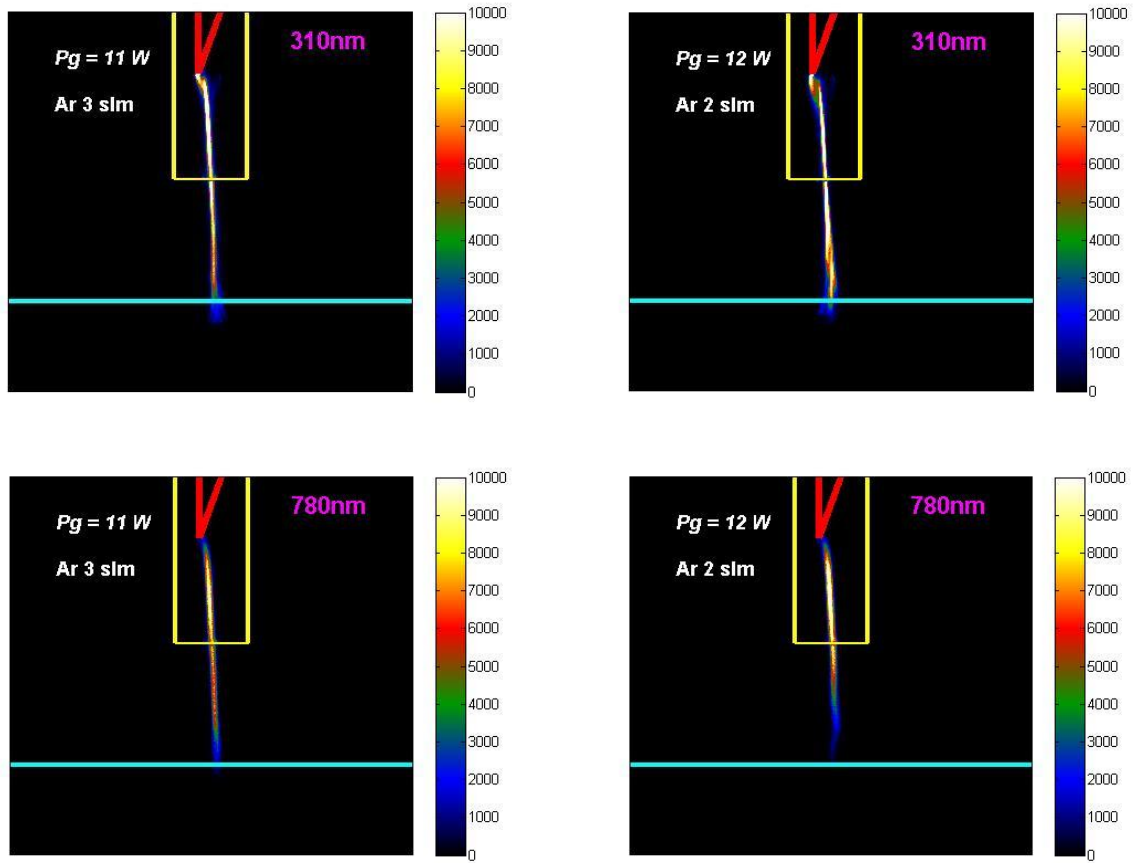
Figure 6.12. The iCCD images (focused on the middle jet) with filters (310 nm and 780 nm). Acquisition parameters, gain 80, exposure time 20 ms, gate pulse width 3 ms.

Figure 6.13 demonstrates the emission measured using 660 nm, 430 nm, and 710 nm filters. Each of these three filters appears to have a distinct emission profile. The 660 nm filtered images show that H_α emission was localized near the bottom of the jet at both flow rates. When 430 nm filters were utilized, N_2 (SPS) and N_2 (FNS) showed in the discharge with a weaker and larger emission profile. Excited argon captured with a 710 nm filter was most intense around the center to the top of the jet, with intensity falling significantly closer to the liquid surface. The strong H_α emission at the bottom of the jet and the excited argon emission at the top of the jet suggested higher plasma excitation in those zones.
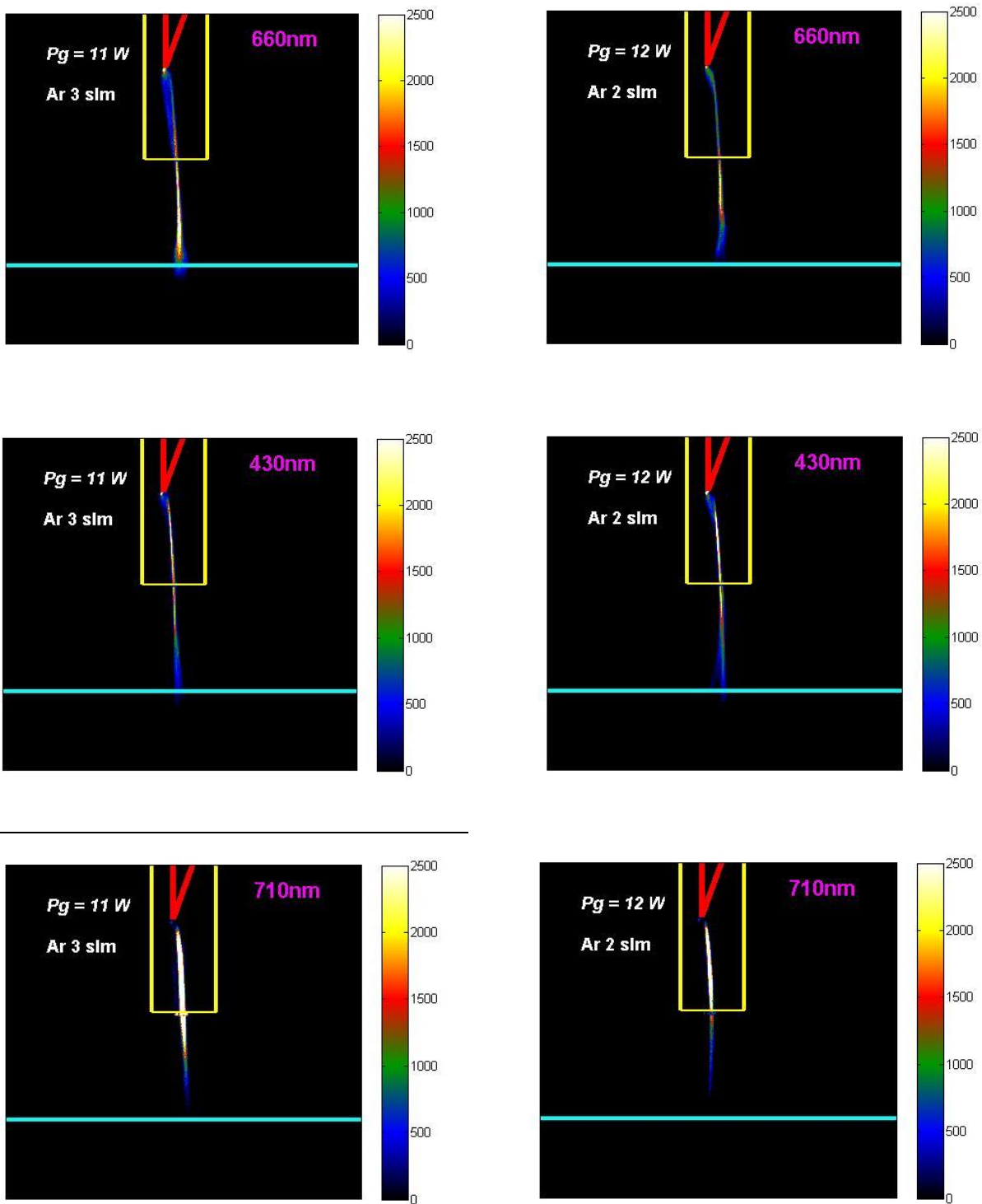
Figure 6.13. The iCCD images (focused on the middle jet) with filters (660 nm, 430 nm and 710 nm). Acquisition parameters, gain 80, exposure time 20 ms, gate pulse width 3 ms.

The 840 nm filtered image is shown in Figure 6.14, and it was observed that there was abundant emission of O· in combination with excited argon in the middle and top of the jet, whereas intensity decreased

when the jet came into contact with the liquid. When the argon flow rate was increased, emission in the bottom of the jet increased progressively.
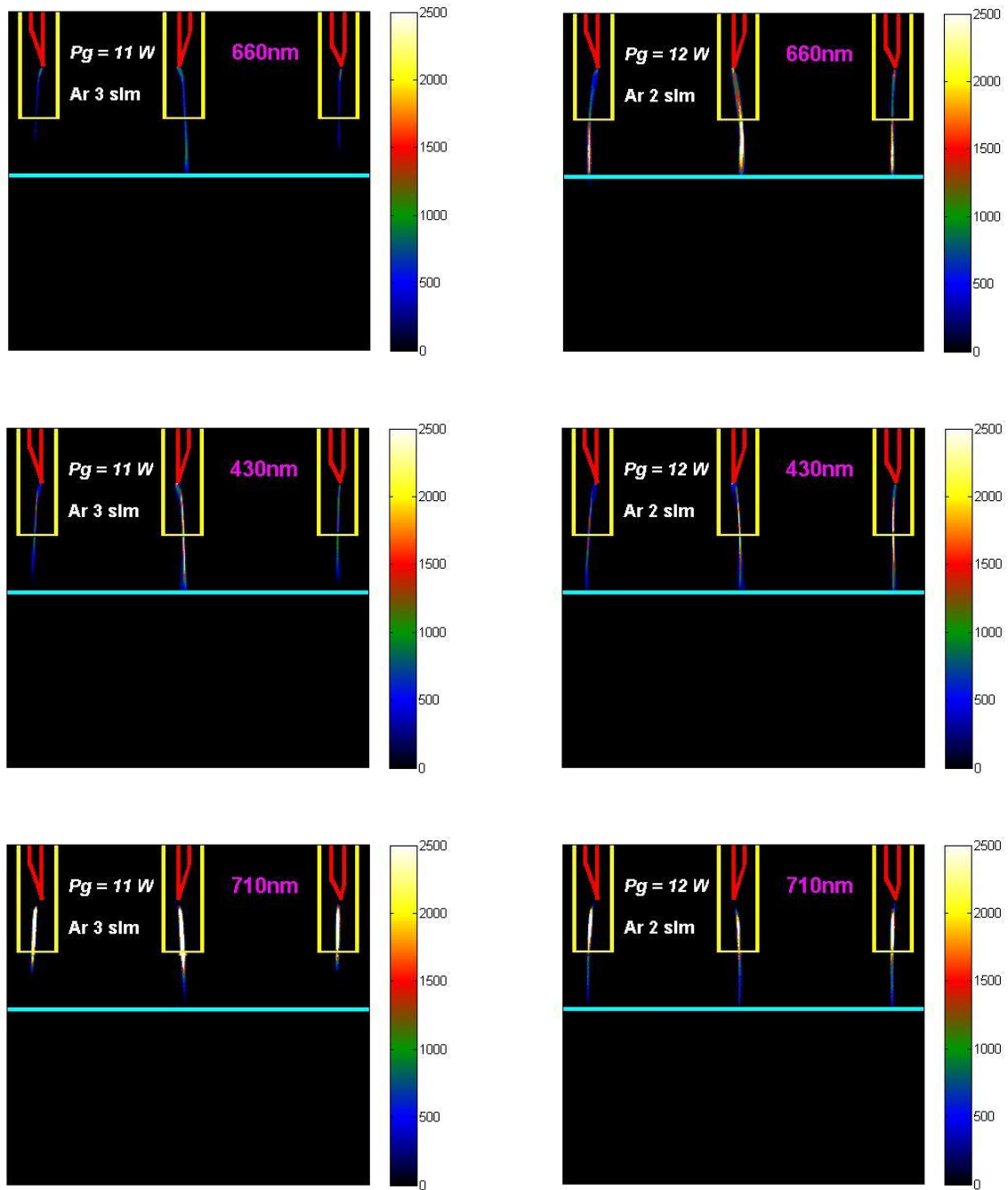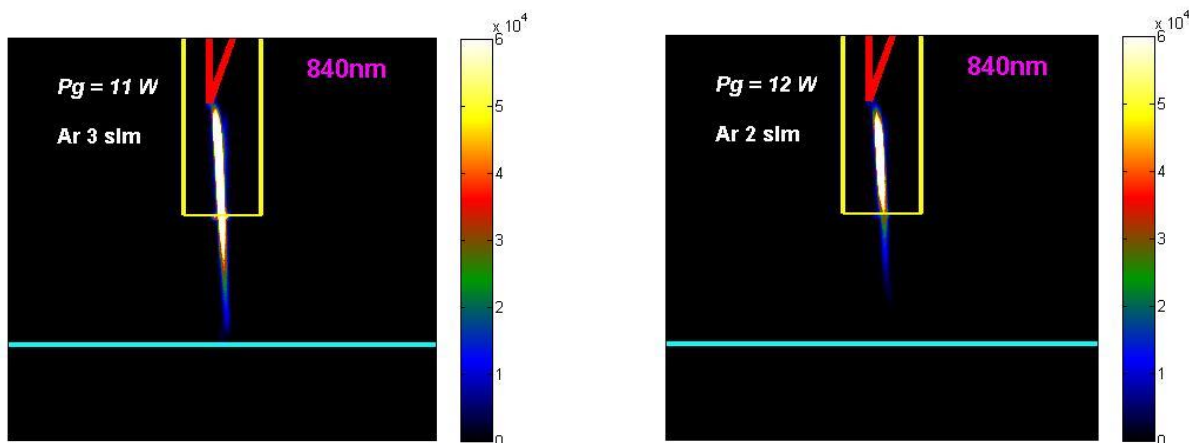

Figure 6.14. The iCCD images (focused on the middle jet) with filters (840 nm). Acquisition parameters, gain 80, exposure time 20 ms, gate pulse width 3 ms.

With all iCCD images captured with filters, it is possible to conclude that main key reactive species responsible for pollution degradation were present in the plasma discharge with varying emission intensities.

6.2. Removal of Acid Blue 25 dye

The plasma source was first subjected to remove the AB25 dye. Initially, the treatment was performed without recirculating the sample; instead, plasma was created on a stationary liquid surface. After that, plasma was generated at the surface of the dye-containing recirculated solution, and the results are briefly discussed.

6.2.1. Effect of initial concentration, initial volume and treatment time

The dye treatment studies were carried out by exposing the plasma directly to AB25-containing water solutions while taking into account a variety of experimental parameters. The degradation data were evaluated and compared across all parameters concisely.

The degradation curve of AB25 in solution as a function of plasma treatment time is depicted in Figure 6.15 (a). Lower initial concentration and volume were found to facilitate faster and higher dye removal. The degradation was more pronounced at the start of plasma exposure, with more than half of the dye destroyed in the first 5 minutes of treatment. After 5 minutes, the degradation pattern changed substantially in all cases. After 20 minutes of plasma treatment at 25 mg/L and 15 ml, approximately 94 % dye degradation was accomplished, while the degradation rate was limited to roughly 76 % at two times higher dye concentration and solution volume. In case of larger volume and higher dye concentration lower degradation was achieved even in the longer period of treatment. Figure 6.15 (b) depicts the removal of dye from the solution as a function of plasma treatment time at constant dye concentration and variable initial volume. There are obvious effects at lower dye concentrations and solution volumes, such as the transition of a dye-colored solution to a clear one, but at double the dye solution volume, the dye does not decompose completely.
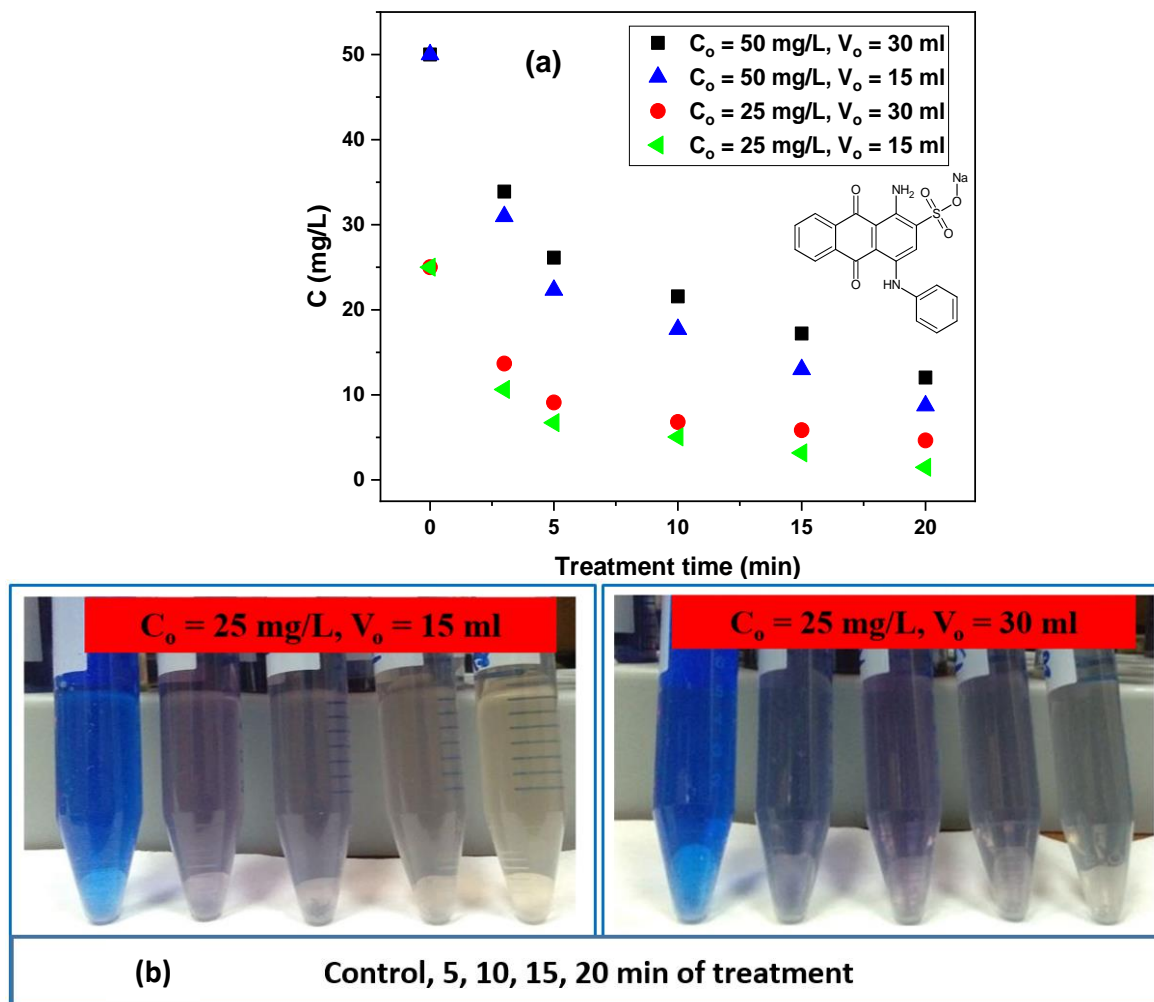
Figure 6.15. (a) Decrease in AB25 concentration (C), and **(b)** rate of decolorization of AB25 dye after plasma treatment. Experiment conditions included an argon flow of 2 slm and a P_{mean} of 14 W at the sample.

Kinetic studies were conducted, and first and second-order models were used to determine the kinetics of the degrading reaction, as shown in Figure 6.16 (a & b). The first-order model best fits the data at lower concentrations and lower initial volumes, while the second-order model best fits the data at higher concentrations and larger initial volumes. $Ln(C/C_0)$ with treatment time and $1/C$ with treatment time depict decolorization rates with first and second-order kinetics, respectively. The first-order equation was already demonstrated in Chapter 5, the equation 6.1 describes the second-order kinetic equation.

$$\frac{1}{Ct} = \frac{1}{Co} + kt \quad (6.1)$$
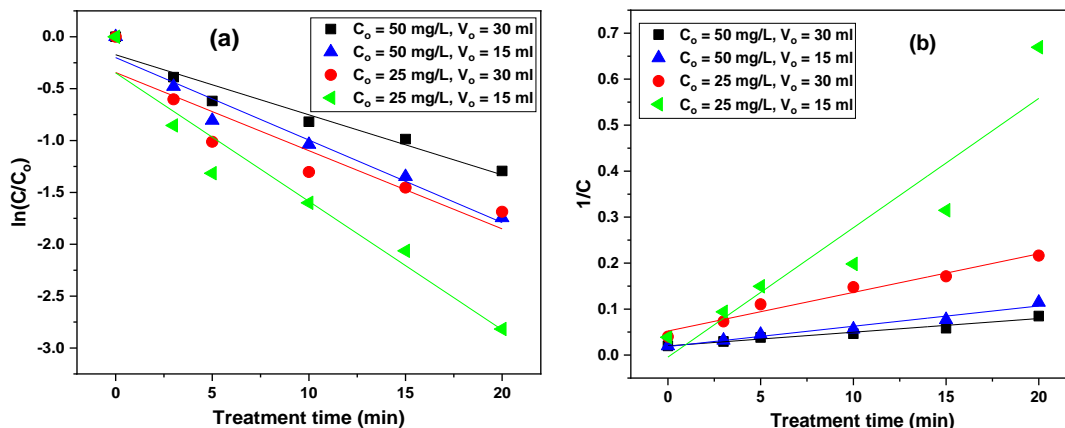
Figure 6.16. (a) First-order **(b)** and second-order degradation of AB25 as a function of treatment time. Experiment conditions, argon flow 2 slm and P_{mean} at sample 14 W.

The first and second-order rates of degradation of AB25 are shown in Table 6.1. Because the kinetic was well fitted with the first order for a solution volume of 15 ml and an AB25 concentration of 25 mg/L, the rate constant was calculated to be around 0.12 min^{-1} ($R^2 = 0.94$). At greater volumes, the rate was around 0.0084 Lmg^{-1}min^{-1} ($R^2 = 0.97$) at a solution volume of 30 ml and an AB25 concentration of 25 mg/L. The reason for second-order reaction decay of AB25 dye in situations of higher concentration and higher initial volume may be attributed to either volume or the AB25 molecules being in abundance, and the quantity of reactive species exposed by plasma remains constant. Another possibility for the rate of constant change is that the reactive species were quenched by byproducts of transformation.

Table 6.1. Data on the kinetics of AB25 degradation under different conditions.

		$C_o = 50$ mg/L, $V_o = 30$ ml	$C_o = 50$ mg/L, $V_o = 15$ ml	$C_o = 25$ mg/L, $V_o = 30$ ml	$C_o = 25$ mg/L, $V_o = 15$ ml
First order	k (min^{-1})	0.0578	0.0795	0.0753	0.1238
	R^2	0.93	0.95	0.85	0.94
Second order	k (Lmg^{-1}min^{-1})	0.0029	0.0044	0.0084	0.0281
	R^2	0.96	0.96	0.97	0.88

For all cases, the pH and conductivity of the solution were computed, and it was confirmed that both varied with plasma treatment time. Figure 6.17 (a) depicts the changes in pH and conductivity values after plasma treatment. In all cases, the pH dropped rapidly at the start of treatment and then progressively reduced over time, and conductivity increased gradually. The lowest pH was attained for the smallest initial volume, although the difference was not statistically significant across all cases. Conductivity was nearly twice as high at lower volumes as it was at larger volumes, and changes in dye concentration had no greater influence on conductivity than changes in solution volume.
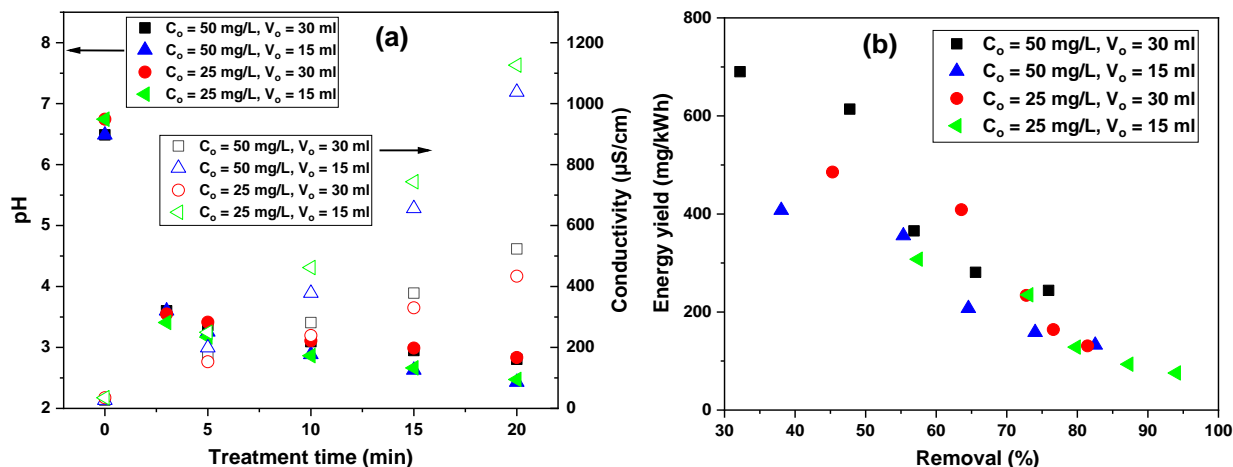
Figure 6.17. (a) Change in solution pH and conductivity as a function of treatment time, **(b)** change in energy yield as a function of removal %. Experiment conditions, argon flow of 2 slm and P_{mean} at sample 14 W.

The energy yields for all of the experimental conditions were estimated and compared. The energy yield as a function of elimination % is depicted in Figure 6.17 (b). The higher the initial dye concentration and volume of dye solution, the greater the energy yield. The highest energy yield was 690 mg/kWh with a removal efficiency of 32 % at 50 mg/L and 30 ml, and the lowest was 76 mg/kWh, with a removal efficiency of 94 % at 25 mg/L of dye concentration and 15 ml of dye solution.

The energy yield for 50 % elimination was also investigated; the greatest was up to 479 mg/kWh at 50 mg/L and 30 ml, and nearly three times lower (144 mg/kWh) at dye concentration of 25 mg/L and dye solution volume of 15 ml. Overall, the following conditions resulted in the highest energy yield at a fixed 50 % dye removal: 50 mg/L, 30 ml > 50 mg/L, 15 ml > 25 mg/L, 30 ml. When the concentration of contaminants and solution volume were high, dye removal became more energy efficient.

6.2.2. Treatment with recirculation system

A previous study on plasma-based treatment processes revealed that most plasma systems operated in batch mode, implying that polluted water was always located beneath plasma throughout treatment and the amount of water was regarded as relatively small. Such plasma reactor configurations are impractical for real-world wastewater treatment when a significant amount of water must be treated in a short time. According to this line of thought, it is more appealing to have a layout in which polluted water can flow and be recirculated, allowing for the treatment of a large volume of polluted water. In this approach, a flow system with plasma generated at flowing and recirculated polluted water samples was designed. The goal was to improve mixing and recirculate polluted water samples in order to facilitate the interaction of plasma-induced reactive species and contaminants.

Treatment of AB25 dye

First, AB25 dye was targeted for treatment with a multi-needle electrodes-APPJ recirculating system. The treatment volume was 250 ml, which is 8 to 16 times greater than the volume without recirculation. During the treatment, dye-treated samples were collected at various intervals and analyzed, and a dye degradation pattern was proposed.

Figure 6.18 (a) displays the dye concentration decreasing with plasma treatment time when APPJ was exposed to a constantly recirculated dye solution. There was no discernible decline in dye concentration over the first 20 minutes. Dye degradation accelerated with increasing plasma exposure time; degradation was most visible after 20 minutes. In 40 minutes, nearly half of the dye had been removed, and 74 % had been removed in 60 minutes. The degradation pattern was tried to fit with various kinetics models, it was found that the zero-order kinetic model ($R^2 = 0.96$) with a rate constant of 0.347 mgL^{-1}min^{-1} best fit and explained the degradation. The pH was calculated and fell from 6.97 to 4.28 after 20 minutes and to 3.48 after 60 minutes.
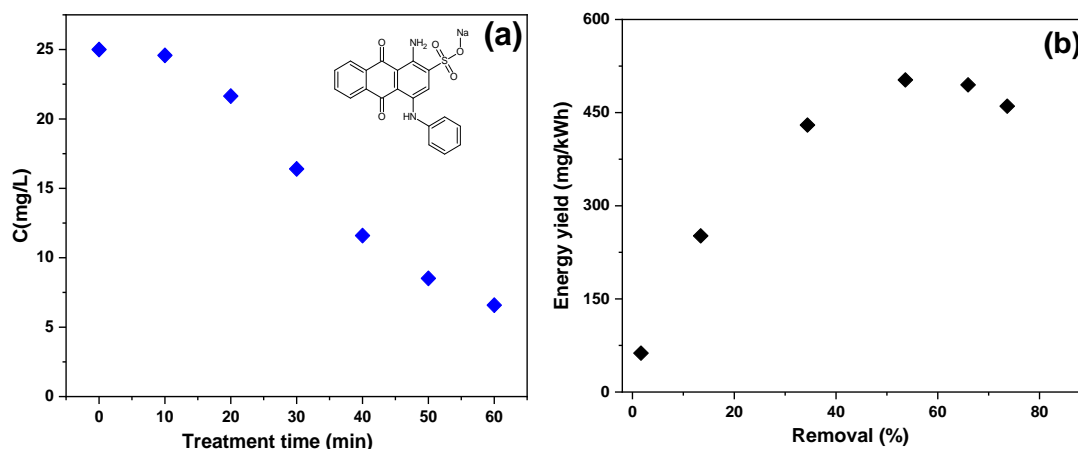
Figure 6.18. (a) Change in AB25 concentration with treatment time, **(b)** energy yield versus removal %. Experimental conditions, C_o = 25 mg/L, V_o = 250 ml, dye solution flow rate 300 ml/min, P_{mean} at the sample 11 W.

The energy yield curve as a function of removal % is depicted in Figure 6.18 (b). It was determined that the energy yield grew with removal % up to a point and then decreased. For example, the energy yield was essentially linear up to about 40 % dye removal, then deviated to 522 mg/kWh at about 50 % removal, and thereafter dropped. The energy yield was higher as compared to dye treatment without a recirculation system (including all treatment conditions).

6.3. Removal of pharmaceutical and industrial chemical

6.3.1. Treatments with recirculation system

Plasma with a recirculation system was also tested for the treatment of DCF and pCBA while retaining the same amount of liquid. The degradation experiment began with DCF, and the results are presented briefly below.

Treatment of DCF

Figure 6.19 (a) shows the degradation behavior of DCF at two different initial concentrations. The concentration of DCF declined as the plasma treatment time increased, and the degradation was considerably rapid at lower DCF concentrations. After 10 minutes of treatment, the degradation of DCF increased rapidly, with about 93 % removal measured, and removal was approximately 46 % at two times greater DCF concentrations. DCF almost totally vanished within 30 minutes of treatment at both 25 mg/L and 50 mg/L. The kinetics of degradation patterns differed between two different initial concentrations of DCF. After fitting the kinetic models, it was determined that lower concentrations of DCF degraded in the first order ($R^2 = 0.95$) while greater concentrations degraded in the zeroth order ($R^2 = 0.97$). Both

the first order rate constant and the zeroth order rate constant was 0.145 min^{-1} and 1.636 (mgL^{-1}min^{-1}), respectively. Such variations in degradation kinetics behavior could be attributed to differences in the oxidation reaction, and competition of reactive species with DCF intermediates.
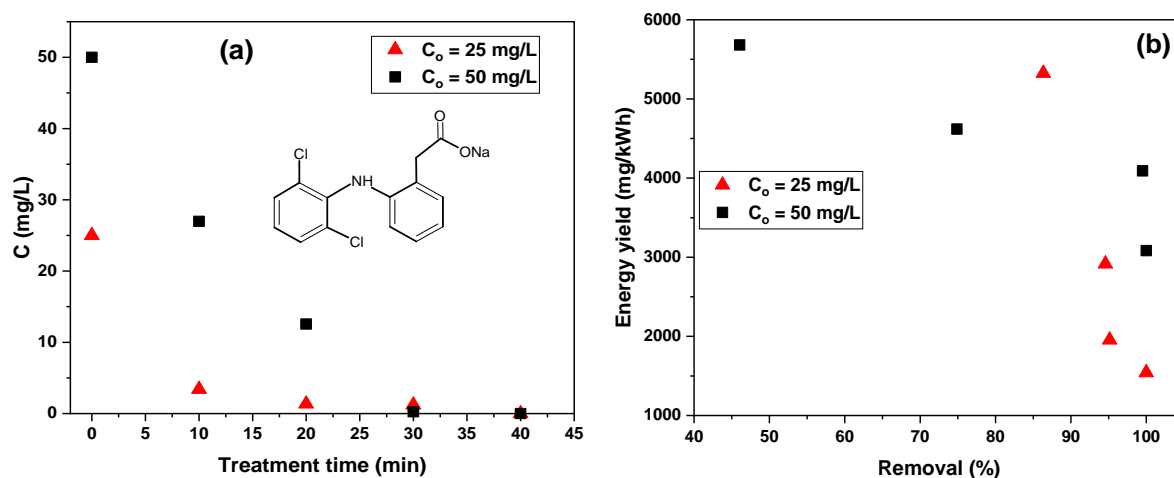
Figure 6.19. (a) Change in DCF concentration with treatment time, **(b)** energy yield versus removal %. Experimental conditions, V_o = 250 ml, argon flow 2 slm, P_{mean} at the sample 8 W.

Because DCF was removed very efficiently at a low treatment time, the energy yield in the instance of DCF removal was greater than that of the other selected compounds. Figure 6.19 (b) demonstrates that the energy yield rose to 5681 mg/kWh at 40 % elimination at higher DCF initial concentrations. The energy yield for the entire DCF elimination was 1542 mg/kWh at 25 mg/L and roughly twice as high at 50 mg/L. At the end of this section, the energy yield was compared to other pollutants and briefly explained.

Treatment of pCBA

The experiment with pCBA was also carried out at an initial concentration of 25 mg/L, the results shown in Figure 6.20. In the case of pCBA treatment, the degradation curve behaved differently than DCF, implying lesser removal. According to the pCBA degradation curve, roughly 15 % removal was observed after 20 minutes and 23 % removal was recorded after 60 minutes. Lower pCBA removal may be explained by the quenching of plasma-induced oxidative species byproducts formed after pCBA degradation. The degradation was also fit with kinetic models throughout three treatment durations, the first order being the best match (R^2 = 0.93) with a degradation rate of 0.00497 min^{-1}.
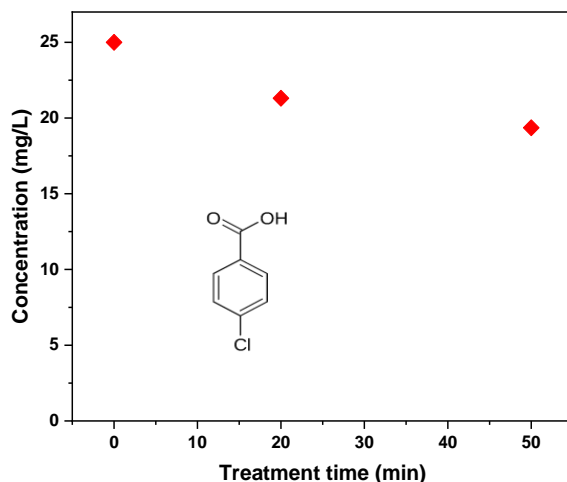
Figure 6.20. Change in pCBA concentration with treatment time. Experimental conditions, at V_o = 250 ml, argon flow 2 slm, P_{mean} at the sample 8 W.

Comparison of energy yields based on 50 % removal

Since data on 50 % pollutant removal is typically available, energy yield estimates based on 50 % pollutant removal are calculated and compared. As shown in Table 6.2, there is a difference in energy yield of at least one order of magnitude between DCF and others (pCBA and AB25). At fixed C_o = 25 mg/L, the energy yield for DFC degradation was roughly 43 times that of pCBA and 12 times that of AB25.

Table 6.2. Energy yield comparison for DCF, pCBA, and AB25 at 50 % removal, V_o = 250 ml.

Compounds	C_o (mg/L)	Maximum energy yield (mg/kWh)
DCF	25	6465
	50	4036
pCBA	25	150
AB25	25	522

The energy yield achieved from this thesis was compared to the earlier cold atmospheric plasma-based DCF and pCBA degradation. For example, Dobrin et al. [74] reported 1000 mg/kWh for 50 % removal and 760 mg/kWh for 90 % removal during DCF decomposition using pulsed corona discharge over a liquid surface. Deng et al. [190] obtained 2458 mg/kWh for 50 % DCF removal and 1332 mg/kWh for 90 % DCF removal utilizing DBD plasma system. Back et al. [191] found that after treating DCF with DBD, energy yield values ranged from 20 to 715 mg/kWh for elimination up to 90 %. In comparison to our studies, the published results demonstrate a rather low DCF removal energy yield. Lesage et al. [178] tested the DBD-recirculation system and plasma was formed above the thin falling layer in the case of pCBA treatment, and they identified 624 mg/kWh of energy yield for 50 % removal. Schönekerl et al. [192] examined the decomposition of pCBA utilizing a plasma-multi electrodes system, giving 320 mg/kWh energy yield for 50 % removal. Data on energy yield for the removal of various OMPs by plasma-based treatment approaches can be found in the literature, where author Malik et al. [109]

conducted a comparative analysis and concluded that gas-phase discharges are more energy efficient than liquid phase discharges. The range of energy yield for various OMPs degradation by plasma could also be found in Kumar et al. [65] review paper.

The energy expenditure in electric energy per order (kWh/m^3) was also calculated. In the best-case scenario, energy consumption for more than 90 % DCF removal was 8 kWh/m^3 at 25 mg/L DCF concentration and 12 kWh/m^3 at 50 mg/L DCF concentration.

According to the results of this experiment, plasma with a recirculation system had substantially more promise and was found to be efficient in terms of energy yield. The enhanced performance for treating a significant amount of water by plasma using a recirculating system can be attributed to the efficient interaction of reactive plasma species and pollutants due to the wider area of plasma-liquid surface interaction. According to the above-mentioned results, the multi-needle electrodes-APPJ with a recirculation system can be deemed an efficient method for the remediation of OMPs-containing wastewater.

6.3.2. Possible degradation pathways of diclofenac

It is also necessary to thoroughly examine the plasma-treated liquid in order to investigate the reaction products left over in the liquid and the involvement of various reaction steps during pollutant removal. In this regard, Orbitrap-LC-MS was utilized to evaluate DCF samples treated with a 3-jet recirculation system; the characterization approach is explained briefly in Chapter 4. Figure 6.21 represents the identified products and their anticipated structures, as well as the possible degradation pathways involved in the process. After the analysis, seven transformation products were identified: DCF-154 ($C_8H_{10}O_3$), DCF-166 ($C_8H_6O_4$), DCF-202 ($C_8H_{10}O_6$), DCF-241 ($C_{14}H_{11}NO_3$), DCF-259 ($C_{14}H_{10}ClNO_2$), DCF-277 ($C_{14}H_9Cl_2NO$) and DCF-308 ($C_{14}H_9Cl_2NO_3$).

The byproducts of DCF degradation have already been investigated utilizing existing AOPs as well as cold atmospheric plasma [74,177,193,194]. The majority of degrading reactions in AOPs are dominated by HO· chemistry. It was revealed that a multi-step mechanism can be engaged in the decomposition of DCF, such as hydroxylation, dechlorination, cyclization, decarboxylation, ring-opening processes, and so on [193,195]. Since plasma interacts with liquid, large RONS can be produced, and so HO· radicals, as well as other plasma-induced oxidants, can cleave DCF in aqueous solution, causing the production of transformation products that can then be destroyed and mineralized [74,190,196]. Investigating the individual contribution of plasma-generated reactive species in the overall decomposition of DCF may be difficult due to a lack of data available in the literature.

The contacts of reactive species with benzene rings are thought to constitute the most important breakdown reactions. For instance, hydroxylation of DCF could occur as a result of a consecutive impact of HO· on the aromatic ring, culminating in the removal of the hydrogen atom and the creation of hydroxylated derivatives. The existence of a Cl-benzyl bond in DCF's aromatic ring caused rapid dechlorination under plasma, causing the production of chloride ions. Cyclization could also be described by the release of H_2O from DCF. A further significant oxidation reaction is DCF decarboxylation, which removes the hydrogen atom from the carboxyl group. The impact of reactive species on the amino group in DCF and the breakage of the aromatic ring bridge can both aid in the splitting of the C-N bond. DCF degradation could continue through ring cleavage and the production of tiny molecules.

As illustrated in Figure 6.21, DCF can be hydroxylated by the electrophilic assault of HO· in the electron-donating position of the aromatic ring, leading to the production of $C_{14}H_{11}NO_3$ (DCF-241) and

$C_{14}H_9Cl_2NO_3$ (DCF-308). Two dechlorination transformation products have been identified: $C_{14}H_{11}NO_3$ (DCF-241) and $C_{14}H_{10}ClNO_2$ (DCF-259). DCF-259 showed a transformation route involved the cyclisation into a carbazole derivative and loss of Cl. The mechanism suggested for the formation of DCF-277 ($C_{14}H_9Cl_2NO$) starts with cyclization and is followed by water elimination.

Subsequently, the cleavage of C-N bonds could occur and form low molecular weight byproducts including $C_8H_{10}O_3$ (DCF-154), $C_8H_6O_4$ (DCF-166) and $C_8H_{10}O_6$ (DCF-202). The cleavage of the C-N bond can be facilitated by the attack of reactive species at the amino group in DCF and breaking the bridge of aromatic rings. Degradation of DCF could continue by cleavage of the ring and the formation of small molecules.
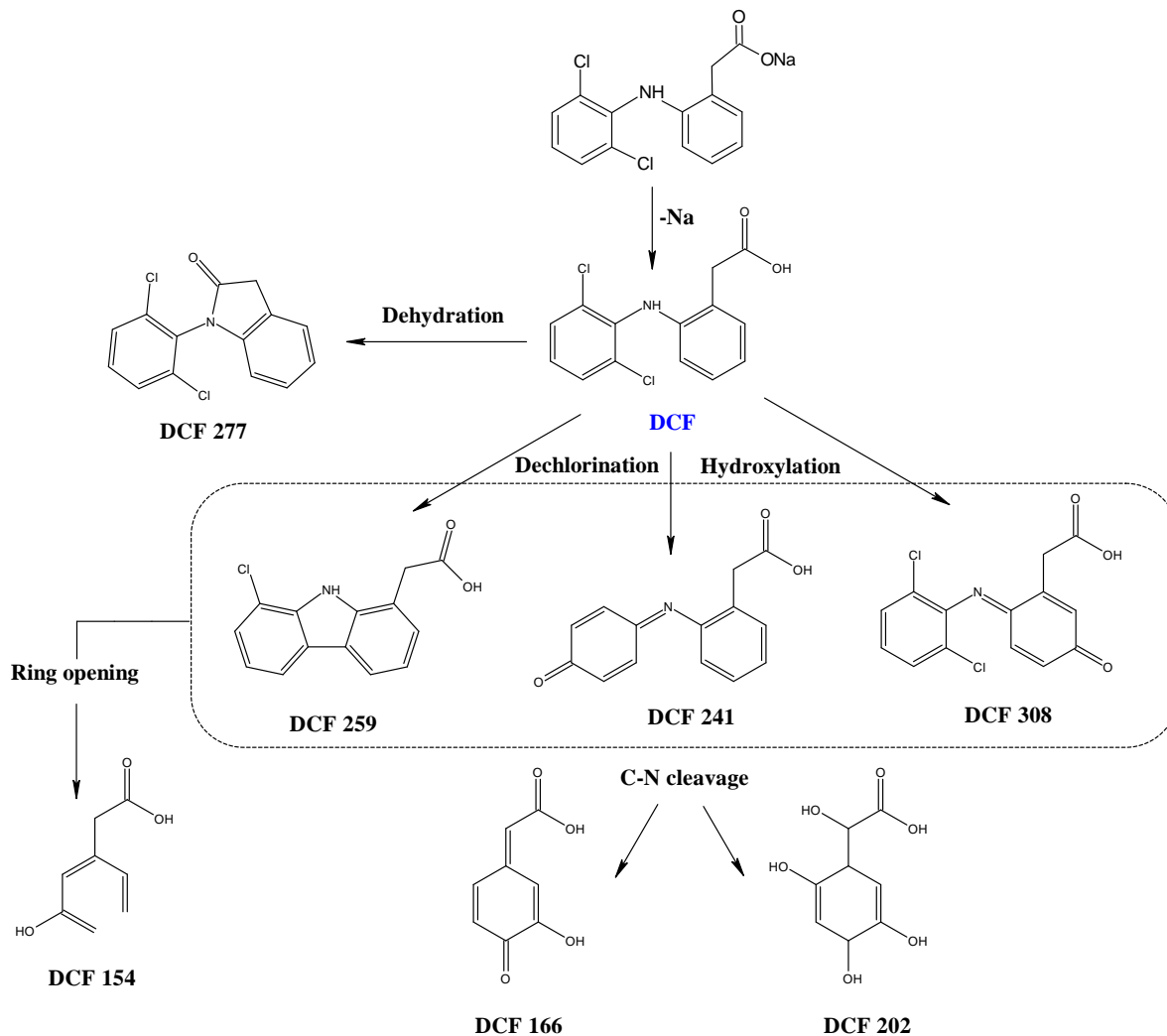
Figure 6.21. Identified products as well as possible DCF degradation pathways.

Toxicity tests were not performed in this study to determine the integrated rate of harmful impact that occurs during diclofenac breakdown in water by plasma. Previously, researchers conducted toxicity tests on diclofenac throughout its degradation using chemical-based AOP as well as plasma [74,176]. For example, Dobrin et al. [74] investigated the breakdown of diclofenac in water using DBD plasma, and a toxicity test was performed to determine the toxicity potential in plasma-treated solution. They discovered that diclofenac breakdown by DBD does not represent a major toxicity to luminous bacteria.

CHAPTER 7

7. Summary, conclusion and future work

7.1. Thesis summary and conclusion

The main goal of this thesis is the design, development and characterization of a cold atmospheric plasma system for wastewater treatment. Cold atmospheric plasma creates a rich chemical environment and, as a result, it is green source of AOPs that does not rely on external chemicals and can be employed to remove a wide range of complex non-biodegradable OMPs from water.

This thesis studies two types of cold atmospheric plasma sources in contact with liquid: pin-APPJ and multi-pin-APPJ (3-jets), both of which are powered by an RF power supply and use argon as a feed gas. Argon plasma was formed at the liquid surface in the presence of surrounding air. During the first phase, pin-APPJ was used to execute experiments with a variety of operational parameters, such as the effect of initial pollutant concentration, treatment time, solution volume, input power and so on. Based on the findings of the pin-APPJ application in treatments of contaminated water and the need to increase plasma-liquid tiny contact area, a novel plasma source with multi-needle electrodes-APPJ was designed, developed and used to treat OMPs. A system for water flow was also designed and plasma was formed on flowing polluted liquid.

The peculiarity of both cold atmospheric pressure plasmas explored in the thesis is that they provide the necessary components for efficient OMPs breakdown in water. Plasma-liquid interactions, for example, can generate electrons, excited species, radicals, ions, and UV radiation, which can drive processes and oxidize pollutants. These plasma sources can treat several forms of contaminated water.

Both plasma sources were electrically and optically characterized. The electrical characterization provides data on discharge characteristics such as operational voltage, current and power delivered to the plasma system. It also provided detailed information on the relationship between voltage and current behavior when plasma was ignited and when plasma was not present. The power deposition was calculated by using the recorded voltage and current values, which is one of the critical parameters in a plasma-based water treatment system. The optical characteristics of plasma were measured using an OES and an iCCD camera. The OES was primarily used to assess the excited reactive species in the gaseous phase of the plasma system during plasma-liquid contact. OES was performed with varying input power in order to compare the effect of power transfer to the plasma on the enhancement of plasma-driven chemistry. Among all the discovered chemical species, HO· and O· are regarded as major ROS that are highly important in water treatment and play a key role in pollutant degradation. The time-integrated distribution of plasma-driven reactive species was investigated using iCCD imaging under varied acquisition settings. Various filters were utilized and set in front of an iCCD camera combined with a lense to track the major plasma-induced reactive species (for example, HO·, O·, H·, N_2, excited argon) in the plasma. It was found that in the majority of cases, reactive species were dispersed throughout the plasma jet, while the intensity of emission varied within the jet.

Plasma was used for treatments of various solutions containing OMPs. In this study, four different model compounds (AB25, DR1, DCF and pCBA) were chosen, each with unique properties. The goal of

selecting these distinct contaminants is to examine how both plasma sources respond during treatment so that plasma technology can be used to treat a variety of pollutants. Several of these selected compounds have previously been detected in the environment as a result of growing demand and usage.

The plasma-treated solutions were examined using several analytical instruments to determine the degradation of each contaminant. Dye plasma treated solutions were assessed by using a spectrophotometer and pharmaceutical degraded was measured using HPLC. A few plasma-treated DCF liquid samples were also studied by using Orbitrap-LC-MS and a possible degradation mechanism was hypothesized based on the observed intermediates products.

Each pollutant degraded in a different way under both plasma sources. DCF was shown to be the pollutant that decreased abruptly with treatment time in both plasma sources under all experimental conditions. AB25, DR1 and pCBA were also efficiently eliminated, but at a lower rate than DCF. Overall, both plasma sources are capable of successfully degrading all of the contaminants tested in this study. In terms of treatment volume, it was demonstrated that a plasma source equipped with multi-needle electrodes-APPJ and a recirculation system was better suitable for treating larger amounts of polluted water.

Lower pollutant concentration, longer treatment duration and higher power were among the experimental conditions that promoted higher degradation of selected OMPs. In all cases, the majority of degradation happened at the start of treatment. The pH and conductivity of the solution were also investigated and it was revealed that after plasma treatment, the pH decreased while the conductivity increased. Lower pH aided in the oxidation of contaminants in some instances due to the quick reactivity of reactive species at lower pH.

A new strategy, such as an experiment with PAW, was conducted to learn more about the role of plasma-generated long-lived RONS in dye degradation in water. PAW can be used in irrigation to purify the water utilized in the irrigation field. PAW can remove pollutants from the water while simultaneously acting as a fertilizer. Since PAW contains a variety of RNS, they may play a key function in plant growth.

The energy yield was calculated, which is an important measure in determining the suitability of plasma-based devices for pollution treatment. Pollutant characteristics, reactor type, initial pollutant concentration, volume and treatment duration all have a significant impact on energy efficiency. The energy yield for elimination varies by order of magnitude; for example, DCF has a higher energy yield than other compounds. A higher energy yield was obtained when a multi-needle electrodes-APPJ recirculating system was used to treat a quarter liter of contaminated water. At 50 % elimination with pin-APPJ, energy yields occurred in the following order for all pollutants: DCF > DR1 > AB25 > pCBA. Because multi-needle electrodes were used to treat three compounds, the highest energy yield was observed after 50 % elimination in the following order: DCF > AB25 > pCBA. In this investigation, higher energy yields were found when compared to some of plasma-based treatment found in the literature.

Overall, the plasma sources utilized in this work shown outstanding performance for the treatment of selected pollutants, implying that they can be used to treat many types of polluted water, such as tertiary treatment in a WWTP, treatment of industrial effluents, and so on. If we look at the treatment volume in this study, it is still on a limited scale. It was attempted to research techniques to boost plasma-liquid

interaction and reaction speed, such as with the treatment of polluted water using a recirculating system. Although plasma water treatment is still in the research and development stage, several attempts have been done by various researchers and industry to treat specific contaminants.

7.2. Future work

Several experimental variables were thoroughly explored in this thesis, various pollutants were treated and diagnostic approaches were applied. There are still numerous experimental parameters to consider in the future in order to conduct a thorough assessment for the treatment of various pollutants utilizing plasma and to efficiently scale up the plasma reactor. The following are some important parameters and ideas to consider:

- Because plasma treatment was performed in a distilled water matrix, it must be investigated using real wastewater samples. The physicochemical properties of the water matrix might influence plasma chemistry and the formation of reactive species. As a result, it is required to study actual wastewater samples containing a complicated mixture of diverse OMPs. It is also necessary to investigate the effect of varied water matrix on the behavior of plasma and plasma-induced aqueous chemistry.

- Other pollutants with different properties, such as solubility, surface tension (after dissolving in liquid), reactivity and functional groups than the intended target pollutants in this study, must also be treated with plasma to identify their degradation patterns. For example, PFAS-based chemicals can be chosen as target pollutants because they tend to cluster at the liquid surface and are mostly reactive with solvated electrons. Cold atmospheric plasma also contains an abundance of solvated electrons, which are very reactive and can cause redox reactions that break the carbon and fluorine bonds in PFAS-based compounds. Because the majority of plasma-induced short-lived reactive species are consumed at the plasma-liquid interface, plasma can be more efficient for such compounds.

- Argon was employed as a feed gas in the treatment; argon plasma was produced in contact with ambient air and no additional gases were introduced. Argon was chosen because it has a lower breakdown potential, which means it can be ignited at a lower voltage and requires less power than air alone. Nevertheless, air can be blended with argon at various concentrations and the effects explored; air can make plasma systems more affordable, while more power may be required to start plasma ignition. If argon can be recycled within a plasma system, it can make plasma more energy efficient and save a lot of money on gas investment.

- Because plasma with 3-jets and recirculation system proved greater removal in cases of the large volume of treatment, approximately 50 times more volume than pin-APPJ, there is potential to add more electrodes so that plasma can be extended across a larger surface of the water. The multi-electrode and recirculation plasma system suggests that the plasma system can be scaled up from lab to pilot scale. Another electrode geometry can be devised to increase the number of reactive species that can interact with contaminants on the plasma liquid contact surface.

As previously stated, plasma is capable of degrading a wide spectrum of substances, lowering the quantity of OMPs in water to astonishing levels. Plasma can be particularly effective in some circumstances if pollutants are extremely complex and resistant to removal by known water treatment processes. Cold atmospheric plasma technologies appear to be practical, prospective and forward-thinking solutions for eliminating aqueous pollutants. Nevertheless, certain obstacles must be overcome in order to meet the industrial demand for continuous research and development. Plasma discharge's future potential for wastewater treatment will be determined primarily by its pollutant degradation efficiency, reduction in transformation residual concentration and energy consumption in comparison to other AOPs and treatment methods in particular. Certain conditions must also be reached before the plasma-based treatment system may be scaled up. A vast number of bench-scale and pilot-plant studies will be required to create cold plasma-based upscaled decontamination systems.

References

[1]   Y. Wada et al., *Modeling Global Water Use for the 21st Century: The Water Futures and Solutions (WFaS) Initiative and Its Approaches*, Geoscientific Model Development **9**, 175 (2016).

[2]   A. Boretti and L. Rosa, *Reassessing the Projections of the World Water Development Report*, Npj Clean Water **2**, 15 (2019).

[3]   S. Pfister, P. Bayer, A. Koehler, and S. Hellweg, *Projected Water Consumption in Future Global Agriculture: Scenarios and Related Impacts*, Science of The Total Environment **409**, 4206 (2011).

[4]   S. Siebert, J. Burke, J. M. Faures, K. Frenken, J. Hoogeveen, P. Döll, and F. T. Portmann, *Groundwater Use for Irrigation – a Global Inventory*, Hydrology and Earth System Sciences **14**, 1863 (2010).

[5]   S. Nishijima et al., *Superconductivity and the Environment: A Roadmap*, Superconductor Science and Technology **26**, 113001 (2013).

[6]   C. He, Z. Liu, J. Wu, X. Pan, Z. Fang, J. Li, and B. A. Bryan, *Future Global Urban Water Scarcity and Potential Solutions*, Nature Communications **12**, 4667 (2021).

[7]   M. M. Mekonnen and A. Y. Hoekstra, *Four Billion People Facing Severe Water Scarcity*, Science Advances **2**, (2016).

[8]   K. Elsaid, N. Bensalah, and A. Abdel-Wahab, *Inland Desalination: Potentials and Challenges*, in *Advances in Chemical Engineering* (InTech, 2012).

[9]   H. a Saliu, E. O. Oriola, and I. P. Ifabiyi, *Water and Politics in Africa : The Need for Regional Cooperation*, Journal of Public Administration and Policy Research **3**, 220 (2011).

[10]   R. Wassmann, S. V. K. Jagadish, K. Sumfleth, H. Pathak, G. Howell, A. Ismail, R. Serraj, E. Redona, R. K. Singh, and S. Heuer, *Chapter 3 Regional Vulnerability of Climate Change Impacts on Asian Rice Production and Scope for Adaptation*, in (2009), pp. 91–133.

[11]   C. A. Schlosser, K. Strzepek, X. Gao, C. Fant, É. Blanc, S. Paltsev, H. Jacoby, J. Reilly, and A. Gueneau, *The Future of Global Water Stress: An Integrated Assessment*, Earth's Future **2**, 341 (2014).

[12]   R. P. Schwarzenbach, B. I. Escher, K. Fenner, T. B. Hofstetter, C. A. Johnson, U. von Gunten, and B. Wehrli, *The Challenge of Micropollutants in Aquatic Systems*, Science **313**, 1072 (2006).

[13]   H. Q. Anh et al., *Antibiotics in Surface Water of East and Southeast Asian Countries: A Focused Review on Contamination Status, Pollution Sources, Potential Risks, and Future Perspectives*, Science of The Total Environment **764**, 142865 (2021).

[14]   J. E. Hardoy and D. Satterthwaite, *Environmental Problems of Third World Cities: A Global Issue Ignored?*, Public Administration and Development **11**, 341 (1991).

[15]   A. Agrawal, R. S. Pandey, and B. Sharma, *Water Pollution with Special Reference to Pesticide Contamination in India*, Journal of Water Resource and Protection **02**, 432 (2010).

[16]   M. Chagnon, D. Kreutzweiser, E. A. D. Mitchell, C. A. Morrissey, D. A. Noome, and J. P. Van der Sluijs, *Risks of Large-Scale Use of Systemic Insecticides to Ecosystem Functioning and*

Services, Environmental Science and Pollution Research **22**, 119 (2015).

[17] J. M. Bullock, J. Aronson, A. C. Newton, R. F. Pywell, and J. M. Rey-Benayas, *Restoration of Ecosystem Services and Biodiversity: Conflicts and Opportunities*, Trends in Ecology & Evolution **26**, 541 (2011).

[18] W. J. Cosgrove and D. P. Loucks, *Water Management: Current and Future Challenges and Research Directions*, Water Resources Research **51**, 4823 (2015).

[19] D. Ziganshina, *Rethinking the Concept of the Human Right to Water*, Santa Clara Journal of International Law **6**, 113 (2008).

[20] P. Neves-Silva, G. I. Martins, and L. Heller, *Human Rights' Interdependence and Indivisibility: A Glance over the Human Rights to Water and Sanitation*, BMC International Health and Human Rights **19**, 14 (2019).

[21] M. Arfanuzzaman and A. Atiq Rahman, *Sustainable Water Demand Management in the Face of Rapid Urbanization and Ground Water Depletion for Social–Ecological Resilience Building*, Global Ecology and Conservation **10**, 9 (2017).

[22] A. Jabeen, X. Huang, and M. Aamir, *The Challenges of Water Pollution, Threat to Public Health, Flaws of Water Laws and Policies in Pakistan*, Journal of Water Resource and Protection **07**, 1516 (2015).

[23] K. D. Ahuja, S., de Andrade, J. B., Dionysiou, D. D., & Hristovski, *Water Challenges and Solutions on a Global Scale*, Vol. 1206 (American Chemical Society, Washington, DC, 2015).

[24] *World Health Organization. (2002). The World Health Report 2002: Reducing Risks, Promoting Healthy Life. World Health Organization* (World Health Organization, Geneva, n.d.).

[25] R. Baum, J. Luh, and J. Bartram, *Sanitation: A Global Estimate of Sewerage Connections without Treatment and the Resulting Impact on MDG Progress*, Environmental Science & Technology **47**, 1994 (2013).

[26] F. D. Owa, *Water Pollution: Sources, Effects, Control and Management*, Mediterranean Journal of Social Sciences (2013).

[27] K. S. Rajmohan, R. Chandrasekaran, and S. Varjani, *A Review on Occurrence of Pesticides in Environment and Current Technologies for Their Remediation and Management*, Indian Journal of Microbiology **60**, 125 (2020).

[28] P. Chakraborty, M. Mukhopadhyay, S. Sampath, B. R. Ramaswamy, A. Katsoyiannis, A. Cincinelli, and D. Snow, *Organic Micropollutants in the Surface Riverine Sediment along the Lower Stretch of the Transboundary River Ganga: Occurrences, Sources and Ecological Risk Assessment*, Environmental Pollution **249**, 1071 (2019).

[29] A. Mukhopadhyay, S. Duttagupta, and A. Mukherjee, *Emerging Organic Contaminants in Global Community Drinking Water Sources and Supply: A Review of Occurrence, Processes and Remediation*, Journal of Environmental Chemical Engineering **10**, 107560 (2022).

[30] W. Gwenzi and N. Chaukura, *Organic Contaminants in African Aquatic Systems: Current Knowledge, Health Risks, and Future Research Directions*, Science of The Total Environment

619–**620**, 1493 (2018).

[31] T. Rasheed, M. Bilal, F. Nabeel, M. Adeel, and H. M. N. Iqbal, *Environmentally-Related Contaminants of High Concern: Potential Sources and Analytical Modalities for Detection, Quantification, and Treatment*, Environment International **122**, 52 (2019).

[32] Y. Abdulrazaq et al., *Classification, Potential Routes and Risk of Emerging Pollutants/Contaminant*, in *Emerging Contaminants* (IntechOpen, 2021).

[33] S. Sun, Y. Chen, Y. Lin, and D. An, *Occurrence, Spatial Distribution, and Seasonal Variation of Emerging Trace Organic Pollutants in Source Water for Shanghai, China*, Science of The Total Environment **639**, 1 (2018).

[34] C. Basheer, J. P. Obbard, and H. K. E. E. Lee, *Persistent Organic Pollutants in Singapore ' S Coastal*, Water, Air, and Soil Pollution **149**, 295 (2003).

[35] F. Ahmadi, M. Rahimi-Nasrabadi, A. Fosooni, and M. Daneshmand, *Synthesis and Application of CoWO4 Nanoparticles for Degradation of Methyl Orange*, Journal of Materials Science: Materials in Electronics **27**, 9514 (2016).

[36] S. P. Azerrad and E. Kurzbaum, *Chemical Decolorization of Textile Wastewater Via Advanced Oxidation Processes: Case Study of Key Parameters with Acid Blue 25*, Water, Air, and Soil Pollution **232**, 1 (2021).

[37] T. A. Nguyen and R.-S. Juang, *Treatment of Waters and Wastewaters Containing Sulfur Dyes: A Review*, Chemical Engineering Journal **219**, 109 (2013).

[38] R. Singla, F. Grieser, and M. Ashokkumar, *Sonochemical Degradation of Martius Yellow Dye in Aqueous Solution*, Ultrasonics Sonochemistry **16**, 28 (2009).

[39] T. N. V. de Souza, M. G. A. Vieira, M. G. C. da Silva, D. do S. B. Brasil, and S. M. L. de Carvalho, *H3PO4-Activated Carbons Produced from Açai Stones and Brazil Nut Shells: Removal of Basic Blue 26 Dye from Aqueous Solutions by Adsorption*, Environmental Science and Pollution Research **26**, 28533 (2019).

[40] C. A. Igwegbe, S. N. Oba, C. O. Aniagor, A. G. Adeniyi, and J. O. Ighalo, *Adsorption of Ciprofloxacin from Water: A Comprehensive Review*, Journal of Industrial and Engineering Chemistry **93**, 57 (2021).

[41] N. H. Torres, G. de O. S. Santos, L. F. Romanholo Ferreira, J. H. P. Américo-Pinheiro, K. I. B. Eguiluz, and G. R. Salazar-Banda, *Environmental Aspects of Hormones Estriol, 17β-Estradiol and 17α-Ethinylestradiol: Electrochemical Processes as next-Generation Technologies for Their Removal in Water Matrices*, Chemosphere **267**, 128888 (2021).

[42] Y. Zhang, S.-U. Geißen, and C. Gal, *Carbamazepine and Diclofenac: Removal in Wastewater Treatment Plants and Occurrence in Water Bodies*, Chemosphere **73**, 1151 (2008).

[43] H. Olvera-Vargas, T. Cocerva, N. Oturan, D. Buisson, and M. A. Oturan, *Bioelectro-Fenton: A Sustainable Integrated Process for Removal of Organic Pollutants from Water: Application to Mineralization of Metoprolol*, Journal of Hazardous Materials **319**, 13 (2016).

[44] V. K. Gupta, A. Fakhri, S. Agarwal, A. K. Bharti, M. Naji, and A. G. Tkachev, *Preparation and*

Characterization of TiO2 Nanofibers by Hydrothermal Method for Removal of Benzodiazepines (Diazepam) from Liquids as Catalytic Ozonation and Adsorption Processes, Journal of Molecular Liquids **249**, 1033 (2018).

[45] T. Gojmerac, Z. Ostojić, D. Pauković, J. Pleadin, and M. Žurić, *Evaluation of Surface Water Pollution with Atrazine, an Endocrine Disruptor Chemical, in Agricultural Areas of Turopolje, Croatia*, Bulletin of Environmental Contamination and Toxicology **76**, 490 (2006).

[46] J. Godard, M. Aimeur, N. Villandier, F. Zermane, F. Bregier, V. Sol, and M. Baudu, *Photodegradation of Tebuconazole Mediated by a Novel Hybrid Phenalenone Based Photosensitizer*, Journal of Photochemistry and Photobiology A: Chemistry **408**, 113124 (2021).

[47] M. S. F. Abedi Koupai J., Nasri Z., Talebi Kh., Mamanpoush A., *Investigation Of Zayandehrud Water Pollution By Diazinon And Its Assimilative Capacity*, WATER AND SOIL SCIENCE (JOURNAL OF SCIENCE AND TECHNOLOGY OF AGRICULTURE AND NATURAL RESOURCES) **15**, 1 (2011).

[48] C. Hosea, Robert, *Exposure of Non-Target Wildlife to Anticoagulant Rodenticides in California*, Proceedings of the Vertebrate Pest Conference **19**, (2000).

[49] R. Katal, H. Zare, S. O. Rastegar, P. Mavaddat, and G. N. Darzi, *Removal of Dye and Chemical Oxygen Demand (COD) Reduction from Textile Industrial Wastewater Using Hybrid Bioreactors*, Environmental Engineering and Management Journal **13**, 43 (2014).

[50] W. Zheng, X. Li, Z. Hao, D. Wang, Q. Yang, and G. Zeng, *Coal Cinder Filtration as Pretreatment with Biological Processes to Treat Pharmaceutical Wastewater*, Water Science and Technology **62**, 15 (2010).

[51] R. Misra, S. Satyanarayan, and N. Potle, *Treatment of Agrochemical / Pesticide Wastewater by Coagulation / Flocculation Process*, **2**, 39 (2013).

[52] V. M. Monsalvo, J. Lopez, A. F. Mohedano, and J. J. Rodriguez, *Treatment of Cosmetic Wastewater by a Full-Scale Membrane Bioreactor (MBR)*, Environmental Science and Pollution Research **21**, 12662 (2014).

[53] F. J. A. da Silva, R. O. de Souza, F. J. F. de Castro, and A. L. C. Araújo, *Prospectus of Waste Stabilization Ponds in Ceará, Northeast Brazil*, Water Science and Technology **63**, 1265 (2011).

[54] M. Roy and R. Saha, *Dyes and Their Removal Technologies from Wastewater: A Critical Review*, in *Intelligent Environmental Data Monitoring for Pollution Management* (Elsevier, 2021), pp. 127–160.

[55] C. Zheng, L. Zhao, X. Zhou, Z. Fu, and A. Li, *Treatment Technologies for Organic Wastewater*, in *Water Treatment* (InTech, 2013).

[56] A. Nagda, M. Meena, and M. P. Shah, *Bioremediation of Industrial Effluents: A Synergistic Approach*, Journal of Basic Microbiology **62**, 395 (2022).

[57] J. Rogowska, M. Cieszynska-Semenowicz, W. Ratajczyk, and L. Wolska, *Micropollutants in Treated Wastewater*, Ambio **49**, 487 (2020).

[58] A. Kot-Wasik, A. Jakimska, and M. Śliwka-Kaszyńska, *Occurrence and Seasonal Variations of*

25 Pharmaceutical Residues in Wastewater and Drinking Water Treatment Plants, Environmental Monitoring and Assessment **188**, 661 (2016).

[59] D. B. Miklos, C. Remy, M. Jekel, K. G. Linden, J. E. Drewes, and U. Hübner, *Evaluation of Advanced Oxidation Processes for Water and Wastewater Treatment – A Critical Review*, Water Research **139**, 118 (2018).

[60] A. G. Capodaglio, *Critical Perspective on Advanced Treatment Processes for Water and Wastewater: AOPs, ARPs, and AORPs*, Applied Sciences **10**, 4549 (2020).

[61] S. de Boer, J. González-Rodríguez, J. J. Conde, and M. T. Moreira, *Benchmarking Tertiary Water Treatments for the Removal of Micropollutants and Pathogens Based on Operational and Sustainability Criteria*, Journal of Water Process Engineering **46**, 102587 (2022).

[62] J. A. Garrido-Cardenas, B. Esteban-García, A. Agüera, J. A. Sánchez-Pérez, and F. Manzano-Agugliaro, *Wastewater Treatment by Advanced Oxidation Process and Their Worldwide Research Trends*, International Journal of Environmental Research and Public Health **17**, 170 (2020).

[63] C. Amor, L. Marchão, M. S. Lucas, and J. A. Peres, *Application of Advanced Oxidation Processes for the Treatment of Recalcitrant Agro-Industrial Wastewater: A Review*, Water **11**, 205 (2019).

[64] J. O. Tijani, O. O. Fatoba, G. Madzivire, and L. F. Petrik, *A Review of Combined Advanced Oxidation Technologies for the Removal of Organic Pollutants from Water*, Water, Air, & Soil Pollution **225**, 2102 (2014).

[65] A. Kumar, N. Škoro, W. Gernjak, and N. Puač, *Cold Atmospheric Plasma Technology for Removal of Organic Micropollutants from Wastewater—a Review*, The European Physical Journal D **75**, 1 (2021).

[66] S. Guerra-Rodríguez, E. Rodríguez, D. Singh, and J. Rodríguez-Chueca, *Assessment of Sulfate Radical-Based Advanced Oxidation Processes for Water and Wastewater Treatment: A Review*, Water **10**, 1828 (2018).

[67] T. Manasfi, *Ozonation in Drinking Water Treatment: An Overview of General and Practical Aspects, Mechanisms, Kinetics, and Byproduct Formation*, in (2021), pp. 85–116.

[68] A. Kumar, N. Škoro, W. Gernjak, D. Povrenović, and N. Puač, *Direct and Indirect Treatment of Organic Dye (Acid Blue 25) Solutions by Using Cold Atmospheric Plasma Jet*, Frontiers in Physics **10**, 1 (2022).

[69] H. Zeghioud, P. Nguyen-Tri, L. Khezami, A. Amrane, and A. A. Assadi, *Review on Discharge Plasma for Water Treatment: Mechanism, Reactor Geometries, Active Species and Combined Processes*, Journal of Water Process Engineering **38**, 101664 (2020).

[70] M. Magureanu, F. Bilea, C. Bradu, and D. Hong, *A Review on Non-Thermal Plasma Treatment of Water Contaminated with Antibiotics*, Journal of Hazardous Materials **417**, 125481 (2021).

[71] P. Gururani, P. Bhatnagar, B. Bisht, V. Kumar, N. C. Joshi, M. S. Tomar, and B. Pathak, *Cold Plasma Technology: Advanced and Sustainable Approach for Wastewater Treatment*, Environmental Science and Pollution Research **28**, 65062 (2021).

[72] B. Topolovec, N. Škoro, N. Puač, and M. Petrovic, *Pathways of Organic Micropollutants*

Degradation in Atmospheric Pressure Plasma Processing – A Review, Chemosphere **294**, 133606 (2022).

[73]   B. R. Locke, M. Sato, P. Sunka, M. R. Hoffmann, and J. S. Chang, *Electrohydraulic Discharge and Nonthermal Plasma for Water Treatment*, Industrial and Engineering Chemistry Research **45**, 882 (2006).

[74]   D. Dobrin, C. Bradu, M. Magureanu, N. B. Mandache, and V. I. Parvulescu, *Degradation of Diclofenac in Water Using a Pulsed Corona Discharge*, Chemical Engineering Journal **234**, 389 (2013).

[75]   Y. Liu, D. Liu, J. Zhang, B. Sun, S. Luo, H. Zhang, L. Guo, M. Rong, and M. G. Kong, *Fluid Model of Plasma–Liquid Interaction: The Effect of Interfacial Boundary Conditions and Henry's Law Constants*, AIP Advances **11**, 055019 (2021).

[76]   C. Sarangapani, N. N. Misra, V. Milosavljevic, P. Bourke, F. O'Regan, and P. J. Cullen, *Pesticide Degradation in Water Using Atmospheric Air Cold Plasma*, Journal of Water Process Engineering **9**, 225 (2016).

[77]   K. D. Weltmann et al., *The Future for Plasma Science and Technology*, Plasma Processes and Polymers **16**, 1 (2019).

[78]   F. F. Chen, *Introduction to Plasma Physics and Controlled Fusion*, Third Edit (Springer International Publishing, Cham, 2016).

[79]   M. Gorenšek, M. Gorjanc, V. Bukošek, J. Kovač, Z. Petrović, and N. Puač, *Functionalization of Polyester Fabric by Ar/N 2 Plasma and Silver*, Textile Research Journal **80**, 1633 (2010).

[80]   N. N. Misra, O. Schlüter, and P. J. Cullen, *Plasma in Food and Agriculture*, in *Cold Plasma in Food and Agriculture* (Elsevier, 2016), pp. 1–16.

[81]   A. Fridman, *Plasma Chemistry*, 1st Editio (Cambridge University Press, Cambridge, 2008).

[82]   C. Tendero, C. Tixier, P. Tristant, J. Desmaison, and P. Leprince, *Atmospheric Pressure Plasmas: A Review*, Spectrochimica Acta Part B: Atomic Spectroscopy **61**, 2 (2006).

[83]   M. A. Lieberman and A. J. Lichtenberg, *Principles of Plasma Discharges and Materials Processing*, Second Edi (John Wiley & Sons, Inc., Hoboken, NJ, USA, 2005).

[84]   M. C. García, M. Mora, D. Esquivel, J. E. Foster, A. Rodero, C. Jiménez-Sanchidrián, and F. J. Romero-Salguero, *Microwave Atmospheric Pressure Plasma Jets for Wastewater Treatment: Degradation of Methylene Blue as a Model Dye*, Chemosphere **180**, 239 (2017).

[85]   J. E. Foster, *Plasma-Based Water Purification: Challenges and Prospects for the Future*, Physics of Plasmas **24**, 055501 (2017).

[86]   P. Bruggeman and R. Brandenburg, *Atmospheric Pressure Discharge Filaments and Microplasmas: Physics, Chemistry and Diagnostics*, Journal of Physics D: Applied Physics **46**, 464001 (2013).

[87]   F. Rezaei, P. Vanraes, A. Nikiforov, R. Morent, and N. De Geyter, *Applications of Plasma-Liquid Systems : A Review*, Materials **12**, 2751 (2019).

[88] D. S. Maletić, Development and Diagnostics of Atmospheric Plasma Jet and Application on Biological Samples, University of Belgrade, 2018.

[89] L. Wu, Q. Xie, Y. Lv, Z. Wu, X. Liang, M. Lu, and Y. Nie, *Degradation of Methylene Blue via Dielectric Barrier Discharge Plasma Treatment*, Water **11**, 1815 (2019).

[90] A. M. Ali, M. A. A. Hassan, and B. I. Abdulkarim, *Thermal Plasma: A Technology for Efficient Treatment of Industrial and Wastewater Sludge*, IOSR Journal of Environmental Science **10**, 63 (2016).

[91] T. Makabe and L. Z. Petrovic, *Plasma Electronics: Applications in Microelectronic Device Fabrication (Vol. 26)*, Second Edi (CRC Press, 2014).

[92] P. Favia, G. Cicala, A. Milella, F. Palumbo, P. Rossini, and R. D'Agostino, *Deposition of Super-Hydrophobic Fluorocarbon Coatings in Modulated RF Glow Discharges*, Surface and Coatings Technology **169–170**, 609 (2003).

[93] S. Živković, N. Puač, Z. Giba, D. Grubišić, and Z. L. Petrović, *The Stimulatory Effect of Non-Equilibrium (Low Temperature) Air Plasma Pretreatment on Light-Induced Germination of Paulownia Tomentosa Seeds*, Seed Science and Technology **32**, 693 (2004).

[94] D. Mance, R. Wiese, T. Kewitz, and H. Kersten, *Atmospheric Pressure Plasma Jet for Biomedical Applications Characterised by Passive Thermal Probe*, The European Physical Journal D **72**, 98 (2018).

[95] N. Puač, M. Gherardi, and M. Shiratani, *Plasma Agriculture: A Rapidly Emerging Field*, Plasma Processes and Polymers **15**, 1700174 (2018).

[96] C. Bradu, K. Kutasi, M. Magureanu, N. Puač, and S. Živković, *Reactive Nitrogen Species in Plasma-Activated Water: Generation, Chemistry and Application in Agriculture*, Journal of Physics D: Applied Physics **53**, 223001 (2020).

[97] L. Bárdos and H. Baránková, *Cold Atmospheric Plasma: Sources, Processes, and Applications*, Thin Solid Films **518**, 6705 (2010).

[98] N. Škoro, D. Marić, G. Malović, W. G. Graham, and Z. L. Petrović, *Electrical Breakdown in Water Vapor*, Physical Review E **84**, 055401 (2011).

[99] A. Schutze, J. Y. Jeong, S. E. Babayan, Jaeyoung Park, G. S. Selwyn, and R. F. Hicks, *The Atmospheric-Pressure Plasma Jet: A Review and Comparison to Other Plasma Sources*, IEEE Transactions on Plasma Science **26**, 1685 (1998).

[100] D. Marić, N. Škoro, P. D. Maguire, C. M. O. Mahony, G. Malović, and Z. L. Petrović, *On the Possibility of Long Path Breakdown Affecting the Paschen Curves for Microdischarges*, Plasma Sources Science and Technology **21**, 035016 (2012).

[101] R. Yuri P., *Gas Discharge Physics*, 1st ed. (Springer Berlin, Heidelberg, Springer Berlin, Heidelberg, 1987).

[102] N. Puač, M. Gherardi, and M. Shiratani, *Plasma Agriculture: A Rapidly Emerging Field*, Plasma Processes and Polymers **15**, 1 (2018).

[103] S. Tomić, A. Petrović, N. Puač, N. Škoro, M. Bekić, Z. L. Petrović, and M. Čolić, *Plasma-*

Activated Medium Potentiates the Immunogenicity of Tumor Cell Lysates for Dendritic Cell-Based Cancer Vaccines, Cancers **13**, 10 (2021).

[104] H. Taghvaei, V. S. S. K. Kondeti, and P. J. Bruggeman, *Decomposition of Crystal Violet by an Atmospheric Pressure RF Plasma Jet: The Role of Radicals, Ozone, Near-Interfacial Reactions and Convective Transport*, Plasma Chemistry and Plasma Processing **39**, 729 (2019).

[105] V. I. Parvulescu, M. Magureanu, and P. Lukes, *Plasma Chemistry and Catalysis in Gases and Liquids*, 1st Editio (John Wiley & Sons., 2012).

[106] J. Peran and S. Ercegović Ražić, *Application of Atmospheric Pressure Plasma Technology for Textile Surface Modification*, Textile Research Journal **90**, 1174 (2020).

[107] E. E. Son and D. V Tereshonok, *Thermal and Plasma Flow Control*, Physica Scripta **T142**, 014039 (2010).

[108] S. Park, W. Choe, S. Y. Moon, and S. J. Yoo, *Electron Characterization in Weakly Ionized Collisional Plasmas: From Principles to Techniques*, Advances in Physics: X **4**, 1526114 (2019).

[109] M. A. Malik, *Water Purification by Plasmas: Which Reactors Are Most Energy Efficient?*, Plasma Chemistry and Plasma Processing **30**, 21 (2010).

[110] K. Takahashi, K. Takaki, and N. Satta, *A Novel Wastewater Treatment Method Using Electrical Pulsed Discharge Plasma over a Water Surface*, in *Sewage - Recent Advances, New Perspectives and Applications* (IntechOpen, 2022).

[111] H. Kempkens and J. Uhlenbusch, *Scattering Diagnostics of Low-Temperature Plasmas (Rayleigh Scattering, Thomson Scattering, CARS)*, Plasma Sources Science and Technology **9**, 492 (2000).

[112] N. Selaković, Mass Spectrometry of Plasma Jet and Application of Electrical Discharches Operating at Atmoshperic Pressure in Biomedicine, University of Belgrade, 2021.

[113] A. Stancampiano, N. Selaković, M. Gherardi, N. Puač, Z. L. Petrović, and V. Colombo, *Characterisation of a Multijet Plasma Device by Means of Mass Spectrometric Detection and ICCD Imaging*, Journal of Physics D: Applied Physics **51**, 484004 (2018).

[114] S. Samukawa et al., *The 2012 Plasma Roadmap*, Journal of Physics D: Applied Physics **45**, 253001 (2012).

[115] R. K. Singh, L. Philip, and S. Ramanujam, *Rapid Degradation, Mineralization and Detoxification of Pharmaceutically Active Compounds in Aqueous Solution during Pulsed Corona Discharge Treatment*, Water Research **121**, 20 (2017).

[116] Y. Liu, D. Liu, J. Zhang, B. Sun, S. Luo, H. Zhang, L. Guo, M. Rong, and M. G. Kong, *Fluid Model of Plasma-Liquid Interaction: The Effect of Interfacial Boundary Conditions and Henry's Law Constants*, AIP Advances **11**, (2021).

[117] M. Magureanu, N. B. Mandache, and V. I. Parvulescu, *Degradation of Pharmaceutical Compounds in Water by Non-Thermal Plasma Treatment*, Water Research **81**, 124 (2015).

[118] M. Hijosa-Valsero, R. Molina, A. Montràs, M. Müller, and J. M. Bayona, *Decontamination of Waterborne Chemical Pollutants by Using Atmospheric Pressure Nonthermal Plasma: A Review*, Environmental Technology Reviews **3**, 71 (2014).

[119] M. Magureanu, N. B. Mandache, and V. I. Parvulescu, *Degradation of Pharmaceutical Compounds in Water by Non-Thermal Plasma Treatment*, Water Research **81**, 124 (2015).

[120] P. J. Bruggeman et al., *Plasma–Liquid Interactions: A Review and Roadmap*, Plasma Sources Science and Technology **25**, 053002 (2016).

[121] I. Yagi, R. Ono, T. Oda, and K. Takaki, *Two-Dimensional LIF Measurements of Humidity and OH Density Resulting from Evaporated Water from a Wet Surface in Plasma for Medical Use*, Plasma Sources Science and Technology **24**, 015002 (2014).

[122] N. Wardenier, Y. Gorbanev, I. Van Moer, A. Nikiforov, S. W. H. Van Hulle, P. Surmont, F. Lynen, C. Leys, A. Bogaerts, and P. Vanraes, *Removal of Alachlor in Water by Non-Thermal Plasma: Reactive Species and Pathways in Batch and Continuous Process*, Water Research **161**, 549 (2019).

[123] Sonia Muradia, Study of Low-Voltage Pulsed Plasma Discharges inside Water Using a Bubble-Generating Porous Ceramic Electrode for Wastewater Treatment, Doctoral dissertation, Shizuoka University, 2013.

[124] A. Tri Sugiarto, T. Ohshima, and M. Sato, *Advanced Oxidation Processes Using Pulsed Streamer Corona Discharge in Water*, Thin Solid Films **407**, 174 (2002).

[125] S. Mededovic and B. R. Locke, *Side-Chain Degradation of Atrazine by Pulsed Electrical Discharge in Water*, Industrial and Engineering Chemistry Research **46**, 2702 (2007).

[126] P. Attri, M. Yusupov, J. H. Park, L. P. Lingamdinne, J. R. Koduru, M. Shiratani, E. H. Choi, and A. Bogaerts, *Mechanism and Comparison of Needle-Type Non-Thermal Direct and Indirect Atmospheric Pressure Plasma Jets on the Degradation of Dyes*, Scientific Reports **6**, 1 (2016).

[127] F. Abdelmalek, M. R. Ghezzar, M. Belhadj, A. Addou, and J. L. Brisset, *Bleaching and Degradation of Textile Dyes by Nonthermal Plasma Process at Atmospheric Pressure*, Industrial and Engineering Chemistry Research **45**, 23 (2006).

[128] N. Škoro, N. Puač, S. Živković, D. Krstić-Milošević, U. Cvelbar, G. Malović, and Z. L. Petrović, *Destruction of Chemical Warfare Surrogates Using a Portable Atmospheric Pressure Plasma Jet*, European Physical Journal D **72**, (2018).

[129] B. Jiang, J. Zheng, S. Qiu, M. Wu, Q. Zhang, Z. Yan, and Q. Xue, *Review on Electrical Discharge Plasma Technology for Wastewater Remediation*, Chemical Engineering Journal **236**, 348 (2014).

[130] M. Russo, G. Iervolino, V. Vaiano, and V. Palma, *Non-Thermal Plasma Coupled with Catalyst for the Degradation of Water Pollutants: A Review*, Catalysts **10**, 1 (2020).

[131] A. Barjasteh, Z. Dehghani, P. Lamichhane, N. Kaushik, E. H. Choi, and N. K. Kaushik, *Recent Progress in Applications of Non-Thermal Plasma for Water Purification, Bio-Sterilization, and Decontamination*, Applied Sciences (Switzerland) **11**, 3372 (2021).

[132] M. Magureanu, D. Piroi, F. Gherendi, N. B. Mandache, and V. Parvulescu, *Decomposition of Methylene Blue in Water by Corona Discharges*, Plasma Chemistry and Plasma Processing **28**, 677 (2008).

[133] J. Li, Z. Zhou, H. Wang, G. Li, and Y. Wu, *Research on Decoloration of Dye Wastewater by*

Combination of Pulsed Discharge Plasma and TiO2 Nanoparticles, Desalination **212**, 123 (2007).

[134] J. Ren, T. Wang, G. Qu, D. Liang, and S. Hu, *Evaluation and Optimization of Electrode Configuration of Multi-Channel Corona Discharge Plasma for Dye-Containing Wastewater Treatment*, Plasma Science and Technology **17**, 1053 (2015).

[135] M. A. Malik, Ubaid-Ur-Rehman, A. Ghaffar, and K. Ahmed, *Synergistic Effect of Pulsed Corona Discharges and Ozonation on Decolourization of Methylene Blue in Water*, Plasma Sources Science and Technology **11**, 236 (2002).

[136] A. Fahmy, A. El-Zomrawy, A. M. Saeed, A. Z Sayed, M. A Ezz El-Arab, H. Shehata, and J. Friedrich, *Degradation of Organic Dye Using Plasma Discharge: Optimization, PH and Energy*, Plasma Research Express **2**, 015009 (2020).

[137] M. Rahimpour, H. Taghvaei, S. Zafarnak, M. R. Rahimpour, and S. Raeissi, *Post-Discharge DBD Plasma Treatment for Degradation of Organic Dye in Water: A Comparison with Different Plasma Operation Methods*, Journal of Environmental Chemical Engineering **7**, 103220 (2019).

[138] D. Piroi, M. Magureanu, N. B. Mandache, and V. I. Parvulescu, *Decomposition of Organic Dyes in Water Using Non-Thermal Plasma*, in *19th International Symposium on Plasma Chemistry* (2009), pp. 1–4.

[139] L. O. de B. Benetoli, B. M. Cadorin, C. Da S. Postiglione, I. G. De Souzaa, and N. A. Debacher, *Effect of Temperature on Methylene Blue Decolorization in Aqueous Medium in Electrical Discharge Plasma Reactor*, Journal of the Brazilian Chemical Society **22**, 1669 (2011).

[140] Q. Tang, W. Jiang, Y. Zhang, W. Wei, and T. M. Lim, *Degradation of Azo Dye Acid Red 88 by Gas Phase Dielectric Barrier Discharges*, Plasma Chemistry and Plasma Processing **29**, 291 (2009).

[141] P. Attri, M. Yusupov, J. H. Park, L. P. Lingamdinne, J. R. Koduru, M. Shiratani, E. H. Choi, and A. Bogaerts, *Mechanism and Comparison of Needle-Type Non-Thermal Direct and Indirect Atmospheric Pressure Plasma Jets on the Degradation of Dyes*, Scientific Reports **6**, 1 (2016).

[142] H. Ghodbane, A. Y. Nikiforov, O. Hamdaoui, P. Surmont, F. Lynen, G. Willems, and C. Leys, *Non-Thermal Plasma Degradation of Anthraquinonic Dye in Water: Oxidation Pathways and Effect of Natural Matrices*, Journal of Advanced Oxidation Technologies **17**, 372 (2014).

[143] B. Jiang, J. Zheng, Q. Liu, and M. Wu, *Degradation of Azo Dye Using Non-Thermal Plasma Advanced Oxidation Process in a Circulatory Airtight Reactor System*, Chemical Engineering Journal **204–205**, 32 (2012).

[144] B. Sun, N. N. Aye, Z. Gao, D. Lv, X. Zhu, and M. Sato, *Characteristics of Gas-Liquid Pulsed Discharge Plasma Reactor and Dye Decoloration Efficiency*, Journal of Environmental Sciences **24**, 840 (2012).

[145] D. He, Y. Sun, L. Xin, and J. Feng, *Aqueous Tetracycline Degradation by Non-Thermal Plasma Combined with Nano-TiO2*, Chemical Engineering Journal **258**, 18 (2014).

[146] S. Rong and Y. Sun, *Wetted-Wall Corona Discharge Induced Degradation of Sulfadiazine Antibiotics in Aqueous Solution*, Journal of Chemical Technology and Biotechnology **89**, 1351 (2014).

[147] H. Krause, B. Schweiger, J. Schuhmacher, S. Scholl, and U. Steinfeld, *Degradation of the Endocrine Disrupting Chemicals (EDCs) Carbamazepine, Clofibric Acid, and Iopromide by Corona Discharge over Water*, Chemosphere **75**, 163 (2009).

[148] R. Banaschik, P. Lukes, H. Jablonowski, M. U. Hammer, K. D. Weltmann, and J. F. Kolb, *Potential of Pulsed Corona Discharges Generated in Water for the Degradation of Persistent Pharmaceutical Residues*, Water Research **84**, 127 (2015).

[149] C. Hao, Z. Yan, K. Liu, and J. Qiu, *Degradation of Pharmaceutical Contaminant Tetracycline in Aqueous Solution by Coaxial-Type DBD Plasma Reactor*, IEEE Transactions on Plasma Science **48**, 471 (2020).

[150] Y. Baloul, D. Hong, S. Chuon, and O. Aubry, *Preliminary Study of a Non-Thermal Plasma for the Degradation of the Paracetamol Residue in Water*, International Journal of Plasma Environmental Science and Technology **10**, 102 (2016).

[151] M. I. Nawaz, C. Yi, P. J. Asilevi, T. Geng, M. Aleem, A. M. Zafar, A. Azeem, and H. Wang, *A Study of the Performance of Dielectric Barrier Discharge under Different Conditions for Nitrobenzene Degradation*, Water. **11**, 842 (2019).

[152] M. Magureanu, D. Piroi, N. B. Mandache, V. David, A. Medvedovici, and V. I. Parvulescu, *Degradation of Pharmaceutical Compound Pentoxifylline in Water by Non-Thermal Plasma Treatment*, Water Research **44**, 3445 (2010).

[153] M. Magureanu, D. Piroi, N. B. Mandache, V. David, A. Medvedovici, C. Bradu, and V. I. Parvulescu, *Degradation of Antibiotics in Water by Non-Thermal Plasma Treatment*, Water Research **45**, 3407 (2011).

[154] J. Smith, I. Adams, and H.-F. Ji, *Mechanism of Ampicillin Degradation by Non-Thermal Plasma Treatment with FE-DBD*, Plasma **1**, 1 (2017).

[155] M. Magureanu, D. Dobrin, N. B. Mandache, C. Bradu, A. Medvedovici, and V. I. Parvulescu, *The Mechanism of Plasma Destruction of Enalapril and Related Metabolites in Water*, Plasma Processes and Polymers **10**, 459 (2013).

[156] L. Gao, L. Sun, S. Wan, Z. Yu, and M. Li, *Degradation Kinetics and Mechanism of Emerging Contaminants in Water by Dielectric Barrier Discharge Non-Thermal Plasma: The Case of 17β-Estradiol*, Chemical Engineering Journal **228**, 790 (2013).

[157] M. Hijosa-Valsero, R. Molina, H. Schikora, M. Müller, and J. M. Bayona, *Removal of Cyanide from Water by Means of Plasma Discharge Technology*, Water Research **47**, 1701 (2013).

[158] V. Vasu, D., Raji, A., Pandiyaraj, K. N., Padmanabhan, P. V. A., & Kandhavelu, *View of Degradation of Telmisartan (TELMA-H) Compounds in Aqueous Solution Using Non-Thermal Atmospheric Pressure Plasma Jet.Pdf*, Frontiers in Advanced Materials Research **1**, 46 (2019).

[159] S. Krishna, A. Maslani, T. Izdebski, M. Horakova, S. Klementova, and P. Spatenka, *Degradation of Verapamil Hydrochloride in Water by Gliding Arc Discharge*, Chemosphere **152**, 47 (2016).

[160] M. El Shaer, M. Eldaly, G. Heikal, Y. Sharaf, H. Diab, M. Mobasher, and A. Rousseau, *Antibiotics Degradation and Bacteria Inactivation in Water by Cold Atmospheric Plasma Discharges Above and Below Water Surface*, Plasma Chemistry and Plasma Processing **40**, 971 (2020).

[161] C. Bradu, M. Magureanu, and V. I. Parvulescu, *Degradation of the Chlorophenoxyacetic Herbicide 2,4-D by Plasma-Ozonation System*, Journal of Hazardous Materials **336**, 52 (2017).

[162] P. Vanraes et al., *Decomposition of Atrazine Traces in Water by Combination of Non-Thermal Electrical Discharge and Adsorption on Nanofiber Membrane*, Water Research **72**, 361 (2015).

[163] M. Hijosa-Valsero, R. Molina, H. Schikora, M. Müller, and J. M. Bayona, *Removal of Priority Pollutants from Water by Means of Dielectric Barrier Discharge Atmospheric Plasma*, Journal of Hazardous Materials **262**, 664 (2013).

[164] Y. Hu, Y. Bai, H. Yu, C. Zhang, and J. Chen, *Degradation of Selected Organophosphate Pesticides in Wastewater by Dielectric Barrier Discharge Plasma*, Bulletin of Environmental Contamination and Toxicology **91**, 314 (2013).

[165] S. P. Li, Y. Y. Jiang, X. H. Cao, Y. W. Dong, M. Dong, and J. Xu, *Degradation of Nitenpyram Pesticide in Aqueous Solution by Low-Temperature Plasma*, Environmental Technology (United Kingdom) **34**, 1609 (2013).

[166] S. Li, X. Ma, Y. Jiang, and X. Cao, *Acetamiprid Removal in Wastewater by the Low-Temperature Plasma Using Dielectric Barrier Discharge*, Ecotoxicology and Environmental Safety **106**, 146 (2014).

[167] M. Markovic, M. Jovi, D. Stankovi, V. Kova, G. Rogli, G. Gojgi, and D. Manojlovi, *Application of Non-Thermal Plasma Reactor and Fenton Reaction for Degradation of Ibuprofen*, Science of The Total Environment **505**, 1148 (2015).

[168] L. Patinglag, D. Sawtell, A. Iles, L. M. Melling, and K. J. Shaw, *A Microfluidic Atmospheric-Pressure Plasma Reactor for Water Treatment*, Plasma Chemistry and Plasma Processing **39**, 561 (2019).

[169] J. Fan, H. Wu, R. Liu, L. Meng, and Y. Sun, *Review on the Treatment of Organic Wastewater by Discharge Plasma Combined with Oxidants and Catalysts*, Environmental Science and Pollution Research **28**, 2522 (2021).

[170] L. da Silva Leite, B. de Souza Maselli, G. de Aragão Umbuzeiro, and R. F. Pupo Nogueira, *Monitoring Ecotoxicity of Disperse Red 1 Dye during Photo-Fenton Degradation*, Chemosphere **148**, 511 (2016).

[171] L. Lonappan, S. K. Brar, R. K. Das, M. Verma, and R. Y. Surampalli, *Diclofenac and Its Transformation Products: Environmental Occurrence and Toxicity - A Review*, Environment International **96**, 127 (2016).

[172] A. Markandya, T. Taylor, A. Longo, M. N. Murty, S. Murty, and K. Dhavala, *Counting the Cost of Vulture Decline-An Appraisal of the Human Health and Other Benefits of Vultures in India*, Ecological Economics **67**, 194 (2008).

[173] J. Bing, L. Li, B. Lan, G. Liao, J. Zeng, Q. Zhang, and X. Li, *Synthesis of Cerium-Doped MCM-41 for Ozonation of p-Chlorobenzoic Acid in Aqueous Solution*, Applied Catalysis B: Environmental **115–116**, 16 (2012).

[174] T. Peng, C. Xu, L. Yang, B. Yang, W. W. Cai, F. Gu, and G. G. Ying, *Kinetics and Mechanism of Degradation of Reactive Radical-Mediated Probe Compounds by the UV/Chlorine Process:*

Theoretical Calculation and Experimental Verification, ACS Omega **7**, 5053 (2022).

[175] F. S. Rocha, A. J. Gomes, C. N. Lunardi, S. Kaliaguine, and G. S. Patience, *Experimental Methods in Chemical Engineering: Ultraviolet Visible Spectroscopy-UV-Vis*, The Canadian Journal of Chemical Engineering **96**, 2512 (2018).

[176] D. Jankunaite, M. Tichonovas, D. Buivydiene, I. Radziuniene, V. Racys, and E. Krugly, *Removal of Diclofenac, Ketoprofen, and Carbamazepine from Simulated Drinking Water by Advanced Oxidation in a Model Reactor*, Water, Air, and Soil Pollution **228**, 1 (2017).

[177] S. Rong, Y. Sun, Z. Zhao, and H. Wang, *Dielectric Barrier Discharge Induced Degradation of Diclofenac in Aqueous Solution*, Water Science and Technology **69**, 76 (2014).

[178] O. Lesage, T. Roques-Carmes, J.-M. Commenge, X. Duten, M. Tatoulian, S. Cavadias, D. Mantovani, and S. Ognier, *Degradation of 4-Chlorobenzoïc Acid in a Thin Falling Film Dielectric Barrier Discharge Reactor*, Industrial & Engineering Chemistry Research **53**, 10387 (2014).

[179] A. Hernandez, V. Lacroze, N. Doudka, J. Becam, C. Pourriere-Fabiani, B. Lacarelle, C. Solas, and N. Fabresse, *Determination of Prenatal Substance Exposure Using Meconium and Orbitrap Mass Spectrometry*, Toxics **10**, 55 (2022).

[180] Z. Zhou, Y. Huang, J. Xiao, H. Liu, Y. Wang, Z. Gong, Y. Li, A. Wang, Y. Li, and L. Zheng, *Chemical Profiling and Quantification of Multiple Components in Jin-Gu-Lian Capsule Using a Multivariate Data Processing Approach Based on UHPLC-Orbitrap Exploris 240 MS and UHPLC-MS/MS*, Journal of Separation Science **45**, 1282 (2022).

[181] F. Guan, C. E. Uboh, L. R. Soma, and J. Rudy, *Erratum to: Sequence Elucidation of an Unknown Cyclic Peptide of High Doping Potential by ETD and CID Tandem Mass Spectrometry*, Journal of the American Society for Mass Spectrometry **27**, 370 (2016).

[182] P. J. Cullen and V. Milosavljević, *Spectroscopic Characterization of a Radio-Frequency Argon Plasma Jet Discharge in Ambient Air*, Progress of Theoretical and Experimental Physics **2015**, 1 (2015).

[183] J. Soler-Arango, G. Brelles-Mariño, A. Rodero, and M. C. Garcia, *Characterization of an Air-Based Coaxial Dielectric Barrier Discharge Plasma Source for Biofilm Eradication*, Plasma Chemistry and Plasma Processing **38**, 535 (2018).

[184] H. Ghodbane and O. Hamdaoui, *Decolorization of Antraquinonic Dye, C.I. Acid Blue 25, in Aqueous Solution by Direct UV Irradiation, UV/H2O2 and UV/Fe(II) Processes*, Chemical Engineering Journal **160**, 226 (2010).

[185] Y. Zambon, N. Contaldo, R. Laurita, E. Várallyay, A. Canel, M. Gherardi, V. Colombo, and A. Bertaccini, *Plasma Activated Water Triggers Plant Defence Responses*, Scientific Reports **10**, 19211 (2020).

[186] V. Stoleru, R. Burlica, G. Mihalache, D. Dirlau, S. Padureanu, G.-C. Teliban, D. Astanei, A. Cojocaru, O. Beniuga, and A. Patras, *Plant Growth Promotion Effect of Plasma Activated Water on Lactuca Sativa L. Cultivated in Two Different Volumes of Substrate*, Scientific Reports **10**, 20920 (2020).

[187] D. Moussa, A. Doubla, G. Kamgang-Youbi, and J. L. Brisset, *Postdischarge Long Life Reactive*

Intermediates Involved in the Plasma Chemical Degradation of an Azoic Dye, IEEE Transactions on Plasma Science **35**, 444 (2007).

[188] B. M. Cadorin, V. D. Tralli, E. Ceriani, L. O. de B. Benetoli, E. Marotta, C. Ceretta, N. A. Debacher, and C. Paradisi, *Treatment of Methyl Orange by Nitrogen Non-Thermal Plasma in a Corona Reactor: The Role of Reactive Nitrogen Species*, Journal of Hazardous Materials **300**, 754 (2015).

[189] Y. He, F. Grieser, and M. Ashokkumar, *Kinetics and Mechanism for the Sonophotocatalytic Degradation of p -Chlorobenzoic Acid*, Journal of Physical Chemistry A **115**, 6582 (2011).

[190] R. Deng, Q. He, D. Yang, Q. Dong, J. Wu, X. Yang, and Y. Chen, *Enhanced Synergistic Performance of Nano-Fe0-CeO2 Composites for the Degradation of Diclofenac in DBD Plasma*, Chemical Engineering Journal **406**, 126884 (2021).

[191] J. O. Back, T. Obholzer, K. Winkler, S. Jabornig, and M. Rupprich, *Combining Ultrafiltration and Non-Thermal Plasma for Low Energy Degradation of Pharmaceuticals from Conventionally Treated Wastewater*, Journal of Environmental Chemical Engineering **6**, 7377 (2018).

[192] S. Schönekerl, A. Weigert, S. Uhlig, K. Wellner, R. Pörschke, C. Pfefferkorn, K. Backhaus, and A. Lerch, *Evaluating the Performance of a Lab-Scale Water Treatment Plant Using Non-Thermal Plasma Technology*, Water **12**, 1956 (2020).

[193] L. Zhang, Y. Liu, and Y. Fu, *Degradation Kinetics and Mechanism of Diclofenac by UV/Peracetic Acid*, RSC Advances **10**, 9907 (2020).

[194] A. Agüera, L. A. Perez Estrada, I. Ferrer, E. M. Thurman, S. Malato, and A. R. Fernandez-Alba, *Application of Time-of-Flight Mass Spectrometry to the Analysis of Phototransformation Products of Diclofenac in Water under Natural Sunlight*, Journal of Mass Spectrometry **40**, 908 (2005).

[195] R. Banaschik, H. Jablonowski, P. J. Bednarski, and J. F. Kolb, *Degradation and Intermediates of Diclofenac as Instructive Example for Decomposition of Recalcitrant Pharmaceuticals by Hydroxyl Radicals Generated with Pulsed Corona Plasma in Water*, Journal of Hazardous Materials **342**, 651 (2018).

[196] F. Liu, J. Liang, L. Chen, M. Tong, and W. Liu, *Photocatalytic Removal of Diclofenac by Ti Doped BiOI Microspheres under Visible Light Irradiation: Kinetics, Mechanism, and Pathways*, Journal of Molecular Liquids **275**, 807 (2019).

Author's biography

I was born in 1992 in northern India. I grew up in Rashulpur, a small village in the district of Maharajganj, Uttar Pradesh, India. I completed my schooling in Bahaduri Bazar and Phulmanha Lehra in Maharajganj. I received my bachelor's degree in mechanical engineering from Dr. A.P.J. Abdul Kalam Technical University in Lucknow, India.

After finishing my undergraduate studies, I relocated to Bangalore, India's southern city. I completed my master's degree in Sustainable Technology at the Centre for Sustainable Technologies (Division of Mechanical Science) at the Indian Institute of Science (IISc) in Bangalore, India. My master's thesis was titled "Experimental investigation of a non-catalytic cold plasma water-gas shift reaction." After obtaining my master's degree, I worked as a research assistant at Combustion Gasification Propulsion Laboratory, Indian Institute of Science in Bangalore, India.

In December 2019, I was selected as a Marie Curie fellow at the MSCA-ITN-H2020 Nowelties. As an early-stage researcher in a double-degree program, I began my PhD studies (European Joint Doctorates) at the Faculty of Technology and Metallurgy, University of Belgrade (Serbia) and The Catalan Institute for Water Research, University of Girona (Spain). My host institute is the Institute of Physics Belgrade. My PhD project is titled "Design, development, and characterization of atmospheric plasma system for wastewater treatment." The majority of my PhD work was done at the Institute of Physics Belgrade. I was on a PhD secondment at The Catalan Institute for Water Research for around 7 months in the year of 2021-2022.

Author's publication

List of publications based on PhD dissertation:

- **Amit Kumar**, Nikola Škoro, Wolfgang Gernjak, Dragan Povrenović and Nevena Puač (2022). Paper title: "Direct and indirect treatment of organic dye (acid blue 25) solutions by using cold atmospheric plasma jet", (**DOI: 10.3389/fphy.2022.835635**).

- **Amit Kumar**, Nikola Škoro, Wolfgang Gernjak and Nevena Puač (2022). Paper title: "Cold atmospheric plasma technology for the removal of organic micropollutants from wastewater – a review", (**DOI: 10.1140/epjd/s10053-021-00283-5**).

- **Amit Kumar**, Nikola Škoro, Wolfgang Gernjak, Olivera Jovanović, Anđelija Petrović, Suzana Živković, Elisabeth Cuervo Lumbaque, Maria José Farré and Nevena Puač (2022). Paper title: "Degradation of Pharmaceuticals in Water by using Cold Atmospheric Plasma Sources (submitted in Science of the Total Environment Journal, under review)".

List of publications based on master dissertation:

- **Amit Kumar**, J Ananthanarasimhan, Anand M Shivapuji, S Dasappa and Lakshminarayana Rao (2020). Paper title: "Experimental investigation of a non-catalytic cold plasma water-gas shift reaction", (**DOI: 10.1088/1361-6463/aba92d**).
- Lakshminarayana Rao, J. Ananthanarasimhan, P.S. Ganesh Subramanian, N. Punith, **Amit Kumar**, M.S. Anand (2021). Paper title: "Application of non-thermal plasmas in medicine and energy-food-water", (**DOI.org/10.34256/famr2122**).

List of attened conferences in PhD

- **Amit Kumar**, Nikola Škoro, Wolfgang Gernjak and Nevena Puač (2021). "Treatment of acid blue 25 dye by using plasma-activated water"; - 23rd symposium on the application of plasma process (SAPP), 4th-5th February 2021, Department of Experimental Physics, Comenius University, Bratislava, Slovakia.

- **Amit Kumar**, Nikola Škoro, Wolfgang Gernjak and Nevena Puač (2022). "Wastewater treatment by using cold atmospheric plasma"; -Nowelties's conference- new materials and inventive wastewater treatment technologies-harnessing resources effectively through innovation, 11th-12th May, 2022 – Dubrovnik, Croatia.

- **Amit Kumar**, Nikola Škoro, Wolfgang Gernjak and Nevena Puač (2022). "Application of cold atmospheric plasma for removal of azo dye from aqueous solution";- 12th Micropol & Ecohazard Conference to be held from June 6th-10th, 2022 in Santiago de Compostela (Galicia, Spain).

- **Amit Kumar**, Nikola Škoro, Wolfgang Gernjak and Nevena Puač (2022). "Design, Development and Characterization of Atmospheric Plasma System for Wastewater Treatment";- 31st Summer School and International Symposium on the Physics of Ionized Gases (SPIG), September 5th-9th, 2022, Belgrade, Serbia.

- N. Škoro, O. Jovanović, **A. Kumar**, A. Petrović, N. Puač (2022). "Correlation between properties of plasma-treated liquids with characteristics of atmospheric pressure plasma devices";-9th Central European Symposium on Plasma Chemistry (CESPC9) + COST Action CA19110 Plasma Applications for Smart and Sustainable Agriculture (PlAgri), September 4th-9th, 2022, Vysoké Tatry, Slovakia.
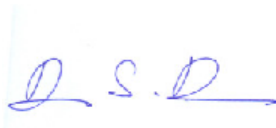
Attachment 4

Statement of originality

ASSESSMENT OF THE REPORT ON THE VERIFICATION OF THE ORIGINALITY OF THE DOCTORAL DISSERTATION

Based on the Rulebook on the evaluation of the originality of doctoral dissertations defended at the University of Belgrade and the findings in the report from the iThenticate program, which checked the originality of the doctoral dissertation **"Design, Development and Characterization of Atmospheric Plasma System for Wastewater Treatment"** by Amit Kumar, I state that the established text match is 20%. This degree of coincidence is due to the citations, personal names, general places and data, as well as the previously published research results of Amit Kumar, which preceded the completion of this doctoral dissertation, which is in accordance with Article 9 of the Regulations. Based on everything stated, and in accordance with Article 8, paragraph 2 of the Rulebook on the evaluation of the originality of doctoral dissertations defended at the University of Belgrade, I declare that the report indicates the originality of the doctoral dissertation, and the prescribed procedure of preparation for its defense can continue.

Advisor

Dr. Dragan Povrenović,

Full professor of the Faculty of Technology and Metallurgy,

University of Belgrade, Belgrade

Attachment 1.

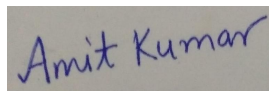# Statement of authorship

The undersigned Amit Kumar

Index number 4037/2019

I declare that the doctoral dissertation is entitled: "Design, development and characterization of plasma systems at atmospheric pressure for water processing"

• the result of own research work,

• that the proposed dissertation, in whole or in parts, was not proposed for obtaining any degree according to the study programs of other higher education institutions,

• that the results are correctly stated i

• that I have not violated copyrights and used the intellectual property of other persons.

Doctoral student's signature

In Belgrade 19.12.2022.

Amit Kumar

_____

Attachment 2.

Statement on the identity of the printed and electronic version of the doctoral thesis

Name and surname of the author: Amit Kumar

Index number: 4037/2019

Study program: Environmental Engineering

The title: "Design, development and characterization of plasma systems at atmospheric pressure for water processing"
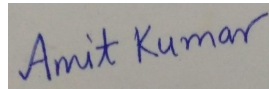
Mentor: Dr. Dragan Povrenović, full professor

The undersigned Amit Kumar

I declare that the printed version of my doctoral thesis is identical to the electronic version that I submitted for publication on the portal of the Digital Repository of the University of Belgrade. I allow the publication of my personal data related to obtaining the academic title of Doctor of Science, such as name and surname, year and place of birth and date of thesis defense. These personal data can be published on the web pages of the digital library, in the electronic catalog and in the publications of the University of Belgrade.

                                        Doctoral student's signature

In Belgrade 19.12.2022.

                                        Amit Kumar
                                        _____

Attachment 3.

Statement of Use

I authorize the "Svetozar Marković" University Library to enter my doctoral dissertation into the Digital Repository of the University of Belgrade under the title:

"Design, development and characterization of plasma systems at atmospheric pressure for water processing"
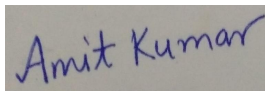
which is my author's work.

I submitted the dissertation with all attachments in an electronic format suitable for permanent archiving. My doctoral dissertation stored in the Digital Repository of the University of Belgrade can be used by anyone who respects the provisions contained in the selected type of Creative Commons license that I chose.

1. Authorship

 2. Authorship - non-commercial

 3. Authorship - non-commercial - no processing

 4. Authorship - non-commercial - share under the same conditions

 5. Authorship - no processing

6. Authorship - share under the same conditions

Doctoral student's signature

In Belgrade 19.12.2022.

Amit Kumar